Chem Soc Rev

REVIEW ARTICLE

View Article Online
View Journal | View Issue

Cite this: *Chem. Soc. Rev.*, 2022, **51**, 5805

Nanomaterials for virus sensing and tracking

Muqsit Pirzada [ab] and Zeynep Altintas *[ab]

The effect of the on-going COVID-19 pandemic on global healthcare systems has underlined the importance of timely and cost-effective point-of-care diagnosis of viruses. The need for ultrasensitive easy-to-use platforms has culminated in an increased interest for rapid response equipment-free alternatives to conventional diagnostic methods such as polymerase chain reaction, western-blot assay, *etc.* Furthermore, the poor stability and the bleaching behavior of several contemporary fluorescent reporters is a major obstacle in understanding the mechanism of viral infection thus retarding drug screening and development. Owing to their extraordinary surface-to-volume ratio as well as their quantum confinement and charge transfer properties, nanomaterials are desirable additives to sensing and imaging systems to amplify their signal response as well as temporal resolution. Their large surface area promotes biomolecular integration as well as efficacious signal transduction. Due to their hole mobility, photostability, resistance to photobleaching, and intense brightness, nanomaterials have a considerable edge over organic dyes for single virus tracking. This paper reviews the state-of-the-art of combining carbon-allotrope, inorganic and organic-based nanomaterials with virus sensing and tracking methods, starting with the impact of human pathogenic viruses on the society. We address how different nanomaterials can be used in various virus sensing platforms (*e.g.* lab-on-a-chip, paper, and smartphone-based point-of-care systems) as well as in virus tracking applications. We discuss the enormous potential for the use of nanomaterials as simple, versatile, and affordable tools for detecting and tracing viruses infectious to humans, animals, plants as well as bacteria. We present latest examples in this direction by emphasizing major advantages and limitations.

Received 6th February 2022

DOI: 10.1039/d1cs01150b

rsc.li/chem-soc-rev

[a] *Technical University of Berlin, Faculty of Natural Sciences and Maths, Straße des 17. Juni 124, Berlin 10623, Germany. E-mail: zeynep.altintas@tu-berlin.de, zeynep.altintas@tf.uni-kiel.de; Fax: +49 30 314 79552; Tel: +49 30 314 23727*
[b] *Institute of Materials Science, Faculty of Engineering, Kiel University, Kaiserstr 2, 24143 Kiel, Germany*

Muqsit Pirzada

Muqsit Pirzada graduated from the Institute of Chemical Technology, Mumbai in 2015. He obtained his MSc in Polymer Materials Science from Martin Luther Universität, Halle (Saale). He completed his MSc thesis in the field of biosensor technology under the supervision of Prof. Altintas at the Technical University of Berlin in 2019. He is currently a third year PhD student in the same group. His research focuses on imprinted polymers, nanomaterials, and diagnostic sensors.

Zeynep Altintas

Zeynep Altintas is full professor and Chair of Bioinspired Materials and Biosensor Technologies at Kiel University, Germany. She has been the Head of Biosensors and Receptor Development Group at Technical University of Berlin since 2016. She completed her PhD on biomedical sensors at the age of 25 with the outstanding PhD student award. Following a one-year postdoc position at Cranfield Biotechnology Centre, she continued her academic career as a faculty member of Biomedical Engineering at Cranfield University (the UK) until 2016. She is the author of >170 publications. She has supervised >35 PhD and MSc students and mentored seven post-doctoral fellows.

1. Introduction

Viruses are pathogenic entities with sizes in the nanometer range.[1] As the number of viruses on the planet exceeds 10^{31}, they are considered the most cornucopian biological units on earth.[2] Their ubiquity in the environment can be inferred from their concentration of 10^{11} virus-like particles (VLPs) per milliliter of seawater.[3] Since the initial discovery of the tobacco mosaic virus in 1898 by Martinus Beijerinck,[4] more than 6500 different species of viruses have been identified.[5] On the basis of their genetic material, they are classified into four realms: (1) duplodnaviria which comprise of double-stranded deoxyribonucleic acid (DNA) responsible for encoding the HK97-fold, a protein essential for capsid assembly;[6] (2) monodnaviria which possess single-stranded deoxyribonucleic acid (DNA) that encodes histidine-hydrophobic residue-histidine endonucleases involved in the rolling circle replication of viruses;[7] (3) riboviria containing ribonucleic acid (RNA) that translates reverse transcriptase or RNA-dependent RNA polymerase which are both involved in replication of viruses such as poliovirus;[8] and (4) varidnaviria that have double-stranded DNA responsible for capsid proteins involved in vertical Swiss roll fold.[5,9] Viruses consist of just one type of nucleic acid encoding a corresponding protein to form a nucleic acid–protein complex. In some viruses like adenoviruses, papillomaviruses and herpesviruses, this complex is enclosed within a capsid protein. However, in the case of flavivirus, parvovirus, picornaviruses and togaviruses, a direct complex between the capsid and the nucleic acid is formed.[1] In certain species such as the severe acute respiratory syndrome coronavirus 2 (SARS-CoV-2) or human immunodeficiency virus (HIV), the capsid may be enveloped by a lipid layer (Fig. 1).

Viruses can infect animals, plants, as well as microorganisms and, are considered crucial machinery for evolution since they can act as instruments of lateral gene transfer.[10] In contrast to most microscopic parasites, viruses are intracellular in nature.[11] Very few genes participate in the production of new viruses as reproduction is incumbent on several enzymes derived from the host cell.[12] In this way, they alter cellular processes to optimize the conditions for their own reproduction. Viruses contain genes and they reproduce as well as survive following the Darwinian concept of natural selection just like living organisms.[13] The defining distinction between viruses and other biological agents includes three characteristics: (1) viruses do not undergo division; (2) they are synthesized by the mere assembly of preformed building blocks; (3) the genetic information essential for the synthesis of ribosomes is absent.[14]

Once they infect the host, viruses may either enter a latent phase or an active replication phase. External stimuli, as well as cellular processes, can activate the repressed viral genome to encourage replication. Infected host cells may face at least one of the four possible consequences subsequently: (1) they are destroyed by various cell death mechanisms such as apoptosis (avian leukosis sarcoma virus,[15] Sendai virus,[16] and reovirus[17]), necroptosis (vaccinia[18] and coxsackie[19] viruses), or pyroptosis (Dengue virus[20] and HIV[21]);[22] (2) they survive with the viral genome (cytomegalovirus[23]) entering a phase of latency;[24,25] (3) they survive with a chronic/persistent viral infection[26] like in the case of varicella virus;[27] (4) they become immortal and achieves the capacity to undergo uninhibited cell division[28] which is often observed in the case of oncoviruses such as human T-cell lymphotropic virus (HTLV) which are responsible for causing adult T-cell lymphoma.[29] Viruses are responsible for several common diseases such as influenza,[30] cold,[31] chickenpox,[32] gastroenteritis, and pneumonia.[33] Serious illnesses including smallpox,[34] acquired immunodeficiency syndrome (AIDS),[35] rabies,[36] severe acute respiratory syndrome (SARS)[37] as well as certain types of cancers are also caused by viral infections.[35]

Viruses have contributed to several major disease outbreaks in human history with high mortality (Fig. 2). Although it is difficult to accurately determine the cause of pre-historic epidemics, viral outbreaks had a cataclysmic impact on human society such as the end of the Bronze age due to the smallpox plague,[38] the fall of Athens in the Peloponnesian war due to viral hemorrhagic fever[39] as well as the rise of monotheism following the Antonine and Cyprian plagues.[40] Epidemics of smallpox,[41] measles,[42] yellow fever,[43] influenza,[44] and dengue[43] were rife in the middle ages due to the development of trade routes and overcrowding of cities without proportional advancement in hygiene practices. Even in modern times, in spite of the advancement in medicines, sanitation as well as an improved understanding of virology and immunology, viral diseases such as the 1918 Spanish flu,[45] HIV-acquired immune deficiency syndrome (HIV)-AIDS[46] pandemic as well as the ongoing coronavirus disease (COVID-19) pandemic have claimed millions of lives.[47]

The treatment of viral diseases and subsequent recovery hinges on the timely detection of analytes such as virions, viral proteins, nucleic acids, or antibodies synthesized as part of the body's immune response to the infection.[69,70] Conventional analytical tools such as enzyme-linked immunosorbent assay (ELISA), polymerase chain reaction (PCR), serological antibody determination, and western blot demand advanced lab instruments which not only require skilled labor but also make testing expensive. Therefore, such analyses are performed in centralized testing institutes thereby prolonging the response time and delaying effective treatment.[12] Such factors cripple the

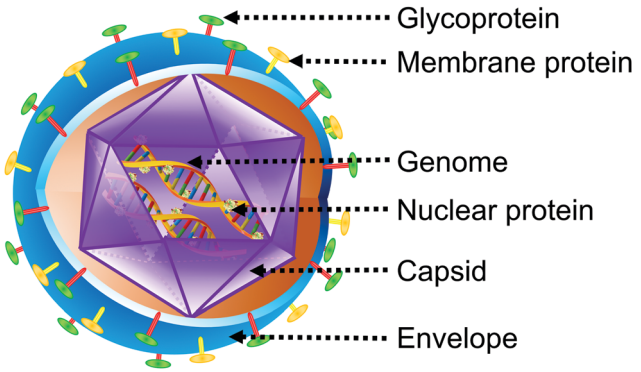

Fig. 1 Structure of a typical enveloped virus.

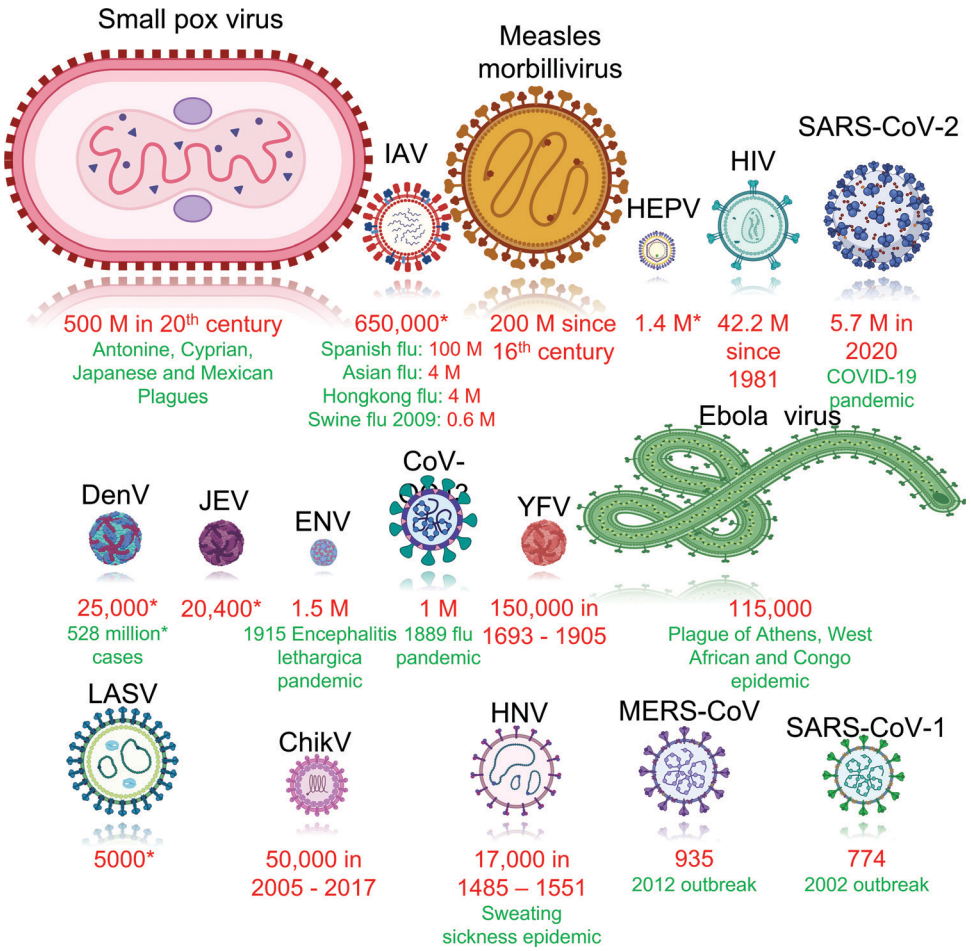

Fig. 2 Viruses responsible for major outbreaks in human history in descending order of fatalities. Abbreviation: *: average number of cases or fatalities each year; ChikV: Chikungunya virus; CoV-OC43: human coronavirus type OC43; DenV: dengue virus; ENV: enterovirus; HEPV: hepatitis viruses; HIV: human immunodeficiency virus; HNV: hantavirus; IAV: influenza A viruses; JEV: japanese encephalitis virus; LASV: lassavirus; MERS-CoV: middle east respiratory syndrome-related coronavirus; SARS-CoV-1: severe acute respiratory syndrome coronavirus 1; SARS-CoV-2: severe acute respiratory syndrome coronavirus 2 (Red: fatalities; green: notable outbreaks). Mortality statistics sourced from literature for: ChikV;[48] CoV-OC43;[49] DenV;[50,51] ebola;[39,52] ENV;[53,54] HIV;[55] HNV;[56] influenza;[54,57–59] LASV;[60] JEV;[61] measles morbillivirus;[62] MERS-CoV;[63] SARS-CoV-1;[64] SARS-CoV-2;[65] smallpox virus;[66] viral hepatitis;[67] yellow fever virus.[68]

response to infections with high virulence such as COVID-19 in developing countries.[71–73] Since biological sensors consist of receptors that exclusively bind to a chosen target analyte, they are highly sensitive and selective.[74,75] As such sensors are facile to manufacture and offer rapid responses capable of real-time detection at a low cost, they are suitable for point-of-care-testing (POCT).[69,76] In addition to early diagnosis, monitoring virus replication and dissemination is essential for prescribing accurate treatment.[77] Tracking the mechanism of viral entry and the resultant cellular response to such cargos constitutes the foundation of antiviral drug development.[78]

We reviewed the integration of nanomaterials to sensing and imaging platforms in our earlier works.[79–83] The typical size of a nanomaterial is lower than the wavelength of electrons which is why most of the atoms in such materials are located on the surface of the substance. These two factors in addition to their extraordinarily high surface area are responsible for the novel physicochemical properties of nanomaterials which are markedly different from the bulk form of the same material.[84,85] Quantum confinement effects in these materials enhance the sensor signal and in turn increase the sensitivity.[74,75] Zero-dimensional nanomaterials such as quantum dots and plasmonic nanoclusters interact with incident electromagnetic radiation resulting in their frequent use for non-invasive disease monitoring.[86,87] Integration of nanomaterials to biomedical applications such as detection and imaging is therefore auspicious.[88,89] Although there are some eminent reviews on nanomaterial-assisted virus recognition, they usually focus on just one type of nanomaterial without discussing viral imaging applications.[84,90–92] Additionally, research works about the latest developments in nanoparticle-mediated virus detection and non-metallic nanoparticles for virus tracking from the previous half-decade are rarely discussed.[93–96] Hence, we aim to present a compendious and detailed overview of the latest advancements in the field of virus recognition using various types of nanomaterials. To the best of our knowledge, this is the first

review wherein nanomaterials other than quantum dots and noble metal nanoparticles are also discussed in the context of virus imaging and tracking.

2. Carbon allotrope-based nanomaterials in virus sensing and tracking

Carbon is abundantly available on earth and has therefore been frequently employed in technological and scientific areas. Elemental carbon can exist as a variety of allotropes based on its hybridization ranging between sp,[97] sp^2,[98] and sp^3.[99] Furthermore, the nanoscale arrangement of these hybridized atoms allows the generation of several allotropes such as graphite, graphene, graphene quantum dots, and buckminsterfullerene all of which are sp^2 hybridized (Fig. 3).[84] Zero-dimensional nanomaterials such as carbon dots (CDs),[100–103] graphene quantum dots (GQDs),[104–106] and buckminsterfullerene (C_{60})[107,108] are capable of undergoing dynamic as well as static quenching, electron transfer, energy transfer, and inner field effect. One-dimensional (1D) carbon nanotubes (CNTs) can be further classified into: (1) single-walled (SWCNTs) with diameters ranging from 7–14 Å; (2) multiwalled (MWCNTs) which is composed of multiple concentric graphene tubes with diameters spanning up to 1000 Å.[84] Their high surface area coupled with long length facilitates the capture of various analytes in electrochemical systems.[109–113] Two-dimensional (2D) carbon allotropes include graphene and its derivatives such as graphene oxide (GO) and reduced graphene oxide (rGO). Owing to the unique structure of the electronic bands of graphene, it shows extraordinary thermal, electrical, and mechanical properties.[114–117] In recent years, other carbon allotropes such as nanohorns,[118] nanodiamonds,[119,120] and nanoparticles[121,122] have also been introduced into sensing and imaging technologies due to their superior fluorescence, impedance, and energy transfer capabilities. These qualities make carbon allotrope-based nanomaterials ideal for incorporation into biosensing and bioimaging platforms.[84]

2.1 Virus sensing

2.1.1 Carbon nanotubes. CNTs, which are graphene sheets rolled into long cylinders, constitute the most abundantly researched carbon allotrope for biosensing purposes. CNT functionalized electrodes can be easily conjugated with various receptors such as aptamers,[123,124] molecularly imprinted polymers (MIPs),[124,125] proteins[109,123,126–128] as well as nucleic acids (Table 1).[111–113] Several different coupling chemistries such as cysteamine,[126] ethyl(dimethylaminopropyl) carbodiimide (EDC) with *N*-hydroxysuccinimide (NHS),[109,123,127] (3-aminopropyl) triethoxysilane (APTES),[123] and glutaraldehyde[129] have been explored to conjugate CNTs with receptors. Choice of a receptor as well as the chemistry employed for its immobilization play a critical role in the sensing properties. Therefore, MWCNTs exhibited a ten-fold higher sensitivity towards pandemic H1N1 with aptamers in comparison to antibodies in a comparative study.[123]

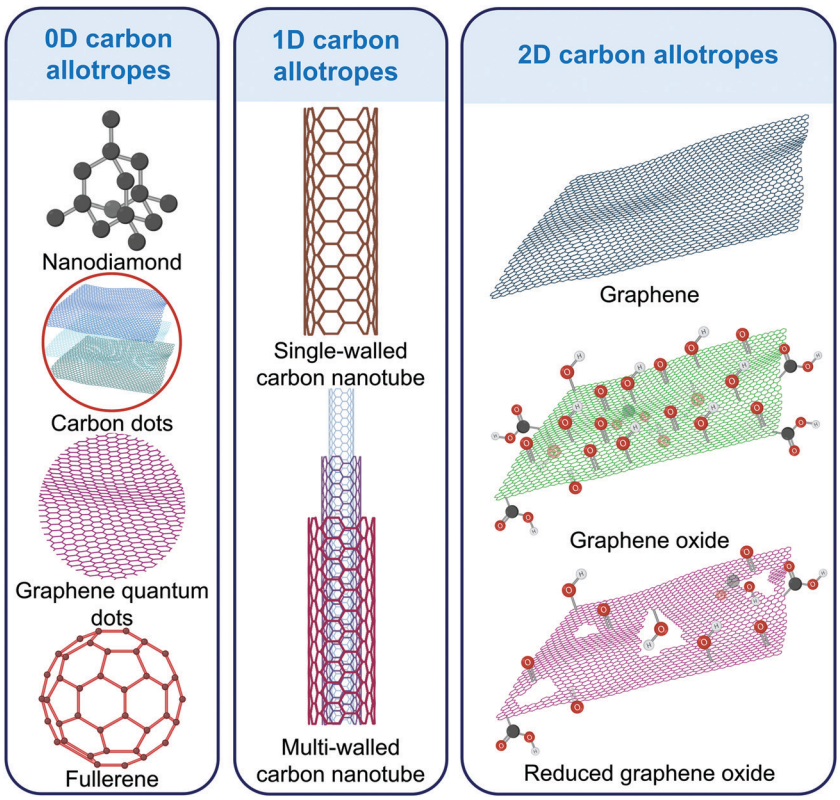

Fig. 3 Carbon allotropes often used in virus detection and imaging.

Table 1 Carbon nanotubes for virus detection

Nanomaterial	Platform	Receptor type	Target	Method	LOD	Ref.
MWCNT/ZNC	FTO	ssDNA	HBV DNA	DPV, CV, EIS	50 copies mL^{-1}	130
aCNT	HA/GCE	Antigen	antiHBV core protein	SWV	34 pg mL^{-1}	131
MWCNT/Chitosan	GCE	MIP	HIV-p24 capsid protein	DPV	83 fg mL^{-1}	125
MWCNT/Chitosan	GCE	MIP	HCV core antigen	DPV	1.67 fg mL^{-1}	124
MWCNT	NH_2rGO/IL	ssDNA	HPV DNA	DPV	1.3 nM	112
Semiconducting SWCNT	Cr/Au IDE	ssDNA	H5N1 DNA	Chemiresistor	20 pM	132
N-doped MWCNT					2 pM	
SWCNT/1-pyrene methylamine	Au IDE	Heparin	DENV-1	Chemiresistor	8.4×10^2 $TCID_{50}$ mL^{-1}	133
CNT	$NiCo_2O_4$ spinel	DNA	HIV-1 DNA	EIS	16.7 fM	134
CNT	Cr, Pt	DNA	Influenza A DNA	FET	1 pM	135
mMWCNT	AuNP/MNP	DNA	H1N1 DNA	LSV	8.4 pM	111
mMWCNT	Pt/IDE	DNA	Norovirus DNA	LSV	8.8 pM	111
MWCNT	AuNP	Antibody	H3N2	Colorimetry	3.4 PFU mL^{-1}	136
AuNP/MWCNT	Silicon chip	Antibody	DENV-2 NS1	DPV	300 fg mL^{-1}	126
AuNP/MWCNT	Ag IDE	Aptamer	H1N1	Volymetric assay	10 fM	123
AuNP/MWCNT	Ag IDE	Antibody	H1N1	Volumetric assay	1 pM	123
AuNP/CNT	AgNP/SPCE	Antibody	HBV surface antigen	SI-DPV	860 pg mL^{-1}	109

Abbreviations: aCNT: aminated carbon nanotubes; AuNPs: gold nanoparticles; CNT: carbon nanotubes; DENV: dengue virus; DPV: differential pulse voltammetry; EIS: electrochemical impedance spectroscopy; FET: fluorescence energy transfer; FTO: fluorine doped tin oxide glass; GCE: glassy carbon electrode; HA: hyaluronic acid; HBV: hepatitis B virus; HCV: hepatitis C virus; HIV: human immunodeficiency virus; HPV: human papilloma virus; IDE: interdigitated electrode; IL: ionic liquid; MIP: molecularly imprinted polymer; mMWCNT: magnetic multi-walled carbon nanotube; MWCNT: multi-walled carbon nanotube; NS: non-structured protein; PFU: plaque forming units; rGO: reduced graphene oxide; SI-DPV: sequential injection differential pulse voltammetry; SPCE: screen printed carbon electrode; ssDNA: single strand deoxyribonucleic acid; SWCNT: single-walled carbon nanotube; SWV: square wave voltammetry; TCID: tissue culture infectious dose; ZNC: zeolite nanocrystal.

This strain of the swine flu virus is responsible for seasonal bouts of influenza.

CNTs are versatile nanomaterials and chemical functionalizations can greatly alter their sensing capabilities (Fig. 4). Carboxylated CNT-based virus sensors are very specific against resemblant circulating viruses[137] such as Zika virus (ZikV) which is responsible for Zika fever. Such devices allow rapid mismatch-tolerant detection for the RNA of highly variable viruses such as HIV which can progress to the life-threatening AIDS illness if left undetected and untreated.[113] These CNTs exhibit excellent electrochemical stability and encourage greater electron transfer through amide bonds with -NH_2 containing moieties. This concept has been harnessed for electrochemically screening ZikV and dengue virus (DenV) by evaluating the presence of nonstructural glycoprotein NS1 in serum and urine samples.[138] Aminated CNTs in immunosensors amplify the charge transfer and provide a stable platform for antigen immobilization. Such platforms are essential for the detection of key serological markers for hepatitis infection such as the antibody to hepatitis B virus (HBV) core antigen.[131] Chitosan functionalized MWCNTs with MIP receptors show ~100% recovery towards viral proteins in serum samples[124,125] and low relative error (−4.7 to 3.4%) against ELISA.[125]

Another strategy for tuning the characteristics of CNT includes decoration with metallic nanoparticles (Fig. 4). For example, gold

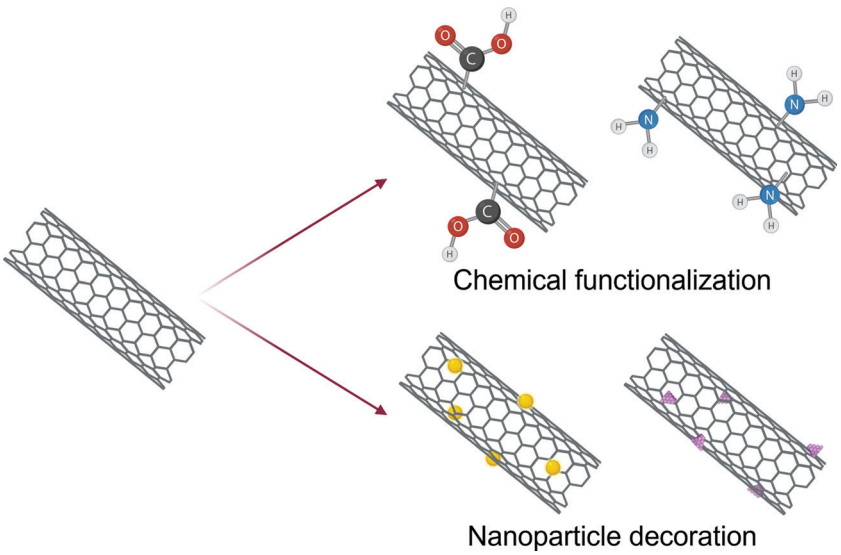

Fig. 4 The two most common types of CNT modifications used in virus sensing.

nanoparticles (AuNPs) have been interspersed on MWCNTs to introduce peroxidase-like activity.[136] These modifications have been reported to enable nearly 500 times higher sensitivity than commercial immunochromatography kits towards H3N2 detection with a 385 times lower LOD in comparison to a typical ELISA.[136] AuNP-decorated CNTs exhibit exceptional specificity towards human pathogenic viruses with proteinaceous as well as nucleic acid receptors.[109,111] Similarly, zinc nanoparticles intercalated on MWCNTs for the detection of Chili leaf curl betasatellite, a plant virus responsible for severe economic loss for pepper and tomato crops, promote the conjugation of single-strand DNA (ssDNA) enabling 3-fold higher specificity against non-complimentary DNA.[139] A similar concept has also been developed integrating a nanocomposite of MWCNTs with zeolite nanocrystals to PCR-based amplification for genosensing HBV DNA.[130] The retention of cavities in metal-organic frameworks (MOFs) embedded with CNTs encourages nucleic acid binding enabling femtomolar detection of HIV DNA.[134] Incorporation of Fe_3O_4@SiO_2 to CNT-based paper biosensor for pseudorabies virus introduced immunomagnetic properties that allows rapid detection within a few minutes without the requirement of skilled labor or expensive equipment making them suitable for POCT.[127] The coexistence of nanoparticles in CNT nanocomposites offers four key benefits: (1) a stronger electrochemical response is obtained due to synergistic electronic interactions, (2) receptor conjugation *via* H bonding, π–π interactions and electrostatic forces is encouraged, (3) increased surface area enhances analyte adsorption, (4) the biocompatibility is improved.[131,134] In addition to physical or chemical modifications, integration of computational modeling to optimize the roughness and alignment in CNT-thin films has been reported to show a higher sensitivity than the viral load observed in clinical samples by two orders of magnitude.[140] Since MWCNTs are cost-effective, they find more abundant application in viral diagnostics than SWCNTs.[111,112,123,128,141] However, interest in SWCNTs is increasing since they have a much larger surface area and allow ultrasensitive detection due to modulation of the Schottky barrier which is absent in MWCNTs.[132,133,142,143] SWCNT-based field-effect transistors (FET) therefore demonstrate picomolar sensitivity towards influenza A virus DNA with a response time of only 1 min.[142]

Interest in carbon nanotube-based sensors for virus detection has risen with 14 164 research works out of 27 916 published in the last five years alone (Web of Science). Electrochemical platforms constitute the largest class of CNT-based biosensors supporting a variety of virus detection mechanisms such as differential pulse voltammetry (DPV),[137,139] electrochemical impedance spectroscopy (EIS),[134] linear sweep voltammetry,[111] cyclic voltammetry[130] and square wave voltammetry[131] (Fig. 5). CNT-based virus biosensors relying on DPV exhibit very high recovery in complex media such as serum[109,125] and cells.[112] CNTs have also been introduced to FET,[129,135,142,144] chemiresistors,[132,133] volumetric assays,[123] optical sensors[136] as well as conventional techniques for viral genome recognition such as PCR[145,146] and loop-mediated isothermal amplification (LAMP).[113] Reverse transcription LAMP-based HIV-1 DNA detection using carboxylated CNTs is even faster than fluorescent PCR

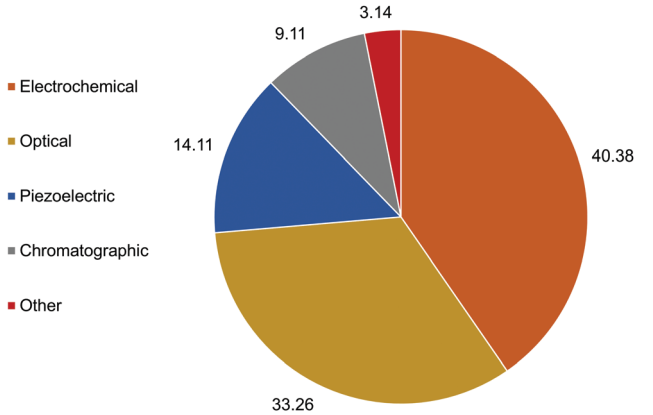

Fig. 5 An illustration of research works published in the last five years on the different types of carbon-nanotube-based sensors for virus detection (Web of Science).

and shows a 96.5% concordance rate with Roche instruments and a Nernstian response factor of 63.567 mV pH^{-1}.[113]

2.1.2 Graphene and its derivates. Graphene consists of a 2-D monoatomic layer of sp^2 hybridized carbon arranged in a honeycomb lattice. It is the second most popular carbon allotrope incorporated in virus sensing platforms. The electrons in graphene maintain a unique band structure giving rise to interesting charge transfer and electronic characteristics.[147] Its outstanding mechanical and thermal properties along with a massive surface area (2630 m^2 g^{-1}) make graphene ideal for biosensors intended for POCT purposes.[84] For example, the use of laser-engraved graphene in a telemedicine platform for the rapid multiplexed detection of SARS-CoV-2 capsid protein, C-reactive protein as well as immunoglobulin M and G in saliva and serum can be fabricated for less than 0.05 $.[117] Furthermore, it has recently been demonstrated that graphene-assisted SARS-CoV-2 immunosensors can show 40 000 times higher sensitivity than ELISA in clinical transport medium while simultaneously being specific against the structurally similar Middle East respiratory syndrome-related coronavirus (MERS-CoV) (Fig. 6).[115] Such a distinction helps in selecting a suitable therapeutic strategy since structurally similar viruses can require radically different treatment methods. Epitaxial graphene has also been employed for SARS-CoV-2 variant B.1.1.7 detection which provided a response within 0.6 s with extraordinary sensitivity (60 copies mL^{-1}).[148] Graphene possesses chiral plasmonic metasurfaces which can be harnessed for polarization-based discrimination of various types of avian influenza viruses.[147] Graphene can also be composited with nanoporous silicon oxide to synthesize HBV sensitive artificial neural network.[149] Such chemical modifications can significantly improve the sensitivity of graphene-based sensors and promote nucleic acid immobilization. Therefore, poly-L-lysine functionalized graphene-based FET sensors show a 113% higher sensitivity than unfunctionalized graphene platforms towards SARS-CoV-2 RNA.[150] The signal-to-noise ratio of graphene FET sensors can be enhanced by ~10% when they are nanocomposited with MXene.[151] Although glutaraldehyde coupling chemistry has been reported,[149] most

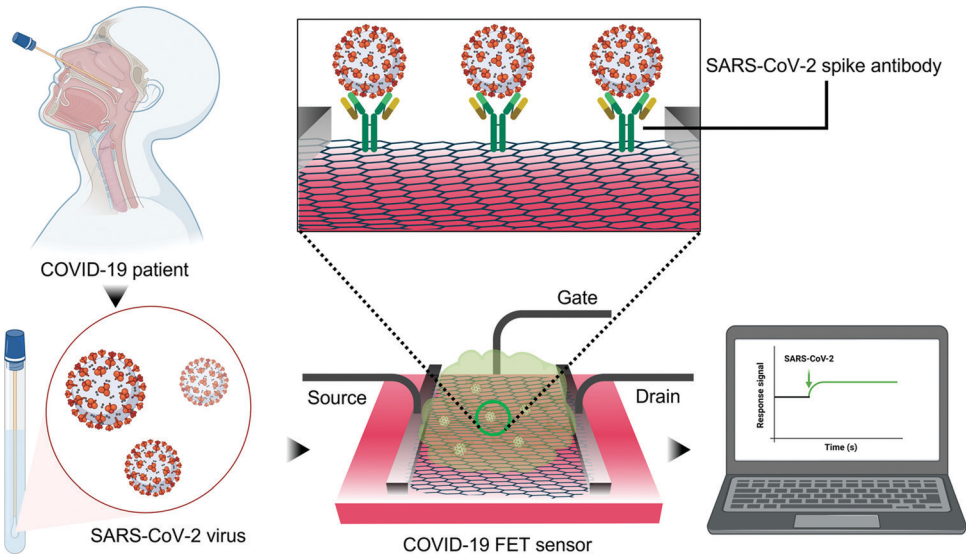

Fig. 6 SARS-CoV-2 detection using a graphene-based FET immunosensor.[115] The FET system is gated with an aqueous solution. The presence of SARS-CoV-2 alters the surface potential of the channel and results in an electrical response when the spike protein attaches to the immobilized antibody.

immunosensors rely on NHS and NHS derivatives for immobilizing the antibodies on graphene.[114–117]

Graphene derivatives such as GO and rGO are considerably influenced by their crystal defects as well as chemical functionalizations. GO is a product of oxidation of exfoliated graphite in which both the graphene surfaces have oxygenated functionalities. The optoelectronic and chemical properties of GO differ widely from graphene since GO has a much higher reactivity and a relatively lower electric conductivity. It also does not interact with the visible portion of the electromagnetic spectrum. Covalent, ionic, or hydrogen bonds between biomolecules and the oxygen-bearing functional groups from the edges and basal plane of GO are auspicious in the development of virus sensing platforms.[84] For example, the negative charge on GO can be used for anchoring the DenV template during the molecular imprinting process.[152] The quantum efficiency of GO can be quenched to avoid chemical modifications and simplify the sensing process. This fluorescence quenching property can be harvested by chemisorbing fluorescein amidate onto GO to generate a DNA-based sensor for Ebola virus (EBV) responsible for a type of viral hemorrhagic fever which is often fatal.[153] Similar principles for HTLV[154] and foot-and-mouth disease virus[155] detection replaced fluorescein with AuNPs for quenching.

Amongst all the 2-D allotropes of carbon, rGO has been the most preferred nanomaterial in virus detection due to its crystal defects, heteroatomic impurities, and low-cost.[156] It is synthesized by reducing GO *via* electrochemical, chemical, or thermal procedures. The reagents used for reduction determine the carbon to oxygen ratio and the crystal defects which in turn affect the electrochemical properties.[84] Reduction with ascorbic acid promotes the integration of ssDNA on rGO surface by direct adsorption through π–π bonding and can thus be used for impedimetric detection of coxsackie virus which causes aseptic meningitis.[157] This type of rGO can also be used as a signal enhancer for femtomolar detection of Japanese encephalitis virus (JEV) non-structural 1 protein.[158] JEV is a *Culex* mosquito-borne virus responsible for Japanese encephalitis, a type of brain infection causing vomiting and seizures in severe cases. GO can also be reduced using porous hydrazine and subsequently conjugated with molybdenum sulfide to generate aptamer-facilitated electrochemical transducers for human papillomavirus (HPV) detection. Undetected HPV can lead to precancerous lesions and is the most common cause of cervical cancer. These hydrazine-reduced GO transducers show not only a high sensitivity (LOD: 1.75 pM) but also excellent recovery in serum (90–98%) as well as saliva (97–105%).[159] Another promising approach for reduction targeted the epoxy and carboxyl groups of GO by refluxing with ethylenediamine to enable electrostatic coupling with AuNPs for the detection of HBV antibodies.[160] A greater variety of biomolecular functionalizations are possible for rGO in comparison to graphene due to the presence of significantly lesser functional groups.[84] These functional groups are easily hydrophilized by amination for conjugating with dendrimers to enhance the sensitivity and facilitate femtomolar detection of viral proteins.[161,162] A 1.25-fold reduction in the detection limit is observed when aminated rGO is wrinkled with CdS quantum dots (QDs).[163] Aminated rGO in a nanohybrid with MWCNTs and ionic liquid shows very high recovery (94–102.5%) in squamous carcinoma cells for HPV DNA.[112]

2.1.3 Zero-dimensional carbon allotropes. Interest in zero-dimensional (0D) carbon allotropes for virus recognition has increased in recent years owing to their exclusive electrical and optical features such as fluorescence, chemiluminescence, photoluminescence (PL), and electrochemiluminescence. These properties arise from their quasispherical/spherical shape in addition to the quantum hall effects prominent at the nanoscale.[164] Allotropes such as CDs are facile and cost-effective to

synthesize, composite as well as functionalize.[84,165] Due to their strong quantum yield, viral assays relying on CDs show a longer lifespan and two orders of magnitude higher sensitivity than those using gold colloid thereby exhibiting an aptitude for POC diagnosis.[103] The polarization value of carbon dots can be increased by conjugating them with a large molecule such as streptavidin to enable the fluorescence-assisted detection of HIV capsid protein. Such sensors, when fabricated on a paper-based platform are 3.5 times cheaper[101] and 65-fold faster than ELISA.[100] Silicon nanospheres can be employed to prevent fluorescence quenching of CDs at high concentrations which facilitates monodispersity and greater quantum yields.[166] Fluorescent carbon dots immobilized on dendritic porous silica have been employed as a colloid for the colorimetric detection of ZikV in a lateral flow format.[167] Such strips perform 100-fold better than AuNP-based lateral flow systems and exhibit a visual detection limit of only 10 pg mL^{-1}. The fluorescence of CDs can be quenched with metallic nanohybrids such as those made of gold and iron oxide. An HTLV genosensor developed on this principle has been shown to discriminate against other blood-borne viruses such as HIV and HBV.[102] However, a 1000-fold increase in the sensitivity and nearly 19-fold wider detection range was reported when a GQD–copper nanocluster hybrid is used instead of the CD nanocomposite.[105] In this case, the GQDs acted as a reference site for the DNA template and allowed the *in situ* generation of copper nanoclusters favored by exonuclease III-assisted target recycling amplification. The signal-to-noise ratio was further amplified by the exonuclease I-assisted cleavage of unbound DNA.[105] The high surface area of GQDs fosters the covalent attachment of a large number of nanoparticles which successively promote the immobilization of more biomolecules such as antibodies[168–170] and nucleic acids.[171] Such immunosensors show negligible interference (<5%) even when the concentration of non-specific molecules is 300 times greater than the target antigen (Fig. 7).[104] Doping the GQDs with different elements can impart interesting properties such as enabling them to discriminate between viral serotypes[172] or introducing magnetic relaxation switches which are useful for designing ultra-low field nuclear magnetic resonance sensors.[173] In GQD-based aptasensors, π–π stacking within the layers of GQDs facilitates interactions between their carboxyl groups with the amine groups from aptamers.[174] One such aptasensor for hepatitis C virus (HCV) displayed high reproducibility (standard deviation <2.3%) and recovery in serum (99–109%).[106] Such π–π interactions between sp^2 hybridized carbon nanoparticles and nucleotides also result in fluorescence resonance energy transfer (FRET). Although these particles have also been used as fluorescence quenchers for silver nanoclusters in HIV detection, a narrow dynamic range is observed which can be attributed to the instability of silver nanoclusters in complex media.[175] GQD-silver nanocomposites can also be harnessed for the naked eye detection of HCV RNA down to 24.84 pM with the help of a catalyzed hairpin assembly reaction.[176]

2.1.4 Other carbon allotropes. Nowadays, interest in other crystalline allotropes of carbon for virus recognition has grown. Due to their small pore size as well as lower impurities, single-walled carbon nanohorns readily physisorb palladium–platinum nanoparticles. Such nanocomposites show promising durability with only 5.8% signal loss in 15 days for horseradish peroxidase-based immunosensing of cytomegalovirus which is often responsible for diseases such as pneumonia and mononucleosis.[118] Crystal defects such as vacancies as well as doping give rise to unique properties at the nanoscale.[177]

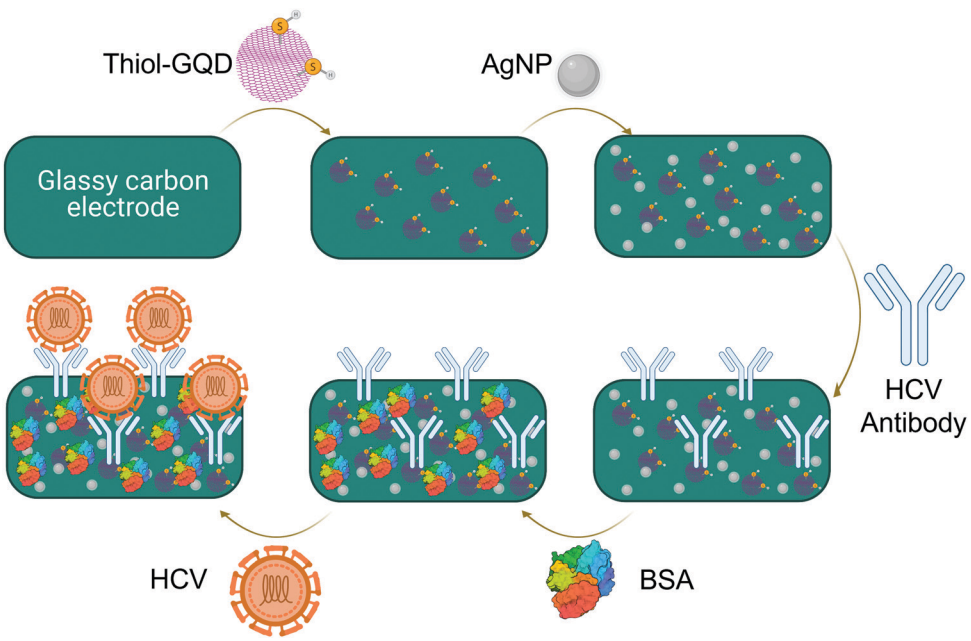

Fig. 7 Thiolated graphene quantum dots for hepatitis virus detection.[104] Abbreviations: AgNP: silver nanoparticles; BSA: bovine serum albumin; GQD: graphene quantum dots; HCV: hepatitis C virus.

Therefore, doping nanodiamonds with boron results in semiconducting behavior and electrodes developed from such materials can be conjugated with polyclonal antibodies to allow the rapid detection of influenza viral proteins[178] as well as whole virions.[119] Similarly, nanodiamonds with nitrogen vacancies exhibit fluorescence. Since these fluorescent nanodiamonds are inexpensive, stable, and highly durable, it is possible to develop virus sensors under 1 $ with attomolar sensitivity and less than a minute of response time.[120] Nanodiamonds are also used for developing aptasensors with attomolar detection limits however, ~33% signal response is lost within just ~11 days.[179] Certain carbon nanoparticles such as C_{60} have also been useful in non-radioactive cell proliferation assays[107] as well as for controlling the window size in virus-sensitive MOFs.[108] Electrodes modified with C_{60} exhibit a broad potential window, durability and stable responses for long time scales allowing the detection of HCV core antigen at the fg mL^{-1} level.[180] This antigen is a surrogate biomarker indicating hepatitis C since their concentration is a direct indicator of viral RNA levels.[181]

Crystalline allotropes of carbon are more numerous and resistant to photobleaching. High purity in addition to exquisite durability make their use in virus detection more widespread than amorphous allotropes. Nevertheless, biomolecules readily adhere to amorphous allotropes of carbon which is an integral requisite for most biosensors.[122] In a recent study, nitrogen-doped porous carbon nanoparticles were synthesized from MOF to promote strong hydrogen bonds with ZikV DNA. This assembly allowed discrimination between 1–2 base mismatches as well as complimentary/non-complimentary DNA.[121] As these particles show lesser residual current than glassy carbon electrodes, they act as ideal substrates for antibody physisorption.[122] However, carbon nanoparticles are also suitable where chemically induced coupling is required. For example, amine-rich carbon nanoparticles derived from chitosan can be conjugated with JeV antibody through EDC-NHS chemistry.[182]

2.2 Virus tracking

2.2.1 Fluorescent nanodiamonds. Although organic fluorophores such as cyanine, coumarin, or rhodamine are still used for imaging purposes, they undergo photobleaching and exhibit photoblinking. With an increase in the intensity of light used, a loss in fluorescent intensity is observed which deteriorates the resolution, reproducibility, and stability.[183] Robust sp^3 hybridized-carbon nanomaterials like fluorescent nanodiamonds (FNDs) have nitrogen vacancies and emit stable fluorescence in the near-infrared region (NIR). This NIR fluorescence exhibits linearity over broad concentration ranges and is largely resistant to interference from non-specific biomolecules. FNDs are recalcitrant to bleaching and display exquisite material durability. In comparison to the widely used QDs,[111] FNDs are non-toxic and photostable. Although nanodiamonds synthesized by detonation exhibit anti-bacterial properties in some cases, such bioincompatible features can be avoided by substituting with crushed high-temperature high-pressure FNDs subjected to oxidative cleaning.[184] FNDs are bioinert and can be easily subjected to chemical modifications. The mass of biomolecules deposited on FNDs is inversely proportional to their size and can therefore be tuned according to the imaging system available. In an *in vivo* imaging-assisted lateral flow assay (LFA), nanodiamonds can be homogeneously distributed with ease and can bind with recombinant as well as wild-type viral glycoproteins without perturbing their immunological function. However, it is essential to optimize the strategy to load the nanoparticles on the test strip as the attachment of multiple FNDs to several wild-type glycoproteins can form large aggregates that retard the flow and induce smearing.[120] FNDs can also be encapsulated with viruses to understand their 3D cell trajectory which is key to understanding cytosis and cellular transport mechanisms.[185] In order to gain a better understanding of viral dissemination, FNDs can also be used for tracking viruses inside bacteria and cells. This can be achieved by forming FND-phage conjugates using an appropriate linking chemistry. Since streptavidin forms strong non-covalent bonds with biotin, streptavidin functionalized FNDs can be easily coupled with biotinylated bacteriophages. These conjugates exhibit highly specific behavior as illustrated in Fig. 8. The FND (red) – phage (cyan) assembly in this case is targeted to bind with the maltoporin receptor on the outer membrane of the bacteria (black). Therefore, no binding between the conjugates and non-target bacteria (yellow) was observed.[184] In this case, it is essential to optimize the FND:phage ratio as free streptavidin FNDs as well as unbound biotinylated phages can result in errors such as false positives or inaccurate visualization. Additional washing steps also help alleviate false-positive results. The streptavidin–biotin chemistry can also be substituted with cysteine-maleimide so that maleimide FNDs attach directly to phages with exposed cysteine groups.[184]

2.2.2 sp^2 hybridized carbon allotropes. In the case of sp^2 hybridized carbon allotropes, supplementary fluorophores such as QDs,[111] rhodamines,[121] metallic nanoparticles,[165] and fluorescein isothiocyanate[78] are often required to strengthen the fluorescence signal. An exception to this rule is the case of boron-nitrogen co-doped single layer GQDs. Due to their low cytotoxicity and high quantum yield (36.5%) such nanomaterials are suitable for imaging viruses in live cells.[186] In addition to experimental imaging, their nucleic acid sensing capabilities have also been confirmed with computational simulations with help of density functional theory. Nanocomposites containing carbon allotropes like graphene alongside metal/magnetic nanoparticles and quantum dots can exhibit multifunctional features such as plasmonic coupling and plasmon resonance energy transfer.[111] These features can be attributed to the synergistic presence of plasmonic and π electrons as well as interactions between the magnetic spins of various elements. Due to delocalization, high-energy unhybridized electrons from graphene can freely move and induce plasmonic coupling with metallic atoms present in such nanocomposites. This coupling, in turn, produces a commensal effect necessary for energy transfer even when the size of the virus is significantly small.[111] The presence of viruses can also be verified by identifying their genetic

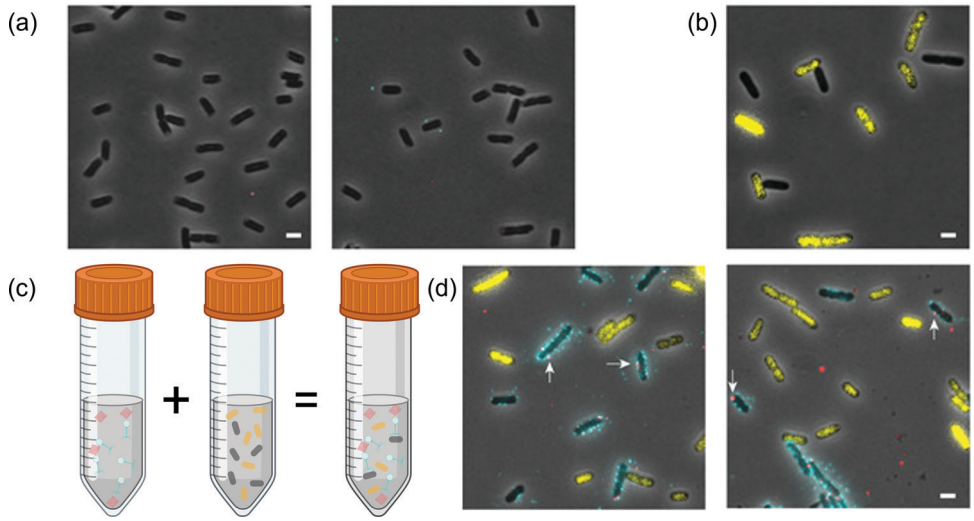

Fig. 8 Host-specific targeting of FND-phage conjugates. (a) Cells without phage receptors do not bind to the FND conjugates; (b) a mixture of target and non-target species of bacteria; (c) scheme of FND-based imaging in the mixture of specific and non-specific bacteria; (d) epifluorescence imaging of FND-phage conjugate. Colors represent FNDs (red), phage (cyan), target bacteria (dark grey), non-target bacteria (yellow). Arrows point towards sites of FND-cell binding.[184]

material. One such strategy involves binding a fluorophore-labeled complementary single-strand nucleic acid to graphitized nitrogen-doped porous carbon nanoparticles.[121] Due to the abundance of N-atoms in the nanoparticles, strong hydrogen bonds are formed with the OH functionality from DNA. The π electrons from the nanoparticles interact with those from the nucleic acid to form a complex capable of FRET. Therefore, the fluorescence of the label is quenched. Since the zeta-potential of the carbon nanoparticles corresponds to incipient instability, the presence of the positively charged target RNA causes electrostatic attraction. As a result, the probe and target nucleic acids bind, and the ensuing conformational changes hide the bases in the double-stranded structure reducing the number of bases that can bind with the nanoparticles. The spectral overlap between the nanoparticles and the fluorophore enables fluorescence recovery in the event of target recognition.[121] This imaging technique shows high specificity against non-complimentary RNA as well as 1–2 base mismatches. Although the presence of mesopores and micropores in the nanoparticles encourages DNA adsorption, the hierarchical structure retards fluorescence recovery resulting in a longer response time. Another drawback of this approach that hinders imaging in real patient samples is the requirement of single-strand DNA when human DNA is double-stranded.

Carbon allotrope-based virus imaging has recently been employed as a high throughput strategy for antiviral drug screening.[78] In this case, an RNA-GO conjugate was developed to target RNA-dependent RNA polymerase, an essential protein present in the genome of all riboviruses such as DenV which causes hemorrhagic fever and shock syndrome. The conjugate was suitable for *in vitro* as well as *in vivo* assays. Here, the GO acted as a quencher for the fluorophore used to label RNA. The quenching-recovery mechanism followed the same approach as the previous method with one minor difference: the target nucleic acid in this case was generated *in situ* by the polymerase enzyme. Therefore, when a drug is successful in eliminating the virus, the fluorescence is not recovered.[78] The main advantages of this strategy include convenient handling due to chemical stability of GO observed in usual room conditions. Additionally, drug screening through virus imaging exhibits high throughput and has the potential to reduce experimental burden as well as research expenditure.

3. Inorganic nanomaterials in virus sensing and tracking

Transition and inner-transition elements have incompletely filled d and f orbitals, respectively. These orbitals contribute to the surplus of high-energy surface electrons that are responsible for the remarkable magnetic, optoelectronic and quantum properties of inorganic materials.[79,187] These features can not only be easily incorporated into the sensing or imaging system as is but also be tuned to best suit the sensor requirements with the help of three strategies: (1) by manipulating the physical features of the nanomaterials such as its size or shape,[188–191] (2) by introducing suitable functionalities to the nanomaterial[192–196] and (3) by combining them with other nanomaterials to generate multifunctional nanocomposites (Fig. 9).[177,197–199] For example, based on the distance between different nanoparticles, localized surface plasmon resonance (LSPR) can be observed. In inorganic nanomaterial-reliant biosensors, this phenomenon can be modulated by the concentration of viruses present in the ambient media.[200,201] Inorganic nanomaterials include metal and metal oxide nanoparticles,[92,202] quantum dots[96,203] as well as silicon-based nanostructures.[93] These nanomaterials come in a variety of shapes such as spheres,[204] cubes,[205] tetrahedrons,[206] octahedrons,[207] bipyramids,[208] cages,[207] wires,[209] core–shell assemblies[210] as well

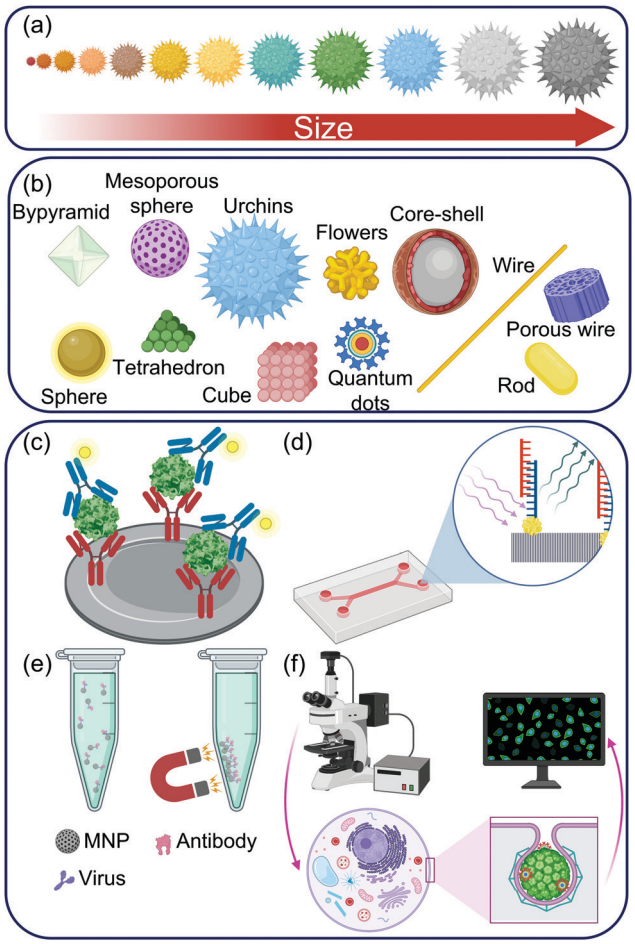

Fig. 9 (a) A hypothetical example of size-dependent variations in the color of inorganic nanomaterials; (b) various shapes of inorganic nanomaterials commonly used in virus sensing and imaging; (c–f) the diverging role of inorganic nanomaterials: (c) as labels in a sandwich assay; (d) as signal amplification tags in a microfluidic optical sensor; (e) for the enrichment of captured virus conjugates; (f) as fluorescent reporters during virus internalization in a host. Abbreviation: MNP: magnetic nanoparticle.

as rods[211] and all these shapes have been harnessed for virus recognition. These nanomaterials can act as transducers,[212] substrates for receptor immobilization,[213] target capture probes,[214] fluorophores,[215] signal amplification tags,[216] and as a part of labels in sandwich assays.[217] Additionally, nanoparticles with magnetic characteristics can also be used to enrich viral assays and enable ultrasensitive detection.[218] Some inorganic nanomaterials show exceptional fluorescent properties and can be used for tracking single virus particles.[96]

3.1 Virus sensing

3.1.1 Gold nanoparticles. Noble metal nanoparticles possess remarkable plasmonic, catalytic, and electronic properties.[199,219] They are capable of interacting with a variety of biomolecules such as oligonucleotides, aptamers, and antibodies.[220–223] Nanomaterials such as AuNPs are biologically inert making them suitable for protein immobilization without the threat of denaturation. Therefore, AuNPs are the most ubiquitous inorganic nanomaterial used for detecting viruses[170,224–229] especially the recent SARS-CoV-2.[230–233] Owing to their high energy valence electrons, AuNPs can intensively amplify electrochemical[234–236] and optical[144,237,238] signals and are frequently used as amplification tags. Mass spectroscopy using AuNPs (13.3 nm) is free from unknown ions and background noise which makes it suitable for single as well as multiplex viral immunoassays.[239] They are especially suited for POCT applications since they are compatible with paper-based,[240] smartphone-based[241,242] as well as lab-on-a-chip[243] sensors. For example, AuNP-assisted LFA strips have recently been developed for the rapid (15 min) detection of SARS-CoV-2 which requires only 10–20 μL of serum.[244] Similar lateral flow strips have also been developed along with colorimetric detection of Tamiflu-resistant H1N1 strains down to 10^4 PFU mL^{-1} (Fig. 10).[243] Tamiflu is an antiviral medication generically known as oseltamivir and resistance to it is particularly concerning in patients with haematologic malignancies. The sensitivity increases 1000-fold when colorimetric visual detection is replaced with the more sophisticated surface-enhanced Raman spectroscopy (SERS).[245] The limit of detection could be reduced down to 1 PFU mL^{-1} by increasing the size of AuNPs from 12 nm to 60 nm in the SERS assay[194] since the AuNP-catalyzed signal transduction is a function of particle size. Another reason to optimize the particle size is to ensure maximum loading of receptor molecules.[246,247] AuNP-based aptasensors have also been developed for POCT applications by shrimp farmers to detect white spot syndrome virus.[223] Although the aptasensors showed lesser sensitivity than the gold-standard PCR, their colorimetric response simplifies virus recognition in the field.

AuNPs have also been incorporated into real-time reverse transcription PCR (nanoPCR) for the detection of foot-and-mouth disease virus which allowed the reduction of threshold cycles to 4.09 from 7.03 which was the value in the case of conventional PCR.[246] Furthermore, the LOD towards the virus improved nearly 1000-fold due to the addition of GO-AuNP nanocomposites to a typical PCR system.[248] NanoPCR shows 10 times higher sensitivity in half the annealing time to bovine respiratory syncytial virus in comparison to conventional PCR.[249] This type of PCR can also be combined with dual-priming oligonucleotides to enable the multiplexed detection of bovine rotavirus, parvovirus and viral diarrhea virus with a 100-fold higher sensitivity than the typical PCR method.[250] These 3 viruses constitute the 3 most important pathogens responsible for diarrhea in new-born calves. NanoPCR is also a promising tool for differentiation between different porcine circovirus gentoypes.[251] Porcine circoviruses are responsible for the most destructive infections affecting the pig farming industry causing multisystemic wasting syndrome. Recently, the contribution of AuNP dimensions and interparticle spacing for surface plasmon resonance (SPR) sandwich immunoassay of SARS-CoV-2 was investigated.[201] Gold nanorods (AuNRs) with a diameter of 10 nm and varying aspect ratios (1–4) were used as labels due to the sensitivity of their longitudinal plasmon

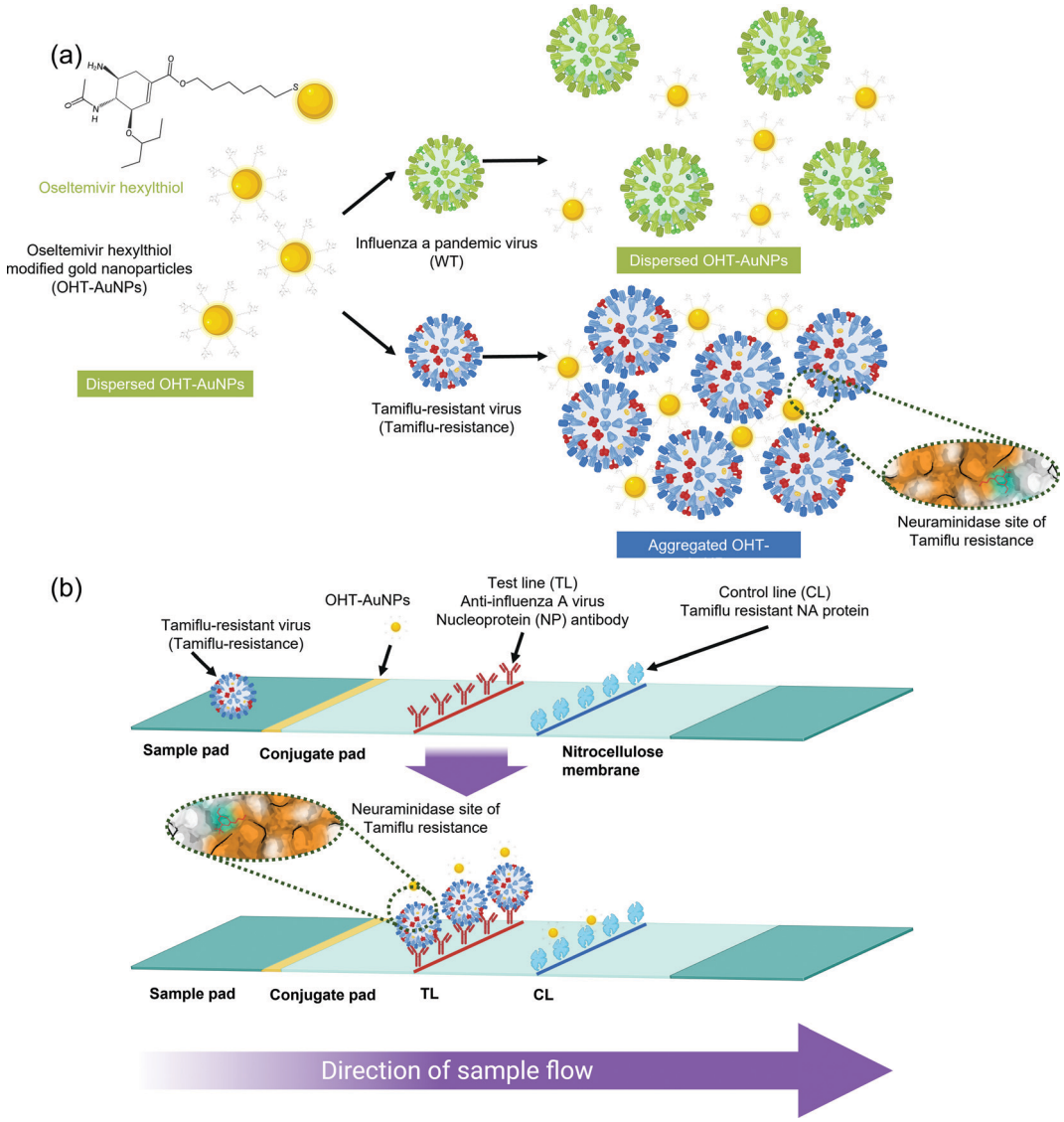

Fig. 10 Schematic illustrations of the AuNP-assisted detection of Tamiflu-resistant influenza virus using (a) colorimetric and (b) lateral-flow assays.[243] https://doi.org/10.1038/s41598-018-31311-x. Used under Creative Commons CC BY 4.0 https://creativecommons.org/licenses/by/4.0/.

bands to small changes in the refractive index. A 50 nm thick gold nanosheet acted as the sensing platform and the distance between AuNRs and the gold nanosheet was varied from 2–14 nm. At an aspect ratio of 4 with a distance of 14 nm, maximum plasmon enhancement was reported and incremental sensitivity of 111.11° RIU^{-1} was achieved. Furthermore, the optimized AuNRs enhanced the evanescent field of the basic gold nanosheet by more than 376%.[201] Such virus sensors have been reported to show tremendous improvement over rapid immunoassays (up to 240 000-fold[252]) due to nanostructure mediated LSPR.[253–256]

In addition to their size, the shape of AuNPs also determines their sensing performance.[257,258] Gold nanocubes (70–140 nm) have a higher surface area than most other morphologies and therefore produce a strong electrochemical signal.[240] Hexagonal AuNPs (30 nm) act as catalysts for tetramethylbenzidine oxidation by H_2O_2.[259] Gold nanocoils (thickness: 200 nm; length: 392 nm) can be functionalized with antibody fragments and coupled with magnetic nanoparticles (MNPs) to facilitate inductive transduction.[260] The superior electron transfer capabilities of nanowires (diameter: 50–70 nm) made with AuNP (6–14 nm) decorated polyaniline is responsible for the high stability of impedimetric sensors for hepatitis E virus (HEV) and white spot syndrome virus.[168] Similar stability is displayed by GQD conjugated gold nanobundles (length: 700 nm; diameter 10 nm) in addition to exceptional optical confinement properties.[261] Gold nanospheres (80 nm) decorated on an excessively tilted fiber grafting exhibit intrinsic LSPR.[262] They magnify the effect of refractive index fluctuations on the core to co-propagating cladding and introduce the bioaffinity necessary for antibody conjugation. Gold nanobipyramids used in colorimetric sensors as substrates for silver deposition change

color depending on the silver film thickness due to virus concentration-induced silver reduction.[208] Chiral gold nanostars (spike length 10 nm; diameter 2 nm) allow the fabrication of circular dichroism-based sensors which show superior sensitivity in comparison to ELISA and commercial diagnostic kits.[263] Similarly, gold nanofilms and nanosheets also enhance sensitivity due to the presence of multiple edges and corners that act as active sites.[264,265] Nanoporous gold electrodes amplify the electrochemical response as well as encourage the covalent binding of probes to reduce baseline current signals.[266,267] This concept can be integrated into PCR-based amplification to reduce the number of reaction cycles.[267]

The concentration of AuNPs is another critical parameter that must be optimized as a higher concentration increases not only the color intensity[241] but also the possibility of nanoparticle agglomeration.[268] Functionalizing the AuNPs with oligonucleotide can protect the AuNPs from aggregating with the help of the electrostatic attractions between the negatively charged nanoparticles and the positively charged nucleobases.[269,270] In such genosensors, the nucleotides form an electric double layer with the negatively charged backbone phosphate groups exposed to repel other similar ssDNA–AuNP assemblies. Although not as sensitive as PCR, such assemblies facilitate naked eye detection in clinically relevant virus concentration range.[269] AuNPs with peptide functionalities also tend to form large agglomerates. Such aggregates can be subjected to explosive enzymatic catalysis to observe an enhanced hypsochromic shift proportional to the concentration of the target virus (Fig. 11).[271] AuNPs (15 ± 0.4 nm) can themselves be used as beacons to induce virus aggregation in 3-(4,5-dimethylthiazol-2-yl)-2,5-diphenyl-2*H*-tetrazolium bromide (MTT) assays.[272] Due to their biocompatibility, they are suitable for application in enzymatic biosensors as immobilization substrates.[266,273] Elemental gold can directly bond with sulfur making AuNPs ideal candidates for immobilization of thiol-activated nucleotides[274–276] and cysteine-rich proteins.[273,277] Therefore, AuNP-based DNA sensors are capable of femtomolar detection with simultaneous virus serotyping.[172,200,278] Since they possess peroxidase-like properties, they are also used as a durable and lucrative substitute to enzymes in virus sensing assemblies that rely on signal amplification *via* hydrogen peroxide reduction.[279–281]

Chemically functionalized AuNPs are emerging as a popular class of AuNPs due to their tailor-made sensing characteristics. AuNP@spherical nucleic acid core–shell assemblies enable the synthesis of reversible self-assembled structures for the picomolar quantification of HIV DNA.[282] Sialic acid-functionalized AuNPs (~20 nm) undergo target specific agglomeration due to the specific binding of the sialic acid receptor with hemagglutinin from the influenza virus.[283,284] The intrinsic properties

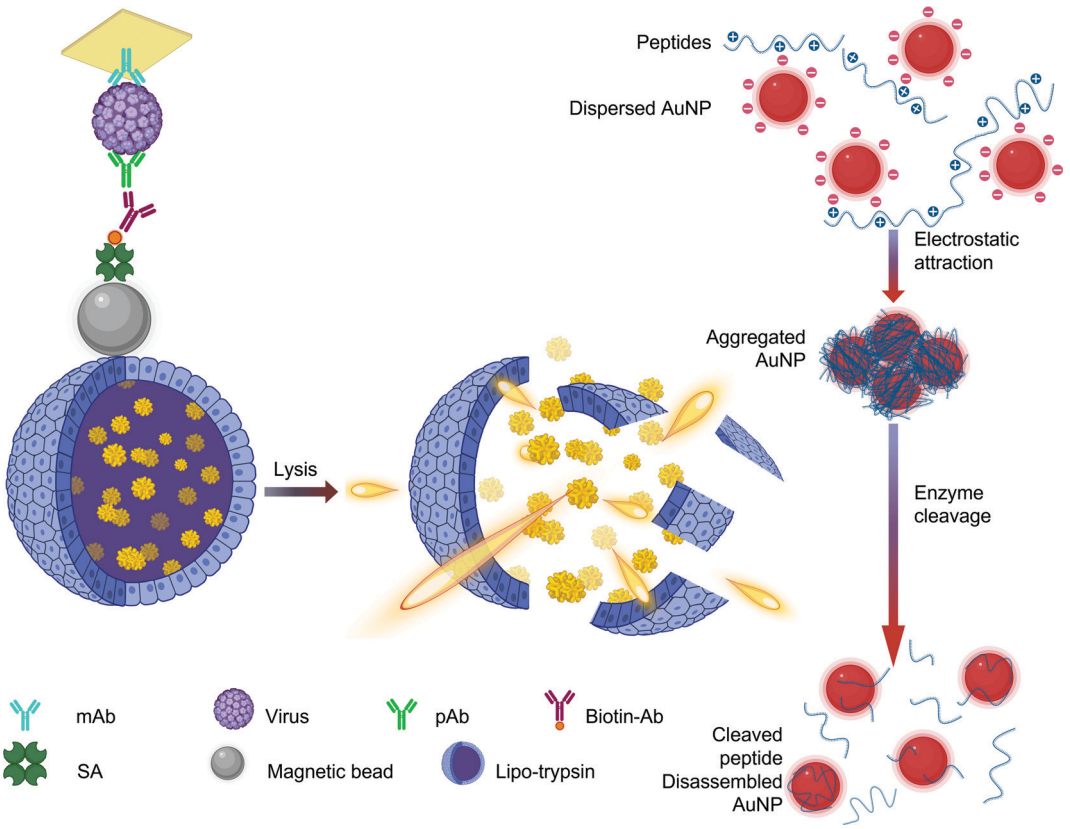

Fig. 11 Scheme for explosive catalysis of gold nanoaggregates for virus detection.[271] Abbreviations: Ab: antibody; AuNP: gold nanoparticles; mAb: monoclonal antibody; pAb: polyclonal antibody; SA: streptavidin. Reprinted with permission from (*ACS Appl. Mater. Interfaces* 2020, **12**, 11, 12525–12532). Copyright (2020) American Chemical Society.

of AuNPs can be further supplemented with other nanomaterials to generate nanohybrids with extraordinary characteristics. For example, AuNP decorated graphitized carbon nitride enhances the permeability of charge transfer[285] as well as photocurrent due to its crystalline structure and superior adsorption. Furthermore, AuNPs provide additional active sites thus facilitating ultrasensitive detection.[286,287] Nanocomposites of AuNP and covalent organic frameworks (COFs) act as biocompatible quenchers for fluorescently labeled DNA and are suitable for *in vitro* and intracellular sensing.[288] Different types of QDs are also common components of AuNP nanocomposites. This is because AuNPs can be employed to modulate their fluorescence.[255] Fluorescent sensors using such nanocomposites have displayed 100-fold higher sensitivity than ELISA.[253] Silica coated AuNR@CdSeTe QD core–shell assemblies show biocompatibility, low toxicity as well as high scattering efficiency and can be functionalized with molecular beacons for the acute recognition of as low as 1.2 copies mL^{-1} of norovirus (NoV) RNA.[289] Norovirus infection is the most prevalent cause of pathogenic gastroenteritis involving abdominal ache, emesis, and diarrhea. The distance between QDs and AuNPs makes it possible to regulate the plasmon resonance and induce high sensitivity to fluctuations in the refractive index of the surrounding medium.[200,253,255,289] It is critical for such ultrasensitive platforms to have negligible background noise to enable precise quantification. An increasingly popular technique to eliminate noise is to add MNPs or magnetic microbeads to enable the selective enrichment of the receptor-target assembly from complex media such as serum, urine, or saliva by applying a magnetic field.[238,273,275,290] Due to the chemiluminescent features of such AuNP nanohybrids, attomolar sensitivity with a broad HTLV detection range of 8 orders of magnitude could be achieved in diluted serum.[291] Such sensors exhibit superior tolerance than quantitative PCR in human cells and hold potential for *in vivo* applications.

3.1.2 Magnetic nanoparticles. Various iron compounds such as Fe_2O_3 and Fe_3O_4 are superparamagnetic at particle size below 1000 nm.[79,83] These MNPs can act as transducers, catalysts as well as complexing agents for magnetic enrichment.[292–298] Since interferents and non-specific molecules in complex biological media are nonmagnetic in nature, virus detection with magnetic sensors is significantly more sensitive than optical and electrochemical techniques.[299] Therefore, several promising techniques such as giant magnetoresistance (GMR),[300,301] magnetic particle spectroscopy (MPS),[302,303] magnetic inductance,[260] and magnetic tunneling junction[304,305] are being explored for virus recognition. Streptavidin functionalized magnetic beads (50 nm) consisting of clusters of 8 nm-sized α-Fe_2O_3 and Fe_3O_4 nanoparticles can be coupled with biotinylated antibodies to develop rapid (response time: 4 min) affordable (6 $ per chip) GMR chips for H1N1 detection in swine nasal swabs down to 250 $TCID_{50}$ mL^{-1}.[300] MPS biosensors are even cheaper than GMR biosensors due to the self-assembly of MNPs although both are suitable for POCT. In MPS, the spectrum of the MNPs (25 nm) changes from higher to lower harmonics in the presence of the target molecules enabling nanomolar detection within 10 seconds.[303] When bionized nanoferrite particles (80 nm) are used to replace these MNPs in MPS-based sensors, 5.9 fmoles of SARS-CoV-2 can be detected within 10 minutes.[302] Bionized nanoferrite particles are nanocomposites with magnetite cores enveloped in a dextran shell. In recent years, similar sensitivities have also been reported with magnetic tunneling junction sensors which are compatible with electronic, microfluidic, and multiplexed systems.[304]

The magnetic nature of MNPs is usually harnessed by using them to capture target molecules and then isolating such complexes under a mild magnetic field. For example, protamine-coated MNPs can be used to concentrate HAV from mussels, strawberries and green onions prior to real-time PCR.[297] The particle size is a function of the method with which the MNPs were synthesized. The use of MNPs in electrochemical, optical, and conventional viral assays is therefore subject to fulfilling the following requirements: their size should never be so large that the colloidal stability is lost during sensing; they must be non-toxic and compatible with the testing matrix; the particles must retain sufficient saturation magnetization to allow their motion without the need for powerful magnets.[79,83] For example, magnetic nanocubes enable the magnetic isolation and concentration of viruses in chronoamperometric immunoassays and reduce the response time to just 160 s.[306] Very high serum recovery was observed when δ-FeOOH induced magnetic separation is supplemented with exonuclease III amplification.[307] MNPs are compatible with a wide array of detection mechanisms as well nanomaterials and their sensing performance can be modulated to suit the required application easily. NoV immunosensors using identically sized MNPs show a higher LOD for electrical resistance measurements (1.16 pg mL^{-1})[308] than DPV (4.1 fg mL^{-1}) and colorimetry (340 fg mL^{-1})[309] since each detection mechanism interacts with MNPs differently. Even when the detection mechanism, sensing medium as well as size is kept constant, MNP nanocomposites show greater sensitivity with QDs (69 NoV RNA copies mL^{-1})[197] than AuNPs (84 NoV RNA copies mL^{-1})[254] and liposomes (136 NoV RNA copies mL^{-1}) (Fig. 12).[187] The synergic effect of MNPs and fluorescent polymer nanoparticles in flow cytometry allows the detection of 100 fold lower concentrations of DenV than polymer nanoparticles alone.[310]

Core–shell morphologies constitute the most common class of MNP nanocomposites. MNPs can act as supports for depositing different types of nanomaterials.[127,192,311,312] MNP cores can be subjected to surface imprinting with whole virus templates to fabricate resonance light scattering (RLS) biosensors capable of picomolar quantification.[311,313] MNP morphology plays a key role in such systems as the response time reduces by more than 7-fold when diamond-shaped particles[313] are replaced with nanospheres.[311] MNP supported noble metal shells are suitable for developing user-friendly lateral flow immunoassays[312] and paper-based genosensors.[240] MNP supports can also act as seeds for growing carbosilane dendrimers[314] as well as silica nanoshells.[192] The layer-by-layer deposition of γ-Fe_2O_3 (320–370 nm) and CdSe/ZnS QDs (7–15 nm) on poly(styrene/acrylamide) copolymer nanospheres generates fluorescent

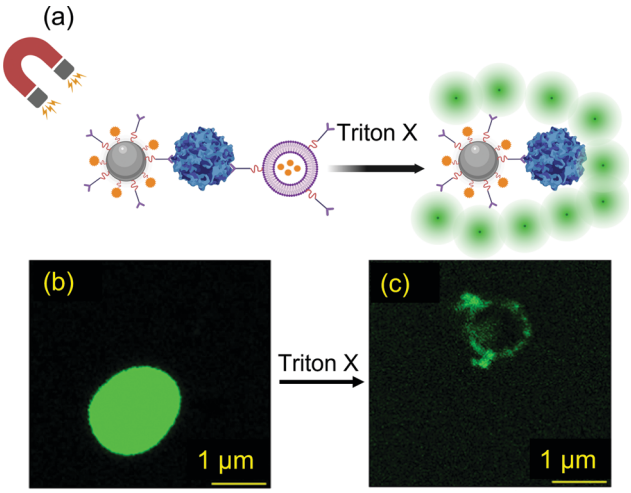

Fig. 12 (a) Schematic illustration of norovirus detection using antibody functionalized SiO_2@magnetic nanoparticles based on liposome rupture using Triton X to release calcein fluorophore; confocal microscopic images of virus bound nanoassemblies (b) before and (c) after fluorophore release.[187] Reprinted with permission from (*ACS Appl. Bio Mater.* 2020, **3**, 6, 3560–3568). Copyright (2020) American Chemical Society.

magnetic catalytic nanoparticles. These catalytic nanoparticles amplify fluorescence as well as electrochemical signals 4-fold more than commercial gold substrates[315] and enable multiplex detection of various influenza viruses in chicken blood.[316] Owing to their excellent catalysis, MNPs have also been employed to accelerate the recognition reactions involved in electrochemiluminescence,[317] rolling circle amplification,[318] RLS,[311] and ELISA.[314]

3.1.3 Quantum dots. Inorganic QDs are made of semiconductors or metallic alloys with an optional metal chalcogenide outer layer and measure only a few nanometers in size. The size of QDs is of the same order as the exciton Bohr radius due to which electron bands in a QD exist in the form of discrete energy levels.[319] When high-energy electrons of QD relax into holes, they emit electromagnetic radiation in the NIR or UV region of the electromagnetic spectrum.[320] This energy gradient is responsible for the attractive properties of QDs such as Stokes shift in fluorescent sensors[321–324] or photocurrent in photoelectrochemical (PEC) sensors.[286,287,325] Such a Stokes shift enhances the signal to noise ratio which in turn enables high luminescence that can allow the detection of the highly infectious NoV at very low concentrations (4.3×10^5 particles mL^{-1}).[326] Fluorescence may also be induced when other plasmonic nanoparticles are present in the immediate environment of the QDs by SPR.[253,327] Therefore, QD nanocomposites with aminated GO allow SPR detection of DenV with high sensitivity (5.49° nM^{-1}) and affinity (K_d: 486.54 nM^{-1}).[327] The quantum tunneling and confinement behaviour in addition to the coulomb blockade present in quantum dots results in extraordinary charging response to alternating potential which can be exploited to develop SARS-CoV-2 sensors which can differentiate between normal and patient samples with nearly 90% accuracy.[328]

QDs form stable links with antibodies *via* EDC–NHS chemistry.[254] For example, CdTe QD (3.1 nm) immunoconjugates show no loss in activity even after 4 months and are capable of ZikV sensing at 100-fold lower concentrations than required for an immune response.[321] They are excellent FRET acceptors[329] and fluorescence enhancers.[322,330] CdTe/ZnS QD nanoprobes employed in FRET-based COVID-19 detection confirm the results of PCR, thus presenting a convenient and cheaper alternative.[324] CdTe QD decorations impart fluorescence to MIPs which can simultaneously detect hepatitis A virus (HAV) and HBV within 20 minutes due to virus-induced quenching.[330] Zinc-doped CdTe QDs can act as supports for the immobilization of black-hole quenchers to inhibit overvalency and allow single-particle detection.[331] Although CdTe QDs encourage the rapid movement of photogenerated charge carriers to improve PEC probes,[286] the reproducibility improved 2-fold when cadmium-free quaternary ZnAgInS QDs (10 nm) were used instead due to higher stability of photocurrent.[287] Another popular variety of cadmium-based binary QDs, CdSe (4.4 nm), has also been used in PEC-mediated genosensors with zeptomolar sensitivity towards HTLV detection.[325] CdSe QDs are ultrasensitive fluorophores that show significantly higher signals than fluorescence dyes and commercial europium-chelates.[192,332] CdSe QD-assisted sensors show specificity against mismatched DNA sequences[332] and are capable of virus serotyping.[278] They are hydrophobic and can also modulate electrochemical signals. Recently, a sensor for the chikungunya virus was developed with CdSe QD (5–7 nm) encapsulated in a liposome and MNPs (26.5 nm) as labels.[193] The MNPs enabled magnetic separation following which chloroform triggered CdSe QD release facilitated dual-modal detection. Such sensors are particularly important in developing nations where chikungunya is often misdiagnosed as Zika fever or dengue due to similarity in symptoms.

The inclusion of additional elements in a QD can modify their intrinsic properties. For example, enhanced fluorescence is observed in sensors that include quaternary QDs such as CdSeTeS.[197,253] In addition to alloying, other techniques such as doping,[331] encapsulation,[192,333] dendronization,[88] intercalation,[316,333] *etc.* are also used to tune the properties of QDs. Therefore, cadmium-QDs are often coated with ZnS[192,332] or ZnSeS[255,278] to inhibit their cytotoxicity since the direct contact of Cd^{2+} ions with reactive oxygen species can cause cell death.[334] ZnSeS coated QDs are also useful for tuning the LSPR performance of AuNPs by modulating the interparticle distance with peptide linkers of appropriate length (Fig. 13).[255] These QDs can be supported on polystyrene nanobeads and further enveloped in SiO_2 to fabricate fluorescent reporters for LFA-assisted SARS-CoV-2 detection within 18 minutes.[192] CdS – dendrimer nanocomposites show higher recovery (100.11–100.33%) in serum for larger QDs (10.507 nm)[88] than in the case of smaller QDs (94.2–96.45%) measuring 3–4 nm.[333]

Traditionally, most QDs were cadmium-based due to their excellent photostability, bright PL, resistance to bleaching, wide excitation range in the ultraviolet spectrum, and narrow emissions.[289,335] However, recent concern over the cytotoxicity

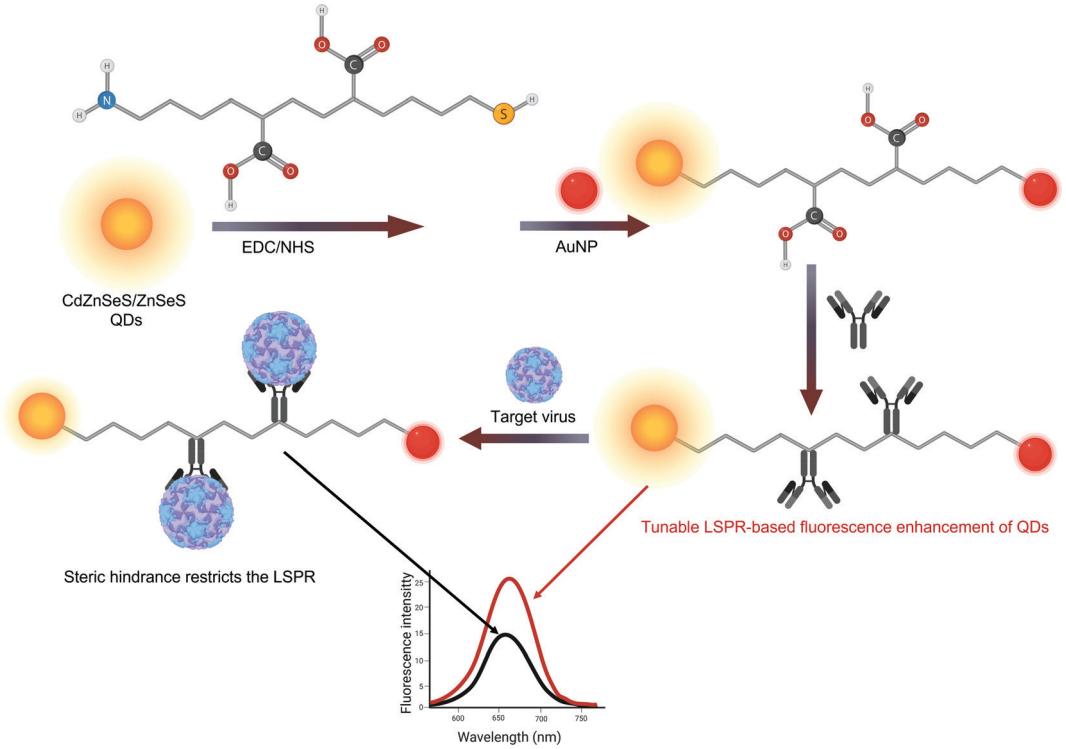

Fig. 13 Schematic representation of the synthesis of peptide-linked quantum dot nanocomposites with gold nanoparticles and their use in norovirus detection.[255]

of cadmium has been gradually shifting the trend towards cadmium-free QDs due to cytotoxicity issues.[334] Although lead quantum dots act as ideal substituents for Cd QDs,[336] additional encapsulation with biocompatible proteins is necessary to avoid toxicity issues.[337] Molybdenum QDs form an important group of cadmium-free QDs. For example, MoS_2 QDs can be used in dual mode sensors since they show chirality as well as PL-induced fluorescence.[338] MoO_3 QDs exhibit a monolayer morphology and semiconductor-based LSPR which is analogous to that of AuNPs or silver nanoparticles (AgNPs) in the NIR and visible spectrum.[339] Zirconium QDs show excellent aqueous dispersibility with blue fluorescence. They readily bind with antibodies and such immunosensors can detect as low as 79.15 EID 50 μL^{-1} of infectious bronchitis virus in blood.[198] This is the only type of coronavirus that infects chickens and the disease is extremely contagious. Kidney inflammation, respiratory distress as well as loss of internal and external egg quality include some of the most common symptoms of infection. Recently, the felicity of Si QDs for immunosensing has also been investigated for H1N1 detection.[320] However, the focus of this study was only to probe the aptitude of Si QDs as substrates for immobilization and parameters like the linear response range, LOD or affinity were not reported.

3.1.4 Silver nanoparticles. Silver nanoparticles (AgNPs), just like AuNPs, are noble metal nanoparticles that are commonly employed for virus sensing.[79,165,239,340–345] Analogous to AuNPs, the optical properties, color, and sensing behavior of AgNPs are dependent on particle dimensions due to LSPR.[170] However, AgNPs are more cost-effective as well as electroactive and have a higher extinction coefficient.[346] In a study on the fluorescence detection of HBV, more than 1500-fold improvement in sensitivity was observed after the addition of AgNPs to the sensing platform.[347] DNA molecules can be labeled with silver nanoclusters for *in vitro* and intracellular sensing.[288] Therefore, AgNPs caged in a DNA tetrahedron show a consistent performance in buffer as well as serum for colorimetric genomic sensing of HIV.[206] Colorimetric sensing has also been achieved *via* the *in situ* deposition of AgNPs using hydroquinone in the presence of AuNPs but 30% of the signal response was lost within 4 weeks.[279] The large value of the fluorescence extinction coefficient can be attributed to discrete energy bands arising from the quantum confinement of excited electrons. Since it is essential to understand the behavior of these electrons in the proximity of proteins, *in silico* modeling has been investigated as a tool for understanding and optimizing the conjugation process.[348] Ag_2S (2.5 ± 1.1 nm) nanocrystals exhibit plasmonic properties in the NIR which facilitates the fluorescence enhancement of C_3N_4 QDs.[177] However, such immunoassays show low sensitivity (100 PFU mL^{-1}) owing to poor size control.

AgNPs show exceptional SERS capacity with plasmon resonance near 500 nm and stable reproducible responses. SERS sensors made of AgNP-assisted LFA have enormous potential for POCT purposes since they are 2000 times more sensitive than standard colloidal gold strip and generate responses within 30 min (Fig. 14).[312] With the latest advancements in

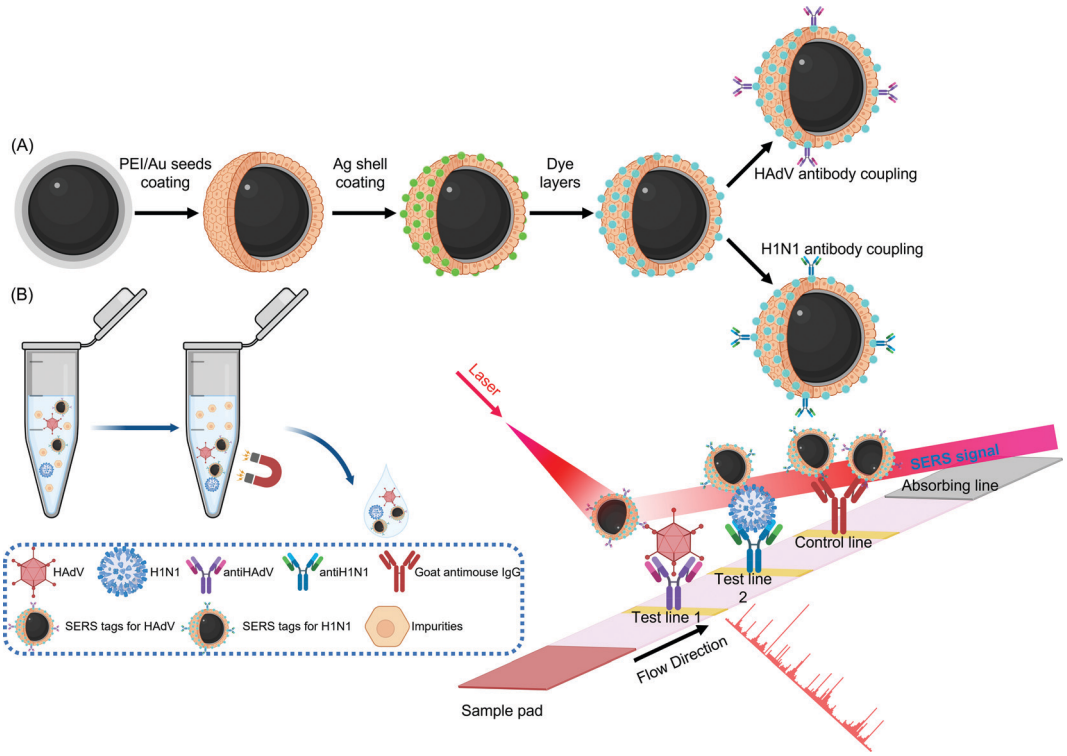

Fig. 14 Schematic illustration of (A) the synthesis of antibody functionalized AgNP SERS tags and (B) their use in a lateral flow assay for sensing respiratory viruses[312] reprinted with permission from (*ACS Appl. Mater. Interfaces* 2019, **11**, 21, 19495–19505). Copyright 2019 American Chemical Society. Abbreviations: Ag: silver; antiHAdV: antibody for human adenovirus; antiH1N1: antibody for H1N1 virus; Au: gold; HAdV: human adenovirus; IgG: immunoglobulin G; SERS: surface-enhanced Raman spectroscopy.

nanolithography, SERS sensors can be fabricated with silver nanoislands. These nanoislands (height: 6 nm; planar size: 20 nm) readily bind with thiol functionalized aptamers to detect as few as 10 virus particles in an assay time of just 12 minutes.[349] Since porous silver nanofilms synthesized using electron beam physical vapor deposition conduct SERS at their sharp edges they have been developed for size-dependent virus capture.[350] A similar non-specific capturing principle has also been adopted in terahertz spectroscopy.[188] Due to their extraordinary electroactivity, AgNP mediated electrochemical sensors display excellent agreement with ELISA.[351] Therefore, AgNPs act as direct signaling tags in voltammetric virus detection.[352,353] AgNPs are capable of improving the detection capacities of other nanomaterials. In a comparison between native AuNPs (2.7 ± 0.6 nm), Au@Ag core–shell nanoparticles (4.4 ± 0.6 nm) and alloyed Ag–AuNPs (2.9 ± 1.1 nm) for ZikV RNA detection, the respective sensitivities observed were 2.9 copies mL^{-1}, 2.4 copies mL^{-1} and 1.7 copies mL^{-1}.[256] Due to their electrochemiluminescence, highly stable AgAuPt nanocubes show high sensitivity (LOD: 65 aM) and recovery (up to 98%) in human serum samples.[354]

3.1.5 Silicon-based nanoparticles. Silicon is the most common metalloid element used in nanomaterial-assisted virus detection since it is cost-effective as well as non-toxic. Nanomaterials such as silicon nanowires (SiNWs) demonstrate a quasi 1D electronic structure and simultaneously possess high electrical conductivity and poor thermal conductivity due to their narrow cross-section. SiNWs are simple and inexpensive to synthesize and exhibit potential for miniaturization as components of nanoelectronic devices.[355] They are mass-producible and can be incorporated in ultrasensitive FET sensors (LOD: 1 fM) due to their high surface-to-volume and signal-to-noise ratios.[356] Ion-selective FET determination of viruses was achieved in the previous year by coupling the functional groups from the SiNW surface (8 nm × 120 nm × 3 μm) with the liquid gate of the sensor to obtain electrical signals.[357] The Stern layer capacitance was extracted to be 26 μF cm^{-1} and the accuracy of the neoteric method was verified with computational simulations. A major challenge in the use of SiNW for sensitive virus detection is the exponential decay of the electric field with increasing distance from the nanowire surface (Debye screening effect). Target molecules farther than the Debye length, which can be as low as 0.8 nm, cannot be registered by the SiNW. To overcome this limitation, aptamers can be used instead of antibodies as receptors because of their small size.[358] The sensitivity can be further improved up to two orders of magnitude with the help of microwave energy.[359] The charge trapping ability of SiNWs is responsible for its photoluminescent activity. Dense SiNW forests (10^{12} NW cm^{-2}) are capable of detecting 20 HBV DNA copies mL^{-1} in real samples which is equivalent to the sensitivity of quantitative PCR.[360] In p-type SiNWs (width: 20 nm; height: 30 nm) conjugated with molecular gate control, the negative charge concentrates on the surface and the resultant accumulation of charge carriers at the

perimeter enhances the electrical signal.[361] In porous SiNW arrays, virus rebinding is observed due to non-specific size-dependent penetration with the help of wavelength shifts in the Fabry – Perot fringes.[362] However, the false-negative rate (0.1 $TCID_{50}$) in such sensors should not be overlooked.[363]

Spherical silica nanoparticles (SiO_2 NPs) constitute the second most popular shape of silicon-based nanoparticles. Although SiO_2 NPs doped with organic dyes cost much less than Au, they show satisfactory signal amplification.[364] They exhibit excellent electrochemiluminescence and a 1000-fold enhancement in sensitivity is observed when SiO_2 NPs are included in the sensor. SiO_2 NPs are also suitable for loading a variety of substances ranging from small quantum dots to large enzymes.[365] For example, pomegranate-shaped SiO_2 NPs (thickness: 5 nm) show high uptake of quantum dots and they can be functionalized with antibodies for rabies lyssavirus detection.[366] Timely detection of the virus is critical since rabies is almost always fatal after the onset of its symptoms such as hydrophobia, nausea, unconsciousness. Glucose oxidase-loaded SiO_2 NPs (120 nm) have been used as supports for poly(acrylic) acid brushes that bind viral DNA.[367] Dendritic SiO_2 nanospheres loaded with red emissive CDs show up to 48.5% quantum yield in aqueous media which is auspicious for lateral flow-based ZikV detection.[166] SiO_2 NP supports can also be used for surface imprinting of viruses.[368] The SiO_2 NPs–MIP nanocomposites show more than 95% cell viability after 24 hours and are therefore ideal for *in vitro* virus detection.[369,370] Silicon nanorods[371] and fouling-based silicon nanomembranes[372] have also been recently explored for virus detection although the use of these materials is not yet common due to scarce literature in the field. Silicon nanomembranes have an advantage over PCR for SARS-CoV-2 detection since they can selectively recognize intact virions thus differentiating between diseased and recently recovered individuals.[372]

3.1.6 Other inorganic nanoparticles. Most metallic nanoparticles offer simplicity in surface modification in addition to a high surface area to volume ratio and the presence of localized surface plasmons. Depending on the element selected, several interesting features can be added to the biosensor. For example, since V_2O_5 nanoparticles possess peroxidase-like properties, they can be used as electrochemical redox mimics for dual-mode optoelectronic NoV determination (Fig. 15).[309] Hollow nanocages of $PtCo_3O_4$ possess similar redox features which can be used for chronoamperometric HEV detection based on water oxidation reaction.[207] These redox features arise from the ability of platinum nanoparticles to facilitate electron transfer resulting in an increased electrochemical response within a few seconds.[373,374] Similarly, ZnO nanoparticles also possess fast electron transfer capability as well as biological inertness and cost much less than platinum. They readily bind with concanavalin A to enable resistivity-based arbovirus discrimination.[375]

In tellurium doped ZnO nanowires (diameter: 50 nm), tellurium promotes the donor-acceptor emissions and simultaneously passivates the essential vacancy parameters due to isoelectronic doping.[376] When such nanowires are doped with molybdenum, charge transfer is promoted and vacant sites are generated for adsorbing DNA.[377] These nanowires show higher precision in comparison to PCR by demonstrating a higher sensitivity against false negatives.[377] Similar nanowires of tin oxide (diameter: 25 nm; length: 3.5 μm) have been grown for EBV genosensing.[378] The evolution of distance and time during SnO_2 growth was described with the help of Cosmol Multiphysics and the nanowires showed high stability with 95% of initial response after 8 weeks. Similar stability is also observed when tin has been used as a dopant in heteroinjected WO_3/In_2O_3 nanowire photoelectrodes.[191,379] The tin heterogeneity

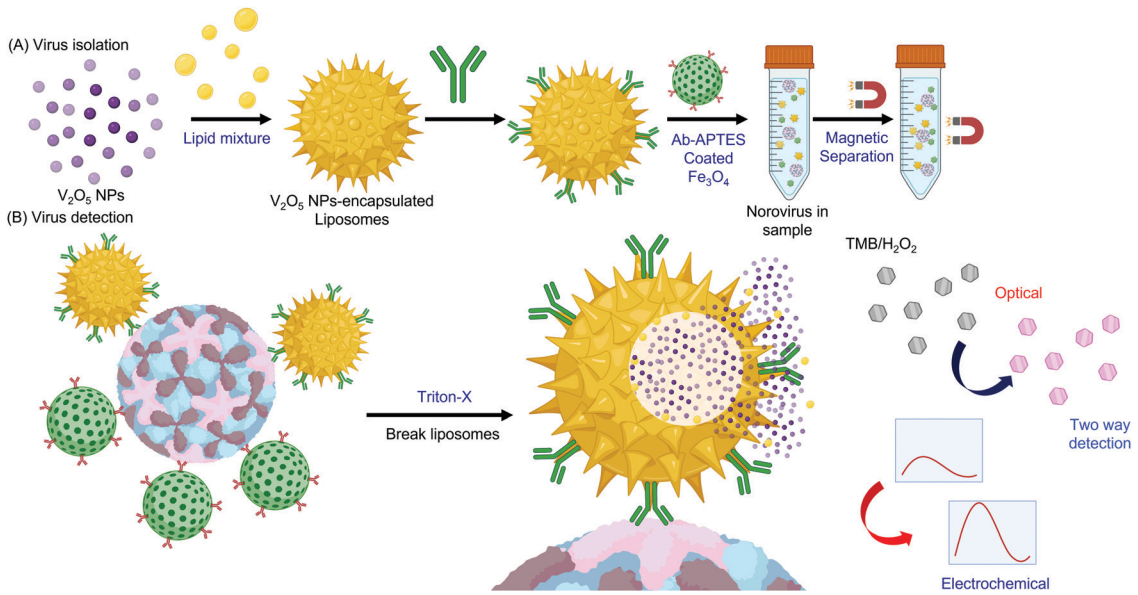

Fig. 15 Fabrication of V_2O_5 liposomes and their use in virus detection.[309] Abbreviation: Ab: antibody; APTES: aminopropyltriethoxy silane; TMB: tetramethylbenzidine.

intensified light absorption by the creation of exciton which allows a dynamic response. Due to this phenomenon, MoS_2 nanosheets increase the electrochemiluminescence of QDs from 27 000 to 76 000 (2.8 times).[190] The introduction of porosity further aids in receptor immobilization due to an increase in the surface area.[134,189]

Nanoflowers of metallic compounds offer a large surface area for nanoparticle immobilization thereby accelerating reaction kinetics and improving the carrier immobility as well as the efficacy of surface reaction.[374,380,381] Anodic aluminum oxide nanohemispheres-based impedimetric sensors show high linear correlation (R^2: 0.983) with real-time PCR detection and a low LOD of only 111 HBV DNA copieas mL^{-1}.[382] Lanthanide-based upconversion nanoparticles show comparable sensitivity to AuNPs due to the excitation of the longer wavelength of light to shorter wavelengths.[383] Recently, phosphorene has been reported as a promising substitute to SARS-CoV-2 sensing due to the tunability of its band gap. Computational simulations reveal a higher Gibb's binding energy between the receptor binding domain of the virus with phosphorene (200.37 kcal mol^{-1}) than with graphene (83.65 kcal mol^{-1}).[384] Therefore, phosphorene is expected to emerge as a promising nanomaterial for virus sensing in the future.[229] Table 2 includes a comprehensive list of various metallic nanoparticles that have been reported for the development of virus biosensors in the last half-decade.

3.2 Virus tracking

3.2.1 Quantum dots. The emission spectra of QDs are narrow and can be tuned by adjusting their size, composition, and shape. Their excitation spectra, on the other hand, are wide which is essential for multicolor imaging where the viral and cellular structures can be imaged at the same time.[86,388] Since they are up to 100 times brighter than organic fluorescent dyes, they provide high-contrast in bioimaging.[389] In nearly all QD-based virus tracking, ZnS coated CdSe QDs are used in order to avoid the toxicity of cadmium ions without compromising on the optical properties.[91] QDs are 100 to 1000-fold more photostable than organic fluorophores making them apt for tracking individual viruses for prolonged periods with excellent temporal resolution.[96,343] This tracking method, so-called single virus tracking (SVT), is an adaptation of the single-particle tracking technology and makes it possible to trace single viruses, track their transport mechanisms and understand viral interactions in host cells. SVT helps visualize the intrinsic mechanisms involved in intracellular processes while targeting each virus particle individually instead of relying on ensemble averages. SVT allows the *in situ* study of dynamic viral behavior inside living cells in real-time.[390,391] Ever since the first use of QD as labels for single lentiviruses was proposed in 2008, the prevalence of QDs in SVT has been growing tremendously.[392]

Table 2 Inorganic nanomaterials for virus detection

Nanomaterial	Size (nm)	Receptor	Virus	Method	LOD	Ref.
Pt NP	3.9 ± 0.5	Ab	ZikV	EIS	10 virus particles μL^{-1}	373
V_2O_5 NP	25 ± 1.5	Ab	NoV	CM; DPV	340 fg mL^{-1}; 4.1 fg mL^{-1}	309
Pt-Co_3O_4 HNC	4–5[a]; 250, 400[b]	Ab	HEV	CA	61 RNA copies mL^{-1}	207
Pt-Pd NF; ZnO NP	200[c]	DNA	DenV	CV/DPV	43 μM	374
PtAgAu NC	100 ± 5	DNA	HBV	ECL	65 aM	354
$NiCo_2O_4$ UANW	8[d]	Ap	HCV	EIS	160 ag mL^{-1}	189
MoS_2 NS; S-BN QDs	7[e]	DNA	HCV	ECL	170 fM	190
UCNP	30[f]; 45[g]	Ab	H5N2 H5N6	NNLFA	10^2 EID_{50} mL^{-1} $10^{3.5}$ EID_{50} mL^{-1}	383
ZnO NR	300[h]; ~2000[i]	Ab	H5N2	CM	8×10^3 EID_{50} mL^{-1}	385
$Cu_3(PO_4)_2$-GO NF	8000	Ap	HBV	DPV	1100 copies mL^{-1}	380
SnO_2 NW	25[h]; 3500[i]	DNA	EBV	DVM	3.2 pM	378
Te-ZnO NW	50[h]	DNA	HBV	EIS	100 fM	376
Sn-WO_3/In_2O_3 NW	50[h]	DNA	HBV	EIS	1 fM	379
WS_2 NF	50–180[j]; 500–800[k]; 4000–5000	NSP	NoV	EIS	2.37[l]/6.21[m] copies mL^{-1}	381
ZnO NR	260[i]	Ab	HCV	CV	0.25 mg mL^{-1}	386
$NiCo_2O_4$@CNT	—	DNA	HIV	EIS	16.7 fM	134
Al–Mo NCM	10[n]	Ab	BHV	LI	90 μg mL^{-1}	387
AAONH	100	DNA	HBV	EIS	111 copies mL^{-1}	382
ITONW	50[h]	DNA	HBV	FET	1 fM	191
Se NP	42	Ab	HIV	SERS	—	258
ZnO NP	—	ConA	ArV	EIS	0.038–0.062 PFU mL^{-1}	375

[a] PtNP dimensions. [b] Nanocage dimensions. [c] Nanocomposite film thickness. [d] Pore size. [e] Diameter of quantum dots. [f] Core size. [g] Total size including shell. [h] Diameter. [i] Length. [j] Petal width. [k] Petal length. [l] LOD in spiked sample. [m] LOD in infected oyster. [n] Thickness. Abbreviations: AAONH: anodic aluminum oxide nanohemisphere; Ab: antibody; Al–Mo NCM: aluminum-molybdenum nanocomposite membrane; Ap: aptamer: ArV: arbovirus; BHV: bovine herpes virus; CA: ahronoamperometry; CM: colorimetry; CNT: carbon nanotube; ConA: conconavalin A; CV: cyclic voltammetry; DenV: dengue virus; DNA: deoxyribonucleic acid; DPV: differential pulse voltammetry; DVM: differential voltage measurement; EBV: ebola virus; ECL: electrochemiluminescence; EIS: electrochemical impedance spectroscopy; FET: field-effect transistor; GO: graphene oxide; HBV: hepatitis B virus; HCV: hepatitis C virus; HEV: hepatitis E virus; HIV: human immunodeficiency virus; HNC: hollow nanocages; ITONW: indium tin oxide nanowire; LI: laser interferometry; LOD: limit of detection; NC: nanocubes; NF: nanoflowers; NNLFA: near-infrared to near-infrared lateral flow assay; NP: nanoparticles; NR: nanorod; NS: nanosheet; NSP: norovirus-specific peptide; NW: nanowire; S-BN QD: sulfur-doped boron nitrogen dots; UCNP: $NaYF_4$:Yb,Tm@$NaYF_4$:Ca up-conversion nanoparticles ZikV: Zika virus.

The significance of QDs as labels for virus imaging can be attributed to the preservation of more than 90% viral infectivity that is observed in the case of single as well as dual-labeling.[393] QD-based SVT has facilitated the understanding of virus infection mechanisms such as virus uncoating, replication, and transport of virus from the extracellular region to the cytoplasm. For example, the uncoating of HIV was recently investigated by labeling the RNA with a red Zn^{2+} doped CdTe QD and the capsid with a green organoarsenic dye as shown in Fig. 16A.[331] In this work, the QDs were initially functionalized with DNA that adopted a stem-loop hairpin structure. After entering the TZM-bI cells, the DNA hybridization caused fluorescence recovery. The poor productive infection of the HIV stocks was further established when only 27 dissociations were recorded in 120 minutes from the 30 000 viruses that were tracked.[331] The combination of QDs with varying emission spectra encourages site-specific labeling of the ribonucleoprotein complex and helps visualize the uncoating process.[86] In a similar study on the internalization of *Dabie bandavirus* which is responsible for causing severe fever with thrombocytopenia syndrome in humans, it was discovered that the rate of membrane fusion was pH-dependent.[388] In this case, multicolor imaging of streptavidin functionalized QDs attached to biotinylated viruses revealed a clathrin-mediated virus transport pathway from the cell periphery to the interior. Since the lipid-specific labeling with QDs preserves native viral infectivity, SVT demonstrates a slow peripheral movement through a dense actin network followed by rapid transport of viral load along microtubules.[394] QD-based confocal imaging revealed that viruses hijack this endosomal sorting complex required for transport machinery and induce a "driver switchover" between the retrograde molecular motor proteins myosin VI and dynein.[395] CdSe@ZnS QDs (8.83 ± 0.8 nm) have been used in conjunction with an inverted microscope with a confocal scanning system to interrogate respiratory syncytial virus-induced endocytosis in Hep-2 cells.[396] The so called "orthopneumovirus" is responsible for bronchiolitis and pneumonia affecting all age groups.[397] For such enveloped viruses, the endocytosis commenced with extensive lipid shifts and culminated with the entry into lysozymes within the perinuclear region. The dependence of such a viral entry on both actins and micropinocytosis was discovered by SVT with QD-Cas9/gRNA complex.[398]

In addition to the common clathrin-mediated viral trafficking pathway, QDs have also been used in SVT for the real-time monitoring of virus internalization *via* clathrin-independent dynamin-dependent internalization (Fig. 16B and C),[399] Rab5 endosomal route as well as autophagy.[400] QDs have also been employed for observing other critical parameters of a viral infection such as their replication kinetics[398] as well as for calculating the intracellular motility.[401] Recently it was reported that certain reoviruses cross the intracellular membrane in 14.8 s and travel through the endosome-lysosome system for sorting and trafficking.[402] This concept was subsequently applied to antiviral drug screening for non-enveloped viruses. Multicolor QDs at dilute concentrations do not exhibit cytotoxicity and

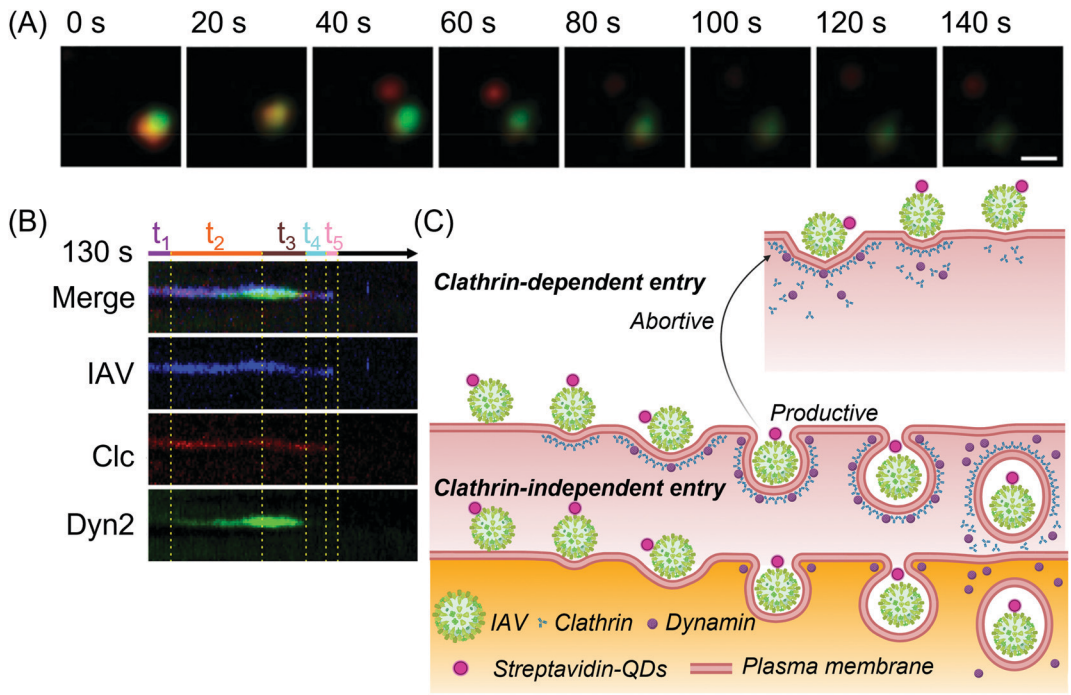

Fig. 16 (A) Fluorescent imaging of the uncoating of the QD-labeled HIV-RNA (green) from its capsid (red)[331] adapted with permission from (*J. Am. Chem. Soc.* 2019, **141**, 34, 13454–13458). Copyright 2019 American Chemical Society. (B) Kymographs of phase-wise clathrin-dependent and independent virus entry and (C) the schematic representation of the proposed internalization mechanism[399] reprinted with permission from (*ACS Nano* 2017, **11**, 5, 4395–4406). Copyright 2017 American Chemical Society. Abbreviations: Clc: clathrin light chains; Dyn2: dynamin 2; QDs: quantum dots; t_1: initiation stage; t_2: dynamin assembly stage; t_3: dynamin disassembly stage; t_4: clathrin disassembly stage; t_5: predirected stage.

they readily undergo budding with viral glycoproteins. Such spontaneous labeling can be used to understand the self-assembly of intraviral components.[403] QD-based SVT also shows potential for differentiating between healthy and disease states in cells. Therefore, the transcription activator-like effectors of the HIV-1 provirus genomic loci can be conjugated with 2 QDs of different emission maxima to induce biorthogonal ligature reactions.[404] These reactions illuminate the mechanism of individual genomic loci regulation as well as their functions within the genomic architecture thus elucidating the virus replication cycle which is a prerequisite for developing antiviral drugs.

3.2.2 Metallic nanoparticles. Metal nanoparticles and nanoclusters such as AuNPs, AgNPs, and MNPs have also been used for the labeling of viruses. Nanomaterials like AuNPs show high stability since they do not biodegrade or photobleach.[405–408] In addition to their extraordinary plasmonic properties, metallic nanoparticles strongly scatter incident light.[409] These signals can be recorded by microscopic techniques that exclude unscattered light from the recorded image.[96,343] Based on this type of scattering, a mixture of AuNPs (5 nm and 50 nm) has been used to study the midgut dissemination of flaviviruses such as ZikV and DenV after blood-meal digestion in mosquito.[87] In this case, the scattered signals were recorded with a scanning electron microscope and scanning transmission electron microscope. AuNPs (100 nm) are also useful in evaluating the amount of force exerted between adherent cells and viruses during uptake.[410] Due to the nano-metal surface energy transfer exhibited by AuNP, their quenching ability can be imaged with the help of time-lapse total internal reflection fluorescence in HeLa cells. Since AuNPs are capable of imaging and their size distribution can be rationally regulated unlike VLPs, membrane-wrapped AuNPs can be used to synthesize artificial virus nanoparticles (AVN) that facilitate the investigation of lipid-mediated viral entry pathway. AuNP-based AVNs provide a non-blinking cross-section. These AVNs help perceive the roles of monosialodihexosylganglioside and phosphatidyl serine in the localization of HIV in tetherin^{+} and CD9^{+} cells with the help of wide-field and confocal microscopy.[411]

The aggregation of AuNPs from 47.4 $\pm$ 0.8 nm particles to 300.1 $\pm$ 198.3 nm clusters enhances the fluorescence intensity enabling the detection of HBV.[347] Such an enhancement is also observed when MNP@AgNP core–shell nanocomposites are bound to fluorescently labeled antibodies.[312] MNPs are also employed in multiplex detection of different influenza virus species using fluorescence imaging.[316] Virus stamping is one of the most interesting applications of MNPs in virus imaging.[412] It is a strategy to introduce virus infection in single cells which shows high efficacy and compatibility with *in vitro*, *ex vivo*, and *in vivo* diagnostics using 2 photon-assisted shadow imaging. Although metallic nanoparticles show promise for virus imaging, the difficulty in sensing multiple species and the scarce availability of several labels are the two primary obstacles that should be overcome to allow widespread applications since their first recorded use for SVT in 2014.[96,413]

4. Organic nanomaterials in virus sensing and tracking

Organic nanomaterials used for virus recognition and tracking are customarily polymeric in nature (Fig. 17). Their synthesis is inexpensive and simple making these materials suitable for developing POCT devices. They are stable across wide temperature ranges and they readily co-ordinate with metals to form structurally detailed and porous frameworks with exceptional fluorescence which can act as substrates for receptor immobilization.[414] Organic nanomaterials can themselves be harnessed as receptors[124] or transducers[415] and are the nanomaterial of choice in optical virus sensors.[11,319,414,416,417] They possess intrinsic bioinertness as well as biocompatibility. Nanomaterials such as MIP nanoparticles (MIP-NPs) offer cost-effective alternatives to the delicate antibodies often used in virus detection.[418] Hyper-branched polymers such as dendrimers improve the conjugation between the target and the sensing platform.[88] Polymeric nanoparticles are also used in nanocomposites to tune the properties of MNPs,[310] AuNPs,[419] CNTs,[124] and QDs.[88,420] Such nanocomposites exhibit a symbiotic combination of unique morphologies with ultrasensitivity and facile fabrication processes. Such substrates effectively suppress background noise and readily bind with oligonucleotides, MIPs as well as antibodies.[285,421,422] They can also act as virus mimics in the development of sensors for highly infectious viruses.[423] Nanoparticles such as polymer dots have the capacity to replace cadmium-based quantum dots in virus sensing and imaging due to their exceptional fluorescent characteristics in addition to their biocompatibility.[424] Apart from polymeric nanoparticles, molecular machines, so called nanomotors or nanodevices, are also emerging as promising virus receptors owing to their sub-nanomolar sensitivities for label-free recognition of viral genomic material.[425]

4.1 Virus sensing

4.1.1 Organic frameworks. Organic frameworks can be broadly classified into two major subtypes: (1) COFs and (2) MOFs. COFs are porous polymeric nanostructures. They exhibit extraordinary thermal stability and low densities. However, due to the absence of high-energy electrons, they have only been used once for virus recognition. In this work, 3.5 nm COF sheets were integrated with AuNPs and Ag nanocluster-labeled DNA for HAV and HBV determination.[288] MOFs, in contrast, are the most quotidian of organic nanomaterials that are in use for virus detection.[426,427] Their surface to volume ratio is high and their pore size can be easily altered. MOFs are fundamentally coordination polymers in which the organic component links metal ions to generate intricate architectures.[90]

Biosensors use MOFs ranging from one to three dimensions or a combination of multiple varieties.[428] Although 1D zinc carboxylate MOFs are water-soluble with aromatic bipyridine peripheral ligands that facilitate nanomolar sensing, they exhibit long assay times.[429] In a comparative study on zwitterionic zinc carboxylate MOFs, it was observed that 2D MOF nanosheets interact with probe DNA more efficiently than 1D

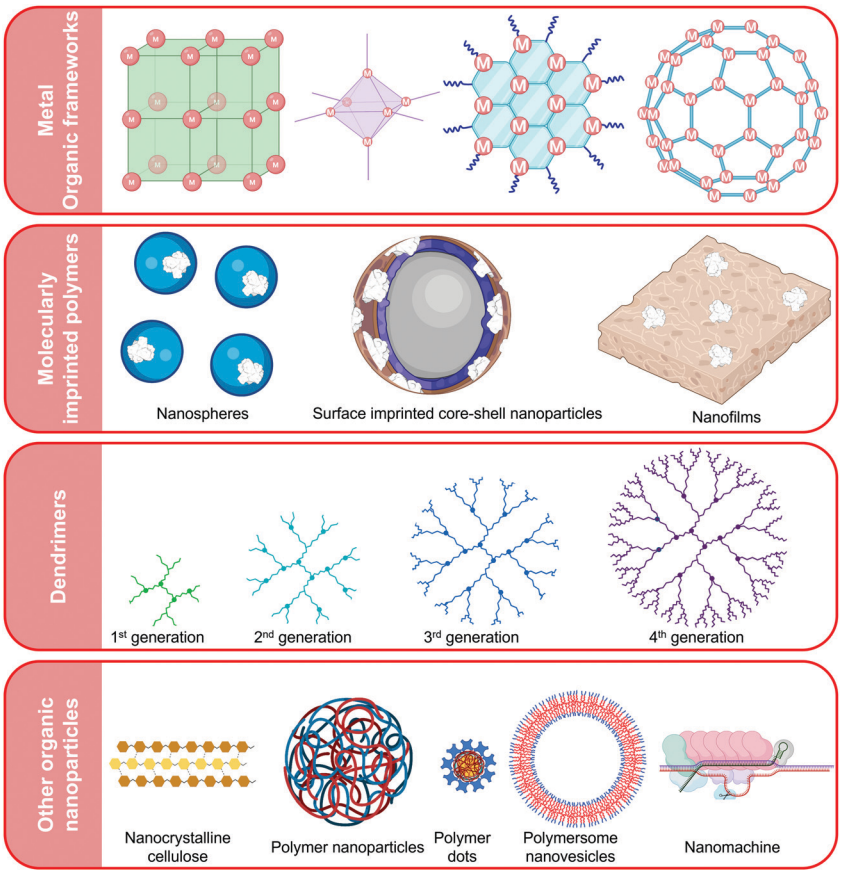

Fig. 17 Different types of organic nanomaterials used in virus detection and imaging.

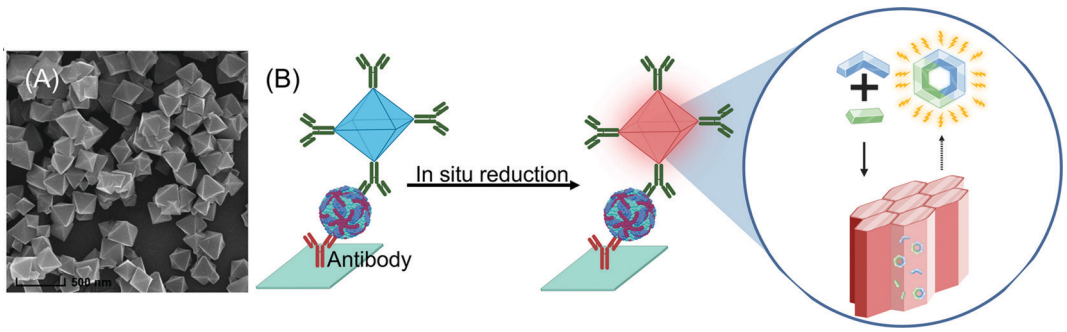

Fig. 18 (A) SEM images of copper organic frameworks; (B) copper organic frameworks as 3D nano for sensing hepatitis B virus.[431] Reprinted with permission from (*Anal. Chem.* 2020, **92**, 4, 2972–2978), Copyright 2020 American Chemical Society.

nanochains, 2D networks as well as 3D polymeric matrices.[428] The LOD was reduced by an order of magnitude when 2D copper MOFs were used.[430] 3D copper MOFs (Fig. 18A) can also be harnessed as nanoreactors for copper-mediated azide-alkyne cycloaddition "click reactions" in time-resolved fluorescence immunoassays for HBV surface antigen (Fig. 18B).[431]

MOFs readily undergo π–π stacking interactions with viral DNA in addition to hydrogen bonds and electrostatic interactions.[108,428,432–434] These interactions have also been confirmed using computational simulations and they enable the picomolar detection of Ebola RNA.[434] Such simulations are also useful for understanding the binding dynamics in the case of synchronous detection of conserved viral nucleic acid sequences.[435] In this study, the planar geometry of the 2D MOF exposed more functional groups on the surface thereby causing fluorescence quenching in the presence of nucleic acid and thus providing contrast for near-dark background fluorescence. These interactions are a function of the size of pores and channels in the framework which are responsible for the impressive loading efficiency of MOFs.[421] For example, the low symmetry from the sp^3 hybridized carbon of methylene can be compensated by metals with high coordination numbers

to form MOF networks with higher dimensions and large pores.[436] Chromium terephthalate MOFs are also used as support in surface imprinting for rapid (20 min) detection of viruses.[414,422] A neoteric morphology of zirconium-based metal-organic gel has recently been explored in a nanocomposite with iron MOF and AuNP decorated graphitized C_3N_4 for electrochemiluminescence-based ZikV sensing.[285] The zirconium nanogel promoted charge transfer owing to the 3D connectivity of its chromophores. It also fostered recombination in the energy rich excited state of carbon nitride.[285]

4.1.2 Dendrimers. Dendrimers are polymeric nanoparticles with three hierarchical constituents: (i) a medial core; (ii) intermediary layers of repeating units termed as ''generations''; (iii) exterior layer of functional groups bound to the outermost generation of the intermediary layers. They possess a globular shape with multiple functionalities on the surface which are useful for biomolecular immobilization. Therefore, a density of 3.6 pmol cm^{-2} for anti-hemagglutinin peptide can be achieved with peptide dendrimers as receptors for influenza viruses.[437] These receptors displayed an almost 80-times wider detection range than antibody-based assays. The abundance of terminal functionalities in dendrimers makes them superb carriers for DNA[438] and antibodies.[439] Since polyamidoamine (PAMAM) dendrimers promote the immobilization of antibodies in a tail-on position, such immunoassays exhibit high affinity (102 pM) and resolution (19.53 nm nM^{-1}) for the target antigen in comparison to antibodies integrated with a side-on orientation.[440]

Dendrimer nanocomposites possess interesting features such as bright fluorescence, sensitivity in complex media, and high reproducibility. The cornucopian tertiary amine groups in PAMAM introduce water solubility and chemical stability in addition to enhancing the capacity for loading QDs.[88,333,420,441] Such nanocomposites shift the resonance angle to a greater extent due to the high molecular weight of PAMAM which encourages antigen recognition.[88,420] In a recent work on the detection of HBV surface antigen, it was observed that the incorporation of PAMAM multiplied the electrochemiluminescence intensity of QDs by 3.42 folds.[333] AgCl nanosphere doped bis(hydroxymethyl)propionic acid dendrimers (4th generation) show low variability for enterovirus detection with intra-assay and inter-assay standard deviations of 4.15% and 6.15% respectively.[439] Nanocomposites of rGO and PAMAM (4th generation) are capable of transporting bioactive agents with high efficacy. SPR sensors using the nanocomposite display high affinity (K_a: 7.6452 TM^{-1}), sensitivity (0.2576° pM^{-1}) along with an ultralow LOD (80 femtomolar).[162]

In recent years, the scope of dendrimers in virus detection has expanded beyond their role as immobilization platforms and nanomaterial carriers. For example, Au–PAMAM (5th generation) nanochains are employed for the visual paper-based detection of HIV capsid-protein p24.[419] Increased levels of p24 are earlier indicators of HIV infection than the frequently targeted patient antibodies. These nanochains are 4-fold more sensitive to the target than AuNPs alone and are promising candidates in the fabrication of POCT HIV-diagnostic devices. Dendrimers derived from coumarin are excellent fluorescent materials for high output screening of viruses in human blood.[442] Lately, dendrimer-based bio-bar codes for HTLV determination have been fabricated owing to the dendritic self-assembly and signal amplification features of polythymidine (Fig. 19).[291] Carbosilane dendrimers (1st and 2nd generation) are compatible with ELISA as they provide the retentive potential to viral antibodies owing to their electrostatic attraction.[314] Such systems present a cost-effective alternative to PCR and reduce the operational time to only 2 h in comparison to 4.5 h required for PCR.

4.1.3 Molecularly imprinted polymeric nanoparticles. Molecularly imprinted polymeric nanoparticles (MIP-NPs) are nanoparticles fabricated as a result of the polymerization of one or more functional monomers in the presence of a template molecule. The template molecules are subsequently removed to reveal high-affinity target-specific nanocavities that are cost-effective and durable substitutes to antibodies.[124] Due to their simplicity of synthesis as well as recalcitrance to extreme environments, MIP-NPs are emerging as promising nanomaterials for virus sensing.[93,443]

The selection of suitable functional monomers is critical for developing assays with high sensitivity and rapid response (Table 3). For example, in the case of MIP-NPs for the RLS-based detection of HAV, (dimethylamino)ethyl methacrylate[414] generated a pH-responsive polymer with a significantly lower LOD (100 fM) and response time (20 min) than *N*-isopryl-acrylamide (LOD: 1.1 pM; response time: 30 min)[369] or dopamine (LOD: 6.2 pM; response time: 150 min).[313] With the help of computational modeling, it is possible to select the functional monomers that show the highest binding affinity with the target thus reducing experimental cost and research time significantly.[444] *In silico* designing can also be used for selecting the most stabile viral epitope as a template peptide to escape the pitfalls of template leakage during rebinding. Such MIP-NPs (65 nm) are resistant to hydrolysis enzymes and are analogous to monoclonal antibodies.[416] However, unlike most anti-bodies, MIP-NPs can be easily regenerated and reused several times.[33,311] The mechanism of virus detection is also a key parameter for improving sensor performance. For example, in the case of JeV imprinting with APTES, nearly 12-fold higher sensitivity was reported when RLS[311] was replaced with fluorescence-based measurement.[445] The detection range widened 7-fold and the imprinting factor increased 2.5 times when APTES was replaced with zinc acrylate as the functional monomer and polyethylene glycol was added as a passivating agent.[422]

The contribution of MIPs to virus sensors has diversified in recent years and it is not restricted to simple target-shaped cavities.[444] Thermoresponsive nanostructured hydrogels synthesized from surface imprinted SiO_2 nanoparticles are eligible for *in vitro* HAV detection.[369] Such MIP-NPs (8 nm) are highly selective against viruses for diseases such as rabies, measles, and rubella[370] and show high recovery in diluted serum.[76] Polythiophene MIP-NPs (200 nm) emit fluorescence (λ: 410 nm) and their thickness can be optimized to obtain a response within 2 minutes.[417]

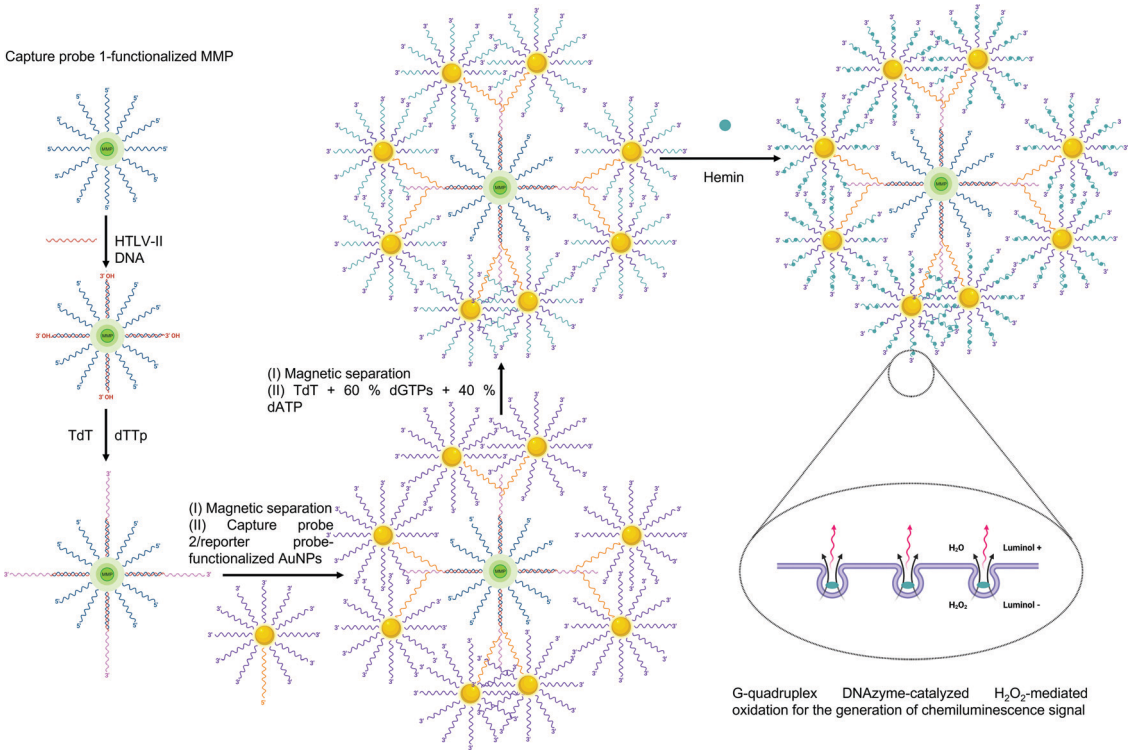

Fig. 19 Scheme for dendrimer-mediated bio-bar codes for sensing viral DNA.[291] Abbreviations: AuNP: gold nanoparticles; dATP: deoxyadenosine triphosphate; dGTP: deoxyguanosine triphosphate; DNA: deoxyribonucleic acid; dTTp: deoxythymidine triphosphate; HTLV-II: human T-lymphotropic virus II; MMP: magnetic microparticle; TdT: terminal deoxynucleotidyl transferase. Used under Creative Commons Attribution-NonCommercial 3.0 Unported Licence https://creativecommons.org/licenses/by-nc/3.0/[L. Wang, M. Ren, L. Liang and C. Zhang, *Chem. Sci.*, 2018, **9**, 4942] – Published by The Royal Society of Chemistry.

Table 3 MIP-NPs for virus detection

Functional monomer	Size (nm)	Template type	Target	Method	LOD	Ref.
NIPAam, BIS, TBAm, AAc	205–238	Virus	MS2	SPR	5×10^6 PFU mL^{-1}	11
Dimethylaminoethylmethacrylate	13	Virus	HAV	RLS	100 fM	414
NIPAam, TBAm, BIS, NPhAam, TFMA	65	Epitope	HIV gp41	Fluorescence	10 nM	416
APTES, TEOS	421	Virus	JEV	Fluorescence	110 fM	445
APTES, TEOS	15	Virus	HAV	Fluorescence	88 pM	76
APTES, TEOS	200[a]	Virus	JEV	RLS	1.3 pM	311
Dopamine	200[b]	Virus	HAV	RLS	6.2 pM	313
Dopamine	70[c]	Virus	HAV	RLS	8.6 pM	370
NIPAam	110[c]	Virus	HAV	RLS	1.1 pM	369
Thiophene	200	Virus	TNV	Fluorescence	2.2 ng L^{-1}	417
Zinc acrylate	50	Virus	JEV	Fluorescence	13 pM	422
2,2′:6′,6″ terpyridine, EGDMA	<100	Pb^{2+}	HIV-1 pol-gene	DPV	300 aM	415

[a] Size of Fe_3O_4@SiO_2 support. [b] Size of diamond-shaped magnetic nanoparticle. [c] Size of SiO_2 support. Abbreviations: AAc: acrylic acid; APTES: (3-aminopropyl)triethoxysilane; BIS: *N*,*N*′-methylenebisacrylamide; DPV: differential pulse voltammetry; EGDMA: ethylene glycol dimethacrylate; gp41: glycoprotein 41; HAV: hepatitis A virus; HIV: human immunodeficiency virus; JEV: japanese encephalitis virus; MS2: bacteriophage MS2; NIPAam: *N*-isopropylacrylamide; NPhAam: *N*-phenylacrylamide; RLS: resonance light scattering; SPR: surface plasmon resonance; TBAm: *N*-*tert*-butylacrylamide; TEOS: tetraethyl orthosilicate; TFMA: trifluoromethyl acrylic acid; TNV: tobacco necrosis virus.

This year, a Pb^{2+} ion-imprinted terpyridine-based polymer was developed as a transducer in the genosensing of the HIV-1 pol-gene.[415]

4.1.4 Other organic nanomaterials. In addition to those previously described, several new organic nanomaterials have been explored as additives in virus detection. Although most of these nanomaterials are polymeric in nature, non-polymeric nanoparticles, especially nucleotide-based nanomachines have also received considerable attention. Fluorescein and adenosine triphosphate copolymer nanoparticles (35 nm) can be easily loaded with Ce(III) ions to generate self-assembled ratiometric probes for fluoroimmunoassays.[446] Polylactic acid–polyethylene glycol copolymer nanoparticles (73 ± 11 nm) with E2 surface functionalization possess virus mimetic properties and are essential for the development of HCV-sensitive 3D biochips.[423] Polyethyleneimine functionalized with polystyrene

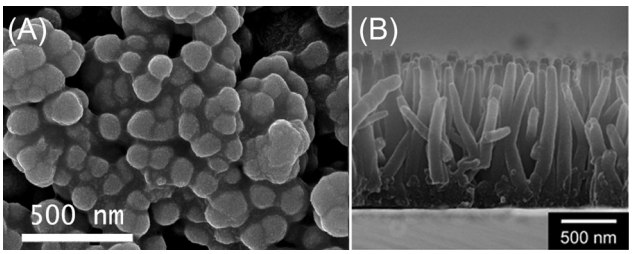

Fig. 20 Scanning electron micrographs of the morphology of (A) polystyrene nanospheres[447] and (B) polypyrrole nanowires.[450] Reprinted with permission from (*ACS Appl. Mater. Interfaces* 2018, **10**, 34, 28412–28419), Copyright 2018, American Chemical Society.

nanospheres (120 nm) *via* coordination polymerization of ferrocene derivatives exhibit a singular morphology as shown in Fig. 20A with a tunable, biocompatible structure.[447] Therefore, the nanospheres act as electron mediators and carriers for other conductive nanomaterials. Similar polymer nanoparticles (129 nm) have also been used to develop a multiplexed lateral flow assays for the rapid detection (<60 min) of SARS-CoV-2.[448] Recently, polystyrene nanobeads have also been employed in a differential impedance sensor for POC dengue antibody detection with an LOD of just 88 pg mL^{-1}.[449] The dye-labeled polymer nanoparticles generated a distinctive, crimson-colored band like modern pregnancy-test kits without the requirement of any expensive instruments.

In flow cytometry, fluorescence latex nanoparticles (200 nm) function as reporters and are responsible for reducing the DenV detection limit from 150 ng mL^{-1} to 2.5 ng mL^{-1}.[310] The intrinsically conducting polypyrrole nanowires shown in Fig. 20B (diameter: 70 nm; length: 1 μm) are conducive to aptamer loading and are capable of distinguishing attomolar concentrations of viral proteins in artificial saliva within 5 s.[450] The blue-emitting polydioctylfluorene dots exhibit theranostic properties due to the synchronous detection and blocking of influenza viruses in the presence of sialyl glycans.[424] Nanocrystalline cellulose (width: ~5 nm; length: ~200 nm) shows low toxicity and special surface chemistry that enables the antibody-mediated agglutination and detection of DenV proteins.[89,451] Fluorescent probes based on carbazole form thermoreversible nanoassemblies with extraordinary solid-state fluorescence.[452] These probes do not form nanoaggregates in the presence of the target virus due to electrostatic association resulting in an immediate change in color.

Molecular machines are nanoscale devices that are capable of propulsion in liquids by themselves or *via* an external fuel. Molecular machines used for virus detection are oligonucleotide-based. Therefore, they show ultrasensitivity to target viruses. For example, a lock-like DNA machine (7.8 nm) with a hairpin DNA and fluorescent ancient DNA opens in the presence of just 900 aM of ZikV gene and subsequently undergoes strand displacement reactions induced by a DNA-based fuel.[453] Although the molecular machine enhanced the fluorescence signal by 360%, a long time (150 min) was required for DNA hybridization. DNA walkers, which combine walking and tracking particles into locked strands of DNAzyme, show good continuity and signal accumulation even though their sensitivity is lower in comparison by 5 orders of magnitude.[454] 3D DNA walker-based sensors show high recovery (99.3–102.0%) in human blood samples but the sensor response takes almost 2 hours.[455] The cascade amplification of SPR signals by double-layer DNA tetrahedron nanodevice facilitates the label- and enzyme-free interrogation of HIV by entropy-driven strand displacement reaction.[425] However, recombinant polymerase-based amplification with Cas13a nanomachine shortens the assays time (5 min–1 h) in comparison to quantitative PCR (2 h) and real-time PCR (7 days).[456]

4.2 Virus tracking

Organic nanoparticles have scarcely received attention for virus tracking and imaging purposes which can be attributed to the scarcity of excited electrons in these particles in comparison to quantum dots and plasmonic nanoparticles. Their large size in comparison to inorganic nanoparticles hinders their internalization into host cells as well as virus capsids. Despite these obstacles, polymer nanoparticles have recently been exploited for imaging and even single virus tracking.[457] For example, latex nanobeads of 20, 100, 300, and 1000 nm elucidate the size-dependent mechanism of virus internalization.[458] It has been observed that 100–300 nm beads followed a clathrin-mediated pathway whereas 1000 nm particles were internalized *via* a caveolae-governed route. Further investigations with stimulated emission depletion super-resolution microscopy (STED) using the 100 and 300 nm particles revealed that the clathrin coat possesses an intrinsic size limit for the synthesis of the endocytic structure and the frequency with which this machinery was recruited was a function of the virus size.[458] STED is also useful for imaging the binding of adenovirus with MIP-NPs (600 nm).[459] The 100 nm virus particle can be accurately resolved in the silane MIPs owing to the synthesis of a Schiff base between the lysine residues of the adenovirus and the aldehyde functionality on the MIP-NP (Fig. 21). Adenoviruses are non-enveloped viruses often responsible for mild respiratory distress in children as well as fatal organ malfunction in immunocompromised individuals. These viruses have also been imaged with polyphenylene dendrimers (1st to 5th generation) to investigate their host-guest interactions as well as manipulate their *in vivo* distribution.[460] In this case, the theranostic features of the dendrimers can be attributed to two factors: (i) they enhanced cellular transduction capabilities of the viral gene-transfer vectors in the absence of coxsackie adenovirus receptor, and (ii) they controlled the interaction between the cargo and the Stuart-Power X enzyme which is the cornerstone of virus interactions in blood.[460]

Dye-loaded polymersome nanovesicles facilitate the study of virus replication and allow high-throughput antiviral drug screening.[461] Initially, dye molecules from the polymersome are discharged to induce an endosomal escape. Subsequently, another dye of a different emission wavelength is targeted towards the Golgi complex. As a result, the budding and proliferation events in the virus replication cycle are tracked with the help of fluorescence imaging.[461] Fluorescent polymer

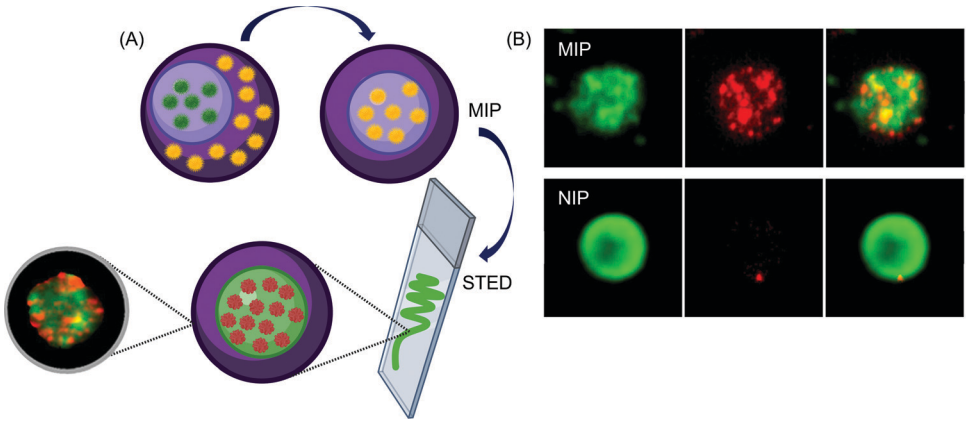

Fig. 21 (A) Schematic illustration of molecularly imprinted polymeric nanoparticles for virus imaging; (B) dual-color imaging stimulated emission depletion (STED) microscopy of molecularly imprinted polymers (top) and non-imprinted polymers in the presence of adenovirus particles[459] redrawn and reprinted with permission from (*Anal. Chem.* 2020, **92**, 4, 3050–3057). Copyright 2020 American Chemical Society.

dots show excellent hole mobility, brightness as well as outstanding blue fluorescence. They are capable of suppressing the fluorescence of dye-stained cells infected with H3N2 without compromising the cell viability hinting at the scope of supramolecular nanomaterials for influenza virus treatment.[424] Organic nanomaterials have also been employed as fluorescence amplifiers[441] and virus substitutes to evaluate the midinfrared photothermal microscopy as a tool for virus-fingerprinting.[462]

5. Conclusions and future prospects

In this work, the latest developments in the role of various nanomaterials for sensing and imaging viruses were discussed. The incorporation of nanomaterials offers multifold benefits to the performance of virus sensors by improving the sensitivity, specificity, response time as well as recovery in complex media. A thorough understanding of nanomaterial interactions in these recognition systems such as nanoparticle size-dependent signal amplification, plasmonic resonance as well as charge transfer abilities could help accelerate the development of virus detection platforms with high veracity. The compatibility of nanomaterials across detection platforms including optical, electrochemical, or piezoelectric makes detection versatile and cost-effective. The spread of the global COVID-19 pandemic has incurred renewed interest in the development of alternatives to conventional virus detection systems such as PCR, ELISA, or flow cytometry. The amalgamation of nanosensors into an affordable paper strip or smartphone systems widens the scope of nanomaterials for POCT of viral pathogens in accordance with the WHO prescribed "ASSURED" (Affordable, Sensitive, Specific, User-friendly, Rapid, Equipment-free, Deliverable to end-users) criteria. Such POCT devices have the potential to timely assess the threat of infection at the patient level thus reducing the risk to healthcare professionals thereby helping curb the spread of epidemic viruses. Furthermore, nanomaterials are emerging to play an instrumental role in upgrading conventional techniques such as the development of nanoPCR as a highly sensitive, selective, rapid and cost-effective alternative to the traditional PCR technique which has often been dubbed as the gold standard in virus detection. Semi-synthetic and synthetic receptors such as aptamers and MIP-NPs are transforming into robust substitutes to the expensive and fragile natural receptors such as antibodies and DNA that previously dominated the field of virus detection. Another trend observed in recent years is the integration of different types of nanomaterials to generate multifunctional nanocomposites that not only positively influence the sensitivity but also improve the signal to noise ratio and make the platform suitable towards commercialization.

In several nanomaterials, the particle size is smaller than the wavelength of the constituent electrons which results in quantum confinement enabling the synthesis of fluorescent nanoparticles. Since these nanoparticles are photostable and resistant to photobleaching, they have emerged as materials of interest for the non-invasive study of virus dissemination. Nanomaterial-mediated SVT helps understand virus internalization pathways and their replication mechanisms which is a prerequisite for adopting any therapeutic discourse. Fluorescent nanoparticles have emerged as promising alternatives to delicate and expensive labels such as green fluorescent protein. They also allow high throughput drug screening thus reducing development and trial costs. Nanoparticles have also been used in imaging studies to test the efficacy of emerging microscopic techniques for virus tracking. Since their size and dielectric constants are close to those of viruses, virus-mimetic nanoparticles are increasingly replacing virus-like particles in the study of intracellular host-guest interactions. Based on the recent trends in virus tracking methodologies, nanoparticles such as quantum dots, gold nanoparticles and nanodiamonds can be expected to contribute as fluorescent labels to a majority of virus imaging and internalization studies.

Conflicts of interest

The authors declare that they have no known competing financial interests or personal relationships that could have appeared to influence the work reported in this paper.

Acknowledgements

This work was supported by the Deutsche Forschungsgemeinschaft (DFG, German Research Foundation) under the project number 428780268. Figure elements were created using BioRender.com.

Notes and references

1 S. Modrow, D. Falke, U. Truyen and H. Schätzl, in *Molecular Virology*, ed. S. Modrow, D. Falke, U. Truyen and H. Schätzl, Springer Berlin Heidelberg, Berlin, Heidelberg, 2013, pp. 17–30.
2 M. Breitbart and F. Rohwer, *Trends Microbiol.*, 2005, **13**, 278–284.
3 Ø. Bergh, K. Y. Børsheim, G. Bratbak and M. Heldal, *Nature*, 1989, **340**, 467–468.
4 M. W. Beijerinck, *Verh. K. Akad. Wet. Amsterdam, Afd. Natuurkd.*, 1898, **6**, 3–21.
5 International Committee on Taxonomy of Viruses, Virus Taxonomy: 2019 Release, **https://talk.ictvonline.org/taxonomy/**.
6 R. L. Duda and C. M. Teschke, *Curr. Opin. Virol.*, 2019, **36**, 9–16.
7 K. J. Tompkins, M. Houtti, L. A. Litzau, E. J. Aird, B. A. Everett, A. T. Nelson, L. Pornschloegl, L. K. Limón-Swanson, R. L. Evans III, K. Evans, K. Shi, H. Aihara and W. R. Gordon, *Nucleic Acids Res.*, 2021, **49**, 1046–1064.
8 J. Shi, J. M. Perryman, X. Yang, X. Liu, D. M. Musser, A. K. Boehr, I. M. Moustafa, J. J. Arnold, C. E. Cameron and D. D. Boehr, *Biochemistry*, 2019, **58**, 3735–3743.
9 C. San Martín and M. J. van Raaij, *Virol. J.*, 2018, **15**, 181.
10 E. V. Koonin, T. G. Senkevich and V. V. Dolja, *Biol. Direct*, 2006, **1**, 1–27.
11 Z. Altintas, M. Gittens, A. Guerreiro, K. A. Thompson, J. Walker, S. Piletsky and I. E. Tothill, *Anal. Chem.*, 2015, **87**, 6801–6807.
12 A. Mokhtarzadeh, R. Eivazzadeh-keihan, P. Pashazadeh, M. Hejazi, N. Gharaatifar, M. Hasanzadeh, B. Baradaran and M. de la Guardia, *Trends Anal. Chem.*, 2017, **97**, 445–457.
13 F. Broecker and K. Moelling, *Ann. N. Y. Acad. Sci.*, 2019, **1447**, 53–68.
14 A. J. Cann, *Principles of molecular virology*, Academic Press, Boston, 6th edn, 2016.
15 J. Brojatsch, J. Naughton, M. M. Rolls, K. Zingler and J. A. T. Young, *Cell*, 1996, **87**, 845–855.
16 K. Peters, S. Chattopadhyay and G. C. Sen, *J. Virol.*, 2008, **82**, 3500 LP–3508.
17 P. Danthi, T. Kobayashi, G. H. Holm, M. W. Hansberger, T. W. Abel and T. S. Dermody, *J. Virol.*, 2008, **82**, 161 LP–172.
18 Y. Cho, S. Challa, D. Moquin, R. Genga, T. D. Ray, M. Guildford and F. K.-M. Chan, *Cell*, 2009, **137**, 1112–1123.
19 K. G. Harris, S. A. Morosky, C. G. Drummond, M. Patel, C. Kim, D. B. Stolz, J. M. Bergelson, S. Cherry and C. B. Coyne, *Cell Host Microbe*, 2015, **18**, 221–232.
20 T. Y. Tan and J. J. H. Chu, *J. Gen. Virol.*, 2013, **94**, 2215–2220.
21 K. M. Monroe, Z. Yang, J. R. Johnson, X. Geng, G. Doitsh, N. J. Krogan and W. C. Greene, *Science*, 2014, **343**, 428 LP–432.
22 P. Danthi, *Annu. Rev. Virol.*, 2016, **3**, 533–553.
23 D. Zhu, C. Pan, J. Sheng, H. Liang, Z. Bian, Y. Liu, P. Trang, J. Wu, F. Liu, C.-Y. Zhang and K. Zen, *Nat. Microbiol.*, 2018, **3**, 503–513.
24 J. Ribeiro, C. Oliveira, M. Malta and H. Sousa, *Futur. Oncol.*, 2017, **13**, 567–579.
25 A. M. Price, J. E. Messinger and M. A. Luftig, *J. Virol.*, 2018, **92**, e01178–17.
26 S. Rasa, Z. Nora-Krukle, N. Henning, E. Eliassen, E. Shikova, T. Harrer, C. Scheibenbogen, M. Murovska and B. K. Prusty, *J. Transl. Med.*, 2018, **16**, 1–25.
27 A. N. Bubak, V. Traina-Dorge, C. N. Como, B. Feia, C. M. Pearce, L. Doyle-Meyers, A. Das, J. Looper, R. Mahalingam and M. A. Nagel, *J. Neurovirol.*, 2020, **26**, 945–951.
28 J. T. Guidry, C. E. Birdwell and R. S. Scott, *Oral Dis.*, 2018, **24**, 497–508.
29 S. Ahmadi Ghezeldasht, S. A. A. Shamsian, J. Gholizadeh Navashenaq, R. Miri, F. Ashrafi, A. Mosavat and S. A. Rezaee, *Rev. Med. Virol.*, 2021, **31**, 1–15.
30 R. E. Malosh, E. T. Martin, J. R. Ortiz and A. S. Monto, *Vaccine*, 2018, **36**, 141–147.
31 O. A. Khomich, S. N. Kochetkov, B. Bartosch and A. V. Ivanov, *Viruses*, 2018, **10**, 392.
32 A. M. Lachiewicz and M. L. Srinivas, *Prev. Med. Rep.*, 2019, **16**, 101016.
33 Z. Altintas, J. Pocock, K. A. Thompson and I. E. Tothill, *Biosens. Bioelectron.*, 2015, **74**, 996–1004.
34 H. Meyer, R. Ehmann and L. Smith, *Viruses*, 2020, **12**, 138.
35 Z.-Y. Jin, X. Liu, Y.-Y. Ding, Z.-F. Zhang and N. He, *Sci. Rep.*, 2017, **7**, 4890.
36 C. R. Fisher, D. G. Streicker and M. J. Schnell, *Nat. Rev. Microbiol.*, 2018, **16**, 241–255.
37 J. A. Otter, C. Donskey, S. Yezli, S. Douthwaite, S. D. Goldenberg and D. J. Weber, *J. Hosp. Infect.*, 2016, **92**, 235–250.
38 P. Norrie, in *A History of Disease in Ancient Times: More Lethal than War*, ed. P. Norrie, Palgrave Macmillan, Cham, 2016, pp. 61–101.
39 P. E. Olson, C. S. Hames, A. S. Benenson and E. N. Genovese, *Emerg. Infect. Dis.*, 1996, **2**, 155–156.
40 S. Sabbatani and S. Fiorino, *Le Infez. Med.*, 2009, **17**, 261–275.
41 A. Suzuki, *Med. Hist.*, 2011, **55**, 313–318.
42 R. Acuna-Soto, D. W. Stahle, M. K. Cleaveland and M. D. Therrell, *Emerg. Infect. Dis.*, 2002, **8**, 360–362.
43 D. J. Rogers, A. J. Wilson, S. I. Hay and A. J. Graham, in *Advances in Parasitology*, ed. S. I. Hay, A. Graham and D. J. B. T.-A. in P. Rogers, Academic Press, 2006, vol. 62, pp. 181–220.
44 D. M. Morens, M. North and J. K. Taubenberger, *Lancet*, 2010, **376**, 1894–1895.

45 T. N. Jilani, R. T. Jamil and A. H. Siddiqui, *H1N1 Influenza (Swine Flu)*, StatPearls Publishing LLC, Treasure Island, Florida, 2019.
46 R. W. Eisinger and A. S. Fauci, *Emerg. Infect. Dis.*, 2018, **24**, 413–416.
47 WHO, *Weekly Epidemiological Update on COVID-19*, 2021.
48 A. S. Lima Neto, G. S. Sousa, O. J. Nascimento and M. C. Castro, *PLoS Negl. Trop. Dis.*, 2019, **13**, e0007575.
49 A. King, *New Sci.*, 2020, **246**, 32–35.
50 J. E. Cogan, Dengue and severe dengue fact sheet, **https://www.who.int/en/news-room/fact-sheets/detail/dengue-and-severe-dengue**.
51 M. Din, M. Asghar and M. Ali, *J. Med. Virol.*, 2020, **93**, 601–602.
52 A. Aruna, P. Mbala, L. Minikulu, D. Mukadi, D. Bulemfu, F. Edidi, J. Bulabula, G. Tshapenda, J. Nsio, R. Kitenge, G. Mbuyi, C. Mwanzembe, J. Kombe, L. Lubula, J. C. Shako, M. Mossoko, F. Mulangu, A. Mutombo, E. Sana, Y. Tutu, L. Kabange, J. Makengo, F. Tshibinkufua, S. Ahuka-Mundeke, J.-J. Muyembe, E. R. Cdc and C. D. C. E. Response, *MMWR Morb. Mortal. Wkly. Rep.*, 2019, **68**, 1162–1165.
53 R. R. Dourmashkin, G. Dunn, V. Castano and S. A. McCall, *BMC Infect. Dis.*, 2012, **12**, 136.
54 R. T. Ravenholt and W. H. Foege, *Lancet*, 1982, **320**, 860–864.
55 UNAIDS, Global HIV & AIDS statistics—2020 fact sheet.
56 P. Heyman, L. Simons and C. Cochez, *Viruses*, 2014, **6**, 151–171.
57 T. Pietrasik, Up to 650 000 people die of respiratory diseases linked to seasonal flu each year, **https://www.who.int/news/item/14-12-2017-up-to-650-000-people-die-of-respiratory-diseases-linked-to-seasonal-flu-each-year**.
58 D. M. Morens and A. S. Fauci, *J. Infect. Dis.*, 2007, **195**, 1018–1028.
59 WHO, *Report of the review committee on the functioning of the international health regulations (2005) in relation to pandemic (H1N1) 2009*, 2011.
60 O. Ogbu, E. Ajuluchukwu and C. J. Uneke, *J. Vector Borne Dis.*, 2007, **44**, 1–11.
61 D. Kumar Pant, T. Tenzin, R. Chand, B. Kumar Sharma and P. Raj Bist, *PLoS One*, 2017, **12**, e0180591.
62 M. Grabowsky, *JAMA Pediatr.*, 2014, **168**, 108–109.
63 ECDC, Geographical distribution of confirmed MERS-CoV cases by probable region of infection and exposure, from 1 January 2020 to 1 September 2020, **https://www.ecdc.europa.eu/en/publications-data/geographical-distribution-confirmed-mers-cov-cases-probable-region-infection-0**.
64 Y. Ding, L. He, Q. Zhang, Z. Huang, X. Che, J. Hou, H. Wang, H. Shen, L. Qiu, Z. Li, J. Geng, J. Cai, H. Han, X. Li, W. Kang, D. Weng, P. Liang and S. Jiang, *J. Pathol.*, 2004, **203**, 622–630.
65 WHO, WHO coronavirus disease (COVID-19) dashboard, **https://covid19.who.int/**.
66 G. A. Roth and E. Fee, *Am. J. Public Health*, 2011, **101**, 1217.
67 S. Smith, H. Harmanci, Y. Hutin, S. Hess, M. Bulterys, R. Peck, B. Rewari, A. Mozalevskis, M. Shibeshi, M. Mumba, L.-V. Le, N. Ishikawa, D. Nolna, L. Sereno, C. Gore, D. J. Goldberg and S. Hutchinson, *JHEP Rep.*, 2019, **1**, 81–89.
68 K. D. Patterson, *Soc. Sci. Med.*, 1992, **34**, 855–865.
69 T. Ozer, B. J. Geiss and C. S. Henry, *J. Electrochem. Soc.*, 2020, **167**, 037523.
70 J. Flint, V. R. Racaniello, G. F. Rall, T. Hatziioannou and A. M. Skalka, *Principles of Virology: Molecular biology, pathogenesis and control*, ASM Press, Washington, DC, 5th edn, 2020.
71 H. H. Zalzala, *New Microbes New Infect.*, 2020, **38**, 100761.
72 M. Nagendran, J. John, K. Annamalai, M. I. Gandhi Sethuraman, N. Balamurugan, H. K. Rajendran, M. A. Deen Fakrudeen, R. Chandrasekar, S. Ranjan and V. C. Padmanaban, *J. Drug Delivery Sci. Technol.*, 2020, 102120.
73 A. K. Giri and D. R. Rana, *Biosaf. Heal.*, 2020, **2**, 53–56.
74 M. Pirzada, E. Sehit and Z. Altintas, *Biosens. Bioelectron.*, 2020, **166**, 112464.
75 E. Sehit, J. Drzazgowska, D. Buchenau, C. Yesildag, M. Lensen and Z. Altintas, *Biosens. Bioelectron.*, 2020, **165**, 112432.
76 L. Luo, W. Feng, W. Hu, C. Chen, H. Gong and C. Cai, *Methods Appl. Fluoresc.*, 2019, **7**, 015006.
77 R. Gaudin and J. G. Goetz, *Trends Cell Biol.*, 2021, **31**, 17–23.
78 S. J. Park, J. Kim, J. Kim, S. Kang, H. J. Cha, H. J. Cha, H. Shin, J. Park, Y. S. Jang, Y. S. Jang, J. S. Woo, J. S. Woo, C. Won, D. H. Min, D. H. Min and D. H. Min, *Sci. Adv.*, 2020, **6**, 1–12.
79 M. Pirzada and Z. Altintas, *Sensors*, 2019, **19**, 5311.
80 M. Kortel, B. D. Mansuriya, N. V. Santana and Z. Altintas, *Micromachines*, 2020, **11**, 866.
81 E. Sehit and Z. Altintas, *Biosens. Bioelectron.*, 2020, **159**, 112165.
82 B. D. Mansuriya and Z. Altintas, *Sensors*, 2020, **20**, 1072.
83 Z. Altintas, *Biosensors and Nanotechnology -Applications in Health Care Diagnostics*, John Wiley & Sons Press, Hoboken, NJ, USA, 2017.
84 H. Ehtesabi, *J. Sci. Adv. Mater. Dev.*, 2020, **5**, 436–450.
85 E. Vermisoglou, D. Panáček, K. Jayaramulu, M. Pykal, I. Frébort, M. Kolář, M. Hajdúch, R. Zbořil and M. Otyepka, *Biosens. Bioelectron.*, 2020, **166**, 112436.
86 C. Qin, W. Li, Q. Li, W. Yin, X. Zhang, Z. Zhang, X.-E. Zhang and Z. Cui, *Proc. Natl. Acad. Sci. U. S. A.*, 2019, **116**, 2577 LP–2582.
87 Y. Cui, D. G. Grant, J. Lin, X. Yu and A. W. E. Franz, *Viruses*, 2019, 11.
88 N. A. S. Omar, Y. W. Fen, J. Abdullah, N. A. A. Anas, N. S. M. Ramdzan and M. A. Mahdi, *Results Phys.*, 2018, **11**, 734–739.
89 N. A. S. Omar, Y. W. Fen, J. Abdullah, C. E. N. C. E. Chik and M. A. Mahdi, *Sens. Bio-Sensing Res.*, 2018, **20**, 16–21.
90 Y. Wang, Y. Hu, Q. He, J. Yan, H. Xiong, N. Wen, S. Cai, D. Peng, Y. Liu and Z. Liu, *Biosens. Bioelectron.*, 2020, **169**, 112604.
91 G. Gao, Y. W. Jiang, W. Sun and F. G. Wu, *Chin. Chem. Lett.*, 2018, **29**, 1475–1485.
92 M. S. Draz and H. Shafiee, *Theranostics*, 2018, **8**, 1985–2017.

93 J. Kang, A. Tahir, H. Wang and J. Chang, *Wiley Interdiscip. Rev.: Nanomed. Nanobiotechnol.*, 2021, **13**, 1700.
94 B. V. Ribeiro, T. A. R. Cordeiro, G. R. Oliveira e Freitas, L. F. Ferreira and D. L. Franco, *Talanta Open*, 2020, **2**, 100007.
95 B. Alhalaili, I. N. Popescu, O. Kamoun, F. Alzubi, S. Alawadhia and R. Vidu, *Sensors*, 2020, 20.
96 S.-L. Liu, Z.-G. Wang, H.-Y. Xie, A.-A. Liu, D. C. Lamb and D.-W. Pang, *Chem. Rev.*, 2020, **120**, 1936–1979.
97 K. Kaiser, L. M. Scriven, F. Schulz, P. Gawel, L. Gross and H. L. Anderson, *Science*, 2019, **365**, 1299–1301.
98 C. Chaicham, T. Tuntulani, V. Promarak and B. Tomapatanaget, *Sens. Actuators, B*, 2019, **282**, 936–944.
99 A. Salaam, D. Dean and V. Thomas, in *Drug Delivery Nanosystems for Biomedical Applications*, ed. C. P. Sharma, Elsevier Inc., 2018, pp. 333–356.
100 A. Kurdekar, L. A. A. Chunduri, E. P. Bulagonda, M. K. Haleyurgirisetty, V. Kamisetti and I. K. Hewlett, *Microfluid. Nanofluid.*, 2016, **20**, 99.
101 L. A. A. Chunduri, M. K. Haleyurgirisetty, S. Patnaik, P. E. Bulagonda, A. Kurdekar, J. Liu, I. K. Hewlett and V. Kamisetti, *Microfluid. Nanofluid.*, 2016, **20**, 1–10.
102 M. Zarei-Ghobadi, S.-H. Mozhgani, F. Dashtestani, A. Yadegari, F. Hakimian, M. Norouzi and H. Ghourchian, *Sci. Rep.*, 2018, **8**, 15593.
103 L.-D. Xu, Q. Zhang, S.-N. Ding, J.-J. Xu and H.-Y. Chen, *ACS Omega*, 2019, **4**, 21431–21438.
104 A. Valipour and M. Roushani, *Biosens. Bioelectron.*, 2017, **89**, 946–951.
105 J. Chen, M. Wang, X. Zhou, Y. Nie and X. Su, *Sens. Actuators, B*, 2021, **326**, 128847.
106 K. Ghanbari, M. Roushani and A. Azadbakht, *Anal. Biochem.*, 2017, **534**, 64–69.
107 J. Ramos-Soriano, J. J. Reina, B. M. Illescas, N. de la Cruz, L. Rodríguez-Pérez, F. Lasala, J. Rojo, R. Delgado and N. Martín, *J. Am. Chem. Soc.*, 2019, **141**, 15403–15412.
108 C. Liu, T. Wang, J. Ji, C. Wang, H. Wang, P. Jin, W. Zhou and J. Jiang, *J. Mater. Chem. C*, 2019, **7**, 10240–10246.
109 J. Upan, P. Banet, P.-H. Aubert, K. Ounnunkad and J. Jakmunee, *Electrochim. Acta*, 2020, **349**, 136335.
110 Z. Chaloupková, A. Balzerová, J. Bařinková, Z. Medříková, P. Šácha, P. Beneš, V. Ranc, J. Konvalinka and R. Zbořil, *Anal. Chim. Acta*, 2018, **997**, 44–51.
111 J. Lee, M. Morita, K. Takemura and E. Y. Park, *Biosens. Bioelectron.*, 2018, **102**, 425–431.
112 L. Farzin, S. Sadjadi, M. Shamsipur and S. Sheibani, *J. Pharm. Biomed. Anal.*, 2020, **179**, 112989.
113 H. Kong, W. Zhang, J. Yao, C. Li, R. Lu, Z. Guo, J. Li, C. Li, Y. Li, C. Zhang and L. Zhou, *Sens. Actuators, B*, 2020, 129118.
114 A. Roberts, N. Chauhan, S. Islam, S. Mahari, B. Ghawri, R. K. Gandham, S. S. Majumdar, A. Ghosh and S. Gandhi, *Sci. Rep.*, 2020, **10**, 14546.
115 G. Seo, G. Lee, M. J. Kim, S.-H. Baek, M. Choi, K. B. Ku, C.-S. Lee, S. Jun, D. Park, H. G. Kim, S.-J. Kim, J.-O. Lee, B. T. Kim, E. C. Park and S. Il Kim, *ACS Nano*, 2020, **14**, 5135–5142.
116 J. Lee, K. Takemura and E. Y. Park, *Sens. Actuators, B*, 2018, **276**, 254–261.
117 R. M. Torrente-Rodríguez, H. Lukas, J. Tu, J. Min, Y. Yang, C. Xu, H. B. Rossiter and W. Gao, *Matter*, 2020, **3**, 1981–1998.
118 W. Huang, G. Xiang, D. Jiang, L. Liu, C. Liu, F. Liu and X. Pu, *Electroanalysis*, 2016, **28**, 1126–1133.
119 K. Siuzdak, P. Niedziałkowski, M. Sobaszek, T. Łęga, M. Sawczak, E. Czaczyk, K. Dziąbowska, T. Ossowski, D. Nidzworski and R. Bogdanowicz, *Sens. Actuators, B*, 2019, **280**, 263–271.
120 G. Z. Feuerstein, M. A. Mansfield, P. I. Lelkes, S. Alesci, C. Marcinkiewicz, N. Butlin and M. Sternberg, *Int. J. Nanomedicine*, 2020, **15**, 7583–7599.
121 J. Li, K. Yang, Z. Wu, X. Li and Q. Duan, *Talanta*, 2019, **205**, 120091.
122 J. Mandli, A. Attar, M. M. Ennaji and A. Amine, *J. Electroanal. Chem.*, 2017, **799**, 213–221.
123 F. Wang, S. C. B. Gopinath and T. Lakshmipriya, *Int. J. Nanomedicine*, 2019, **14**, 8469–8481.
124 K. Ghanbari and M. Roushani, *Sens. Actuators, B*, 2018, **258**, 1066–1071.
125 Y. Ma, X. L. Shen, Q. Zeng, H. S. Wang and L. S. Wang, *Talanta*, 2017, **164**, 121–127.
126 Q. Palomar, X. X. Xu, C. Gondran, M. Holzinger, S. Cosnier and Z. Zhang, *Microchim. Acta*, 2020, **187**, 1–10.
127 X. Guo, J. Hou, Z. Yuan, H. Li and S. Sang, *Nanotechnology*, 2021, **32**, 355102.
128 M. Sudan Guray, P. Minakshi, B. Brar, R. Rani and U. P. Lambe, *J. Nanosci. Nanotechnol.*, 2021, **21**, 3513–3523.
129 P. G. Gopinath, V. R. Anitha and S. Aruna Mastani, *Alexandria Eng. J.*, 2018, **57**, 671–681.
130 J. Narang, C. Singhal, N. Malhotra, S. Narang, A. K. P. N., R. Gupta, R. Kansal and C. S. Pundir, *Biosens. Bioelectron.*, 2016, **86**, 566–574.
131 D. G. A. Cabral, E. C. S. Lima, P. Moura and R. F. Dutra, *Talanta*, 2016, **148**, 209–215.
132 Y. Fu, V. Romay, Y. Liu, B. Ibarlucea, L. Baraban, V. Khavrus, S. Oswald, A. Bachmatiuk, I. Ibrahim, M. Rümmeli, T. Gemming, V. Bezugly and G. Cuniberti, *Sens. Actuators, B*, 2017, **249**, 691–699.
133 D. Wasik, A. Mulchandani and M. V. Yates, *Biosens. Bioelectron.*, 2017, **91**, 811–816.
134 Z. Jia, Y. Ma, L. Yang, C. Guo, N. Zhou, M. Wang, L. He and Z. Zhang, *Biosens. Bioelectron.*, 2019, **133**, 55–63.
135 T. L. Tran, T. T. Nguyen, T. T. Huyen Tran, V. T. Chu, Q. Thinh Tran and A. Tuan Mai, *Phys. E*, 2017, **93**, 83–86.
136 S. R. Ahmed, J. Kim, T. Suzuki, J. Lee and E. Y. Park, *Biosens. Bioelectron.*, 2016, **85**, 503–508.
137 G. Cabral-Miranda, A. R. Cardoso, L. C. S. Ferreira, M. G. F. Sales and M. F. Bachmann, *Biosens. Bioelectron.*, 2018, **113**, 101–107.
138 P. D. Mendonça, L. K. B. Santos, M. V. Foguel, M. A. B. Rodrigues, M. T. Cordeiro, L. M. Gonçalves, E. T. A. Marques and R. F. Dutra, *Anal. Bioanal. Chem.*, 2021, **413**, 4873–4885.

139 M. A. Tahir, S. Hameed, A. Munawar, I. Amin, S. Mansoor, W. S. Khan and S. Z. Bajwa, *J. Virol. Methods*, 2017, **249**, 130–136.
140 S. Y. Kim, J.-C. Lee, G. Seo, J. H. Woo, M. Lee, J. Nam, J. Y. Sim, H.-R. Kim, E. C. Park and S. Park, *Small Sci.*, 2021, **n/a**, 2100111.
141 Z. S. Miripour, R. Sarrami-Forooshani, H. Sanati, J. Makarem, M. S. Taheri, F. Shojaeian, A. H. Eskafi, F. Abbasvandi, N. Namdar, H. Ghafari, P. Aghaee, A. Zandi, M. Faramarzpour, M. Hoseinyazdi, M. Tayebi and M. Abdolahad, *Biosens. Bioelectron.*, 2020, **165**, 112435.
142 C. T. Xuan, N. T. Thuy, T. T. Luyen, T. T. T. Huyen and M. A. Tuan, *J. Electron. Mater.*, 2017, **46**, 3507–3511.
143 R. L. Pinals, F. Ledesma, D. Yang, N. Navarro, S. Jeong, J. E. Pak, L. Kuo, Y.-C. Chuang, Y.-W. Cheng, H.-Y. Sun and M. P. Landry, *Nano Lett.*, 2021, **21**, 2272–2280.
144 M. A. Zamzami, G. Rabbani, A. Ahmad, A. A. Basalah, W. H. Al-Sabban, S. Nate Ahn and H. Choudhry, *Bioelectrochemistry*, 2022, **143**, 107982.
145 Y.-T. Yeh, Y. Tang, A. Sebastian, A. Dasgupta, N. Perea-Lopez, I. Albert, H. Lu, M. Terrones and S.-Y. Zheng, *Sci. Adv.*, 2016, **2**, e1601026.
146 S. Jeong, E. González-Grandío, N. Navarro, R. L. Pinals, F. Ledesma, D. Yang and M. P. Landry, *ACS Nano*, 2021, **15**, 10309–10317.
147 M. Amin, O. Siddiqui, H. Abutarboush, M. Farhat and R. Ramzan, *Carbon N. Y.*, 2021, **176**, 580–591.
148 S. Kim, H. Ryu, S. Tai, M. Pedowitz, J. R. Rzasa, D. J. Pennachio, J. R. Hajzus, D. K. Milton, R. Myers-Ward and K. M. Daniels, *Biosens. Bioelectron.*, 2022, **197**, 113803.
149 J. Basu, N. Samanta, S. Jana and C. RoyChaudhuri, *Microelectron. Reliab.*, 2018, **91**, 154–159.
150 J. Gao, C. Wang, C. Wang, Y. Chu, S. Wang, M. Yuan Sun, H. Ji, Y. Gao, Y. Wang, Y. Han, F. Song, H. Liu, Y. Zhang and L. Han, *Anal. Chem.*, 2022, **94**, 1626–1636.
151 Y. Li, Z. Peng, N. J. Holl, M. R. Hassan, J. M. Pappas, C. Wei, O. H. Izadi, Y. Wang, X. Dong, C. Wang, Y.-W. Huang, D. Kim and C. Wu, *ACS Omega*, 2021, **6**, 6643–6653.
152 K. Navakul, C. Warakulwit, P. Yenchitsomanus, A. Panya, P. A. Lieberzeit and C. Sangma, *Nanomedicine*, 2017, **13**, 549–557.
153 J. Wen, W. Li, J. Li, B. Tao, Y. Xu, H. Li, A. Lu and S. Sun, *Sens. Actuators, B*, 2016, **227**, 655–659.
154 M. Z. Ghobadi, S.-H. Mozhgani, F. Hakimian, M. Norouzi, S. A. Rezaee and H. Ghourchian, *Heliyon*, 2018, **4**, e00996.
155 J.-W. Kim, K.-W. Park, M. Kim, K. K. Lee and C.-S. Lee, *Nanomaterials*, 2022, 12.
156 R. Tarcan, O. Todor-Boer, I. Petrovai, C. Leordean, S. Astilean and I. Botiz, *J. Mater. Chem. C*, 2020, **8**, 1198–1224.
157 B. Nagar, M. Balsells, A. de la Escosura-Muñiz, P. Gomez-Romero and A. Merkoçi, *Biosens. Bioelectron.*, 2019, **129**, 238–244.
158 A. Roberts, V. Kesarwani, R. Gupta and S. Gandhi, *Biosens. Bioelectron.*, 2022, **198**, 113837.
159 F. Chekin, K. Bagga, P. Subramanian, R. Jijie, S. K. Singh, S. Kurungot, R. Boukherroub and S. Szunerits, *Sens. Actuators, B*, 2018, **262**, 991–1000.
160 M. F. Abd Muain, K. H. Cheo, M. N. Omar, A. S. Amir Hamzah, H. N. Lim, A. B. Salleh, W. S. Tan and A. Ahmad Tajudin, *Bioelectrochemistry*, 2018, **122**, 199–205.
161 N. A. S. Omar, Y. W. Fen, J. Abdullah, Y. Mustapha Kamil, W. M. E. M. M. Daniyal, A. R. Sadrolhosseini and M. A. Mahdi, *Sci. Rep.*, 2020, **10**, 2374.
162 N. A. S. Omar, Y. W. Fen, J. Abdullah, A. R. Sadrolhosseini, Y. M. Kamil, N. I. M. Fauzi, H. S. Hashim and M. A. Mahdi, *Nanomaterials*, 2020, **10**, 1–14.
163 N. A. S. Omar, Y. W. Fen, J. Abdullah, M. H. M. Zaid and M. A. Mahdi, *Optik*, 2018, **171**, 934–940.
164 V. Georgakilas, J. A. Perman, J. Tucek and R. Zboril, *Chem. Rev.*, 2015, **115**, 4744–4822.
165 O. J. Achadu, F. Abe, F. Hossain, F. Nasrin, M. Yamazaki, T. Suzuki and E. Y. Park, *Biosens. Bioelectron.*, 2021, **193**, 113540.
166 L.-D. Xu, S.-W. Wang, J. Zhu, T. Zhou and S.-N. Ding, *ChemistrySelect*, 2021, **6**, 9787–9793.
167 L.-D. Xu, F.-L. Du, J. Zhu and S.-N. Ding, *Analyst*, 2021, **146**, 706–713.
168 K. Takemura, J. Satoh, J. Boonyakida, S. Park, A. D. Chowdhury and E. Y. Park, *J. Nanobiotechnol.*, 2020, **18**, 152.
169 S. Savas and Z. Altintas, *Materials*, 2019, **12**, 2189.
170 N. Li, L. Shi, X. Zou, T. Wang, D. Wang, Z. Gong and M. Fan, *Microchem. J.*, 2022, **173**, 107046.
171 Q. Xiang, J. Huang, H. Huang, W. Mao and Z. Ye, *RSC Adv.*, 2018, **8**, 1820–1825.
172 A. D. Chowdhury, A. B. Ganganboina, F. Nasrin, K. Takemura, R. Doong, D. I. S. Utomo, J. Lee, I. M. Khoris and E. Y. Park, *Anal. Chem.*, 2018, **90**, 12464–12474.
173 Y. Li, P. Ma, Q. Tao, H.-J. Krause, S. Yang, G. Ding, H. Dong and X. Xie, *Sens. Actuators, B*, 2021, **337**, 129786.
174 J. L. Gogola, G. Martins, A. Gevaerd, L. Blanes, J. Cardoso, F. K. Marchini, C. E. Banks, M. F. Bergamini and L. H. Marcolino-Junior, *Anal. Chim. Acta*, 2021, **1166**, 338548.
175 Y.-D. Ye, L. Xia, D.-D. Xu, X.-J. Xing, D.-W. Pang and H.-W. Tang, *Biosens. Bioelectron.*, 2016, **85**, 837–843.
176 Y. Li, J. Li, Y. Cao, P. Jiang, Y. Tang, Z. Chen and K. Han, *Anal. Chim. Acta*, 2022, **1203**, 339693.
177 O. J. Achadu, D. X. Lioe, K. Kagawa, S. Kawahito and E. Y. Park, *Microchim. Acta*, 2020, **187**, 466.
178 D. Nidzworski, K. Siuzdak, P. Niedziałkowski, R. Bogdanowicz, M. Sobaszek, J. Ryl, P. Weiher, M. Sawczak, E. Wnuk, W. A. Goddard, A. Jaramillo-Botero and T. Ossowski, *Sci. Rep.*, 2017, **7**, 15707.
179 S. Ramanathan, S. C. B. Gopinath, Z. H. Ismail, M. K. Md Arshad and P. Poopalan, *Biosens. Bioelectron.*, 2022, **197**, 113735.
180 A. Valipour and M. Roushani, *Microchim. Acta*, 2017, **184**, 2015–2022.
181 A. Pérez-García, A. Aguinaga, A. Navascués, J. Castilla and C. Ezpeleta, *Int. J. Infect. Dis.*, 2019, **89**, 131–136.
182 H. C. Lai, S. F. Chin, S. C. Pang, M. S. Henry Sum and D. Perera, *J. Nanomater.*, 2017, **2017**, 3615707.

183 M. S. Purdey, J. G. Thompson, T. M. Monro, A. D. Abell and E. P. Schartner, *Sensors*, 2015, **15**, 31904–31913.
184 J. T. Trinh, M. H. Alkahtani, I. Rampersaud, A. Rampersaud, M. Scully, R. F. Young, P. Hemmer and L. Zeng, *Biotechnol. Bioeng.*, 2018, **115**, 1427–1436.
185 Y. Wu, S. Cao, M. N. A. Alam, M. Raabe, S. Michel-Souzy, Z. Wang, M. Wagner, A. Ermakova, J. J. L. M. Cornelissen and T. Weil, *J. Mater. Chem. B*, 2021, **9**, 5621–5627.
186 R. S. Li, B. Yuan, J. H. Liu, M. L. Liu, P. F. Gao, Y. F. Li, M. Li and C. Z. Huang, *J. Mater. Chem. B*, 2017, **5**, 8719–8724.
187 A. D. Chowdhury, S. Sharmin, F. Nasrin, M. Yamazaki, F. Abe, T. Suzuki and E. Y. Park, *ACS Appl. Bio Mater.*, 2020, **3**, 3560–3568.
188 J. T. Hong, S. W. Jun, S. H. Cha, J. Y. Park, S. Lee, G. A. Shin and Y. H. Ahn, *Sci. Rep.*, 2018, **8**, 15536.
189 Z. Rahmati, M. Roushani and H. Hosseini, *Surf. Interfaces*, 2021, **22**, 100813.
190 Y. Liu, Y. Nie, M. Wang, Q. Zhang and Q. Ma, *Biosens. Bioelectron.*, 2020, **148**, 111823.
191 M. Shariati, *Biosens. Bioelectron.*, 2018, **105**, 58–64.
192 C. Li, Z. Zou, H. Liu, Y. Jin, G. Li, C. Yuan, Z. Xiao and M. Jin, *Talanta*, 2021, **225**, 122064.
193 F. Nasrin, A. D. Chowdhury, A. B. Ganganboina, O. J. Achadu, F. Hossain, M. Yamazaki and E. Y. Park, *Microchim. Acta*, 2020, **187**, 674.
194 G. Eom, A. Hwang, H. Kim, S. Yang, D. K. Lee, S. Song, K. Ha, J. Jeong, J. Jung, E.-K. Lim and T. Kang, *ACS Sens.*, 2019, **4**, 2282–2287.
195 Q. Lv, Y. Wang, C. Su, T. Lakshmipriya, S. C. B. Gopinath, K. Pandian, V. Perumal and Y. Liu, *Int. J. Biol. Macromol.*, 2019, **134**, 354–360.
196 S. R. Ahmed, J. C. Corredor, É. Nagy and S. Neethirajan, *Nanotheranostics*, 2017, **1**, 338–345.
197 A. B. Ganganboina, A. D. Chowdhury, I. M. Khoris, R. Doong, T.-C. Li, T. Hara, F. Abe, T. Suzuki and E. Y. Park, *Biosens. Bioelectron.*, 2020, **170**, 112680.
198 S. R. Ahmed, S. W. Kang, S. Oh, J. Lee and S. Neethirajan, *Heliyon*, 2018, **4**, e00766.
199 D. H. Mohsin, M. S. Mashkour and F. Fatemi, *Chem. Pap.*, 2021, **75**, 279–295.
200 A. D. Chowdhury, K. Takemura, I. M. Khorish, F. Nasrin, M. M. Ngwe Tun, K. Morita and E. Y. Park, *Nanoscale Adv.*, 2020, **2**, 699–709.
201 C. M. Das, Y. Guo, G. Yang, L. Kang, G. Xu, H.-P. Ho and K.-T. Yong, *Adv. Theory Simulations*, 2020, **3**, 2000185.
202 J.-E. Park, K. Kim, Y. Jung, J.-H. Kim and J.-M. Nam, *ChemNanoMat*, 2016, **2**, 927–936.
203 S. Manivannan and K. Ponnuchamy, *Appl. Organomet. Chem.*, 2020, **34**, e5887.
204 M. S. Draz, A. Vasan, A. Muthupandian, M. K. Kanakasabapathy, P. Thirumalaraju, A. Sreeram, S. Krishnakumar, V. Yogesh, W. Lin, X. G. Yu, R. T. Chung and H. Shafiee, *Sci. Adv.*, 2020, **6**, eabd5354.
205 P. Kannan, P. Subramanian, T. Maiyalagan and Z. Jiang, *Anal. Chem.*, 2019, **91**, 5824–5833.
206 X. Ma and P. Miao, *J. Mater. Chem. B*, 2019, **7**, 2608–2612.
207 A. B. Ganganboina, I. M. Khoris, A. D. Chowdhury, T.-C. Li and E. Y. Park, *ACS Appl. Mater. Interfaces*, 2020, **12**, 50212–50221.
208 S. Xu, W. Ouyang, P. Xie, Y. Lin, B. Qiu, Z. Lin, G. Chen and L. Guo, *Anal. Chem.*, 2017, **89**, 1617–1623.
209 M. Shariati, M. Vaezjalali and M. Sadeghi, *Anal. Chim. Acta*, 2021, **1156**, 338360.
210 Y. Zhang, G. Wu, J. Wei, Y. Ding, Y. Wei, Q. Liu and H. Chen, *Microchim. Acta*, 2021, **188**, 3.
211 S. Yadav, S. Senapati, D. Desai, S. Gahlaut, S. Kulkarni and J. P. Singh, *Colloids Surf., B*, 2021, **198**, 111477.
212 A. Cossettini and L. Selmi, *IEEE Trans Nanobioscience*, 2018, **17**, 102–109.
213 R. Viter, M. Savchuk, N. Starodub, Z. Balevicius, S. Tumenas, A. Ramanaviciene, D. Jevdokimovs, D. Erts, I. Iatsunskyi and A. Ramanavicius, *Sens. Actuators, B*, 2019, **285**, 601–606.
214 B. Negahdari, M. Darvishi and A. A. Saeedi, *Artif. Cells, Nanomed., Biotechnol.*, 2019, **47**, 455–461.
215 D. Li, H. Chen, X. Gao, X. Mei and L. Yang, *ACS Sens.*, 2021, **6**, 613–627.
216 M. W. Kim, H.-J. Park, C. Y. Park, J. H. Kim, C. H. Cho, L. M. T. Phan, J. P. Park, S. K. Kailasa, C.-H. Lee and T. J. Park, *RSC Adv.*, 2020, **10**, 29759–29764.
217 Z. Ghafary, R. Hallaj, A. Salimi and K. Akhtari, *ACS Omega*, 2019, **4**, 15323–15336.
218 S.-L. Hong, N. Zhang, L. Qin, M. Tang, Z. Ai, A. Chen, S. Wang and K. Liu, *Analyst*, 2021, **146**, 930–936.
219 C. Srisomwat, A. Yakoh, N. Chuaypen, P. Tangkijvanich, T. Vilaivan and O. Chailapakul, *Anal. Chem.*, 2021, **93**, 2879–2887.
220 G. Qiu, Z. Gai, Y. Tao, J. Schmitt, G. A. Kullak-Ublick and J. Wang, *ACS Nano*, 2020, **14**, 5268–5277.
221 M. Steinmetz, D. Lima, A. G. Viana, S. T. Fujiwara, C. A. Pessôa, R. M. Etto and K. Wohnrath, *Biosens. Bioelectron.*, 2019, **141**, 111351.
222 M. R. Rakhshani, *IEEE Sens. J.*, 2022, 1.
223 P. Etedali, M. Behbahani, H. Mohabatkar and G. Dini, *Aquaculture*, 2022, **548**, 737628.
224 S. Cajigas, D. Alzate and J. Orozco, *Microchim. Acta*, 2020, **187**, 594.
225 E. Ç. Yeter, S. Şahin, M. O. Caglayan and Z. Üstündağ, *Chem. Pap.*, 2021, **75**, 77–87.
226 L. A. Layqah and S. Eissa, *Microchim. Acta*, 2019, **186**, 224.
227 A. S. Mohammed, R. Nagarjuna, M. N. Khaja, R. Ganesan and J. Ray Dutta, *Microchim. Acta*, 2019, **186**, 566.
228 J. S. Gootenberg, O. O. Abudayyeh, M. J. Kellner, J. Joung, J. J. Collins and F. Zhang, *Science*, 2018, **360**, 439 LP–444.
229 H. Jiang, Z. Sun, C. Zhang and X. Weng, *Sens. Actuators, B*, 2022, **354**, 131232.
230 Z. Yao, Q. Zhang, W. Zhu, M. Galluzzi, W. Zhou, J. Li, A. V. Zayats and X.-F. Yu, *Nanoscale*, 2021, **13**, 10133–10142.
231 N. Cennamo, L. Pasquardini, F. Arcadio, L. Lunelli, L. Vanzetti, V. Carafa, L. Altucci and L. Zeni, *Talanta*, 2021, **233**, 122532.

232 G. Qiu, Z. Gai, L. Saleh, J. Tang, T. Gui, G. A. Kullak-Ublick and J. Wang, *ACS Nano*, 2021, **15**, 7536–7546.
233 W. A. El-Said, A. S. Al-Bogami and W. Alshitari, *Spectrochim. Acta, Part A*, 2022, **264**, 120237.
234 J. Lin, S. C. B. Gopinath, T. Lakshmipriya, Y. Chen, W. R. Yuan and M. Yang, *Int. J. Biol. Macromol.*, 2019, **141**, 564–569.
235 A. D. Chowdhury, K. Takemura, T.-C. Li, T. Suzuki and E. Y. Park, *Nat. Commun.*, 2019, **10**, 3737.
236 W.-P. Lin, W.-J. Wang, C.-H. Lee, F.-J. Jan and G.-J. Wang, *Sens. Actuators, B*, 2022, **350**, 130875.
237 F. Inci, M. G. Karaaslan, A. Mataji-Kojouri, P. A. Shah, Y. Saylan, Y. Zeng, A. Avadhani, R. Sinclair, D. T.-Y. Lau and U. Demirci, *Appl. Mater. Today*, 2020, **20**, 100709.
238 Y. Sun, L. Xu, F. Zhang, Z. Song, Y. Hu, Y. Ji, J. Shen, B. Li, H. Lu and H. Yang, *Biosens. Bioelectron.*, 2017, **89**, 906–912.
239 H.-W. Chu, C.-S. Lai, J.-Y. Ko, S. G. Harroun, C.-I. Chuang, R. Y. L. Wang, B. Unnikrishnan and C.-C. Huang, *ACS Sens.*, 2019, **4**, 1543–1551.
240 C. Singhal, A. Dubey, A. Mathur, C. S. Pundir and J. Narang, *Process Biochem.*, 2018, **74**, 35–42.
241 P. Brangel, A. Sobarzo, C. Parolo, B. S. Miller, P. D. Howes, S. Gelkop, J. J. Lutwama, J. M. Dye, R. A. McKendry, L. Lobel and M. M. Stevens, *ACS Nano*, 2018, **12**, 63–73.
242 P. Teengam, W. Siangproh, S. Tontisirin, A. Jiraseree-amornkun, N. Chuaypen, P. Tangkijvanich, C. S. Henry, N. Ngamrojanavanich and O. Chailapakul, *Sens. Actuators, B*, 2021, **326**, 128825.
243 S. G. Hwang, K. Ha, K. Guk, D. K. Lee, G. Eom, S. Song, T. Kang, H. Park, J. Jung and E.-K. Lim, *Sci. Rep.*, 2018, **8**, 12999.
244 C. Huang, T. Wen, F.-J. Shi, X.-Y. Zeng and Y.-J. Jiao, *ACS Omega*, 2020, **5**, 12550–12556.
245 G. Eom, A. Hwang, D. K. Lee, K. Guk, J. Moon, J. Jeong, J. Jung, B. Kim, E.-K. Lim and T. Kang, *ACS Appl. Bio Mater.*, 2019, **2**, 1233–1240.
246 M. E. Hamdy, M. Del Carlo, H. A. Hussein, T. A. Salah, A. H. El-Deeb, M. M. Emara, G. Pezzoni and D. Compagnone, *J. Nanobiotechnol.*, 2018, **16**, 48.
247 H. H. Fakih, M. M. Itani and P. Karam, *Sens. Actuators, B*, 2017, **250**, 446–452.
248 J.-W. Kim, M. Kim, K. K. Lee, K. H. Chung and C.-S. Lee, *Nanomater.*, 2020, 10.
249 Z. Liu, J. Li, Z. Liu, J. Li, Z. Li, C. Wang, J. Wang and L. Guo, *BMC Vet. Res.*, 2019, **15**, 110.
250 M. Wang, Y. Yan, R. Wang, L. Wang, H. Zhou, Y. Li, L. Tang, Y. Xu, Y. Jiang, W. Cui and X. Qiao, *Front. Microbiol.*, 2019, **10**, 2884.
251 L. Zhang, Y. Luo, L. Liang, J. Li and S. Cui, *Infect., Genet. Evol.*, 2018, **60**, 1–6.
252 F. Zang, Z. Su, L. Zhou, K. Konduru, G. Kaplan and S. Y. Chou, *Adv. Mater.*, 2019, **31**, 1902331.
253 F. Nasrin, A. D. Chowdhury, K. Takemura, J. Lee, O. Adegoke, V. K. Deo, F. Abe, T. Suzuki and E. Y. Park, *Biosens. Bioelectron.*, 2018, **122**, 16–24.
254 K. Takemura, J. Lee, T. Suzuki, T. Hara, F. Abe and E. Y. Park, *Sens. Actuators, B*, 2019, **296**, 126672.
255 F. Nasrin, A. D. Chowdhury, K. Takemura, I. Kozaki, H. Honda, O. Adegoke and E. Y. Park, *Anal. Chim. Acta*, 2020, **1109**, 148–157.
256 O. Adegoke, M. Morita, T. Kato, M. Ito, T. Suzuki and E. Y. Park, *Biosens. Bioelectron.*, 2017, **94**, 513–522.
257 M. Shariati, M. Ghorbani, P. Sasanpour and A. Karimizefreh, *Anal. Chim. Acta*, 2019, **1048**, 31–41.
258 S. L. Manoto, A. El-Hussein, R. Malabi, L. Thobakgale, S. Ombinda-Lemboumba, Y. A. Attia, M. A. Kasem and P. Mthunzi-Kufa, *Saudi J. Biol. Sci.*, 2021, **28**, 78–89.
259 S. Oh, J. Kim, V. T. Tran, D. K. Lee, S. R. Ahmed, J. C. Hong, J. Lee, E. Y. Park and J. Lee, *ACS Appl. Mater. Interfaces*, 2018, **10**, 12534–12543.
260 E. Alipour, S. P. Shariatpanahi, H. Ghourchian, B. Piro, M. Fathipour, S. M. Boutorabi, S. L. Znoyko and P. I. Nikitin, *Microchim. Acta*, 2020, **187**, 463.
261 S. R. Ahmed, J. Mogus, R. Chand, E. Nagy and S. Neethirajan, *Biosens. Bioelectron.*, 2018, **103**, 45–53.
262 B. Luo, Y. Xu, S. Wu, M. Zhao, P. Jiang, S. Shi, Z. Zhang, Y. Wang, L. Wang and Y. Liu, *Biosens. Bioelectron.*, 2018, **100**, 169–175.
263 S. R. Ahmed, É. Nagy and S. Neethirajan, *RSC Adv.*, 2017, **7**, 40849–40857.
264 A. Karimizefreh, F. A. Mahyari, M. VaezJalali, R. Mohammadpour and P. Sasanpour, *Microchim. Acta*, 2017, **184**, 1729–1737.
265 S. R. Ahmed, J. Kim, V. T. Tran, T. Suzuki, S. Neethirajan, J. Lee and E. Y. Park, *Sci. Rep.*, 2017, **7**, 44495.
266 Y. Zhang, Y. Gao, X. Zhang, H. Wang, T. Xia, C. Bian, S. Liang, X. Tang and X. Wang, *Sens. Actuators, B*, 2019, **284**, 296–304.
267 L. E. Ahangar and M. A. Mehrgardi, *Bioelectrochemistry*, 2017, **117**, 83–88.
268 S. C. Razo, V. G. Panferov, I. V. Safenkova, Y. A. Varitsev, A. V. Zherdev, E. N. Pakina and B. B. Dzantiev, *Sensors*, 2018, 18.
269 R. Jin, L. Zhai, Q. Zhu, J. Feng and X. Pan, *Aquaculture*, 2020, **528**, 735554.
270 A. Bosak, N. Saraf, A. Willenberg, M. W. C. Kwan, B. W. Alto, G. W. Jackson, R. H. Batchelor, T. D. Nguyen-Huu, V. Sankarapani, G. D. Parks, S. Seal and B. J. Willenberg, *RSC Adv.*, 2019, **9**, 23752–23763.
271 L.-H. Xiong, S. Huang, Y. Huang, F. Yin, F. Yang, Q. Zhang, J. Cheng, R. Zhang and X. He, *ACS Appl. Mater. Interfaces*, 2020, **12**, 12525–12532.
272 X. Mi, E. M. Lucier, D. G. Turpeinen, E. L. L. Yeo, J. C. Y. Kah and C. L. Heldt, *Analyst*, 2019, **144**, 5486–5496.
273 L. Zhan, W. B. Wu, C. M. Li and C. Z. Huang, *J. Anal. Test.*, 2017, **1**, 298–305.
274 M. Khater, A. de la Escosura-Muñiz, D. Quesada-González and A. Merkoçi, *Anal. Chim. Acta*, 2019, **1046**, 123–131.
275 T. Ngamdee, L. S. Yin, S. Vongpunsawad, Y. Poovorawan, W. Surareungchai and B. Lertanantawong, *Anal. Chim. Acta*, 2020, **1134**, 10–17.

276 M. Khater, A. de la Escosura-Muñiz, L. Altet and A. Merkoçi, *Anal. Chem.*, 2019, **91**, 4790–4796.
277 J. Kim, S. Y. Oh, S. Shukla, S. B. Hong, N. S. Heo, V. K. Bajpai, H. S. Chun, C.-H. Jo, B. G. Choi, Y. S. Huh and Y.-K. Han, *Biosens. Bioelectron.*, 2018, **107**, 118–122.
278 O. Adegoke and E. Y. Park, *J. Mater. Chem. B*, 2017, **5**, 3047–3058.
279 I. M. Khoris, A. D. Chowdhury, T.-C. Li, T. Suzuki and E. Y. Park, *Anal. Chim. Acta*, 2020, **1110**, 64–71.
280 L. Zhan, T. Yang, C. M. Li, W. B. Wu and C. Z. Huang, *Sens. Actuators, B*, 2018, **255**, 1291–1297.
281 S. R. Ahmed, K. Takemeura, T.-C. Li, N. Kitamoto, T. Tanaka, T. Suzuki and E. Y. Park, *Biosens. Bioelectron.*, 2017, **87**, 558–565.
282 A. Karami and M. Hasani, *Anal. Chim. Acta*, 2020, **1102**, 119–129.
283 C. Lee, P. Wang, M. A. Gaston, A. A. Weiss and P. Zhang, in *Biosensors and Biodetection. Methods in Molecular Biology*, ed. A. Rasooly and B. Prickril, Humana Press, New York, NY, 2017, Vol. 157, pp. 109–116.
284 Y. Horiguchi, T. Goda, A. Matsumoto, H. Takeuchi, S. Yamaoka and Y. Miyahara, *Langmuir*, 2019, **35**, 1798–1806.
285 Y.-W. Zhang, W.-S. Liu, J.-S. Chen, H.-L. Niu, C.-J. Mao and B.-K. Jin, *Sens. Actuators, B*, 2020, **321**, 128456.
286 B. Sun, J. Dong, L. Cui, T. Feng, J. Zhu, X. Liu and S. Ai, *Biosens. Bioelectron.*, 2019, **124–125**, 1–7.
287 Y. Hu, Y. Huang, Y. Wang, C. Li, W. Wong, X. Ye and D. Sun, *Anal. Chim. Acta*, 2018, **1035**, 136–145.
288 Y. Tian, Q. Lu, X. Guo, S. Wang, Y. Gao and L. Wang, *Nanoscale*, 2020, **12**, 7776–7781.
289 Z. Han, L. Chen, Q. Weng, Y. Zhou, L. Wang, C. Li and J. Chen, *Sens. Actuators, B*, 2018, **258**, 508–516.
290 T. A. Freitas, C. A. Proença, T. A. Baldo, E. M. Materón, A. Wong, R. F. Magnani and R. C. Faria, *Talanta*, 2019, **205**, 120110.
291 L. Wang, M. Ren, L. Liang and C. Zhang, *Chem. Sci.*, 2018, **9**, 4942–4949.
292 M. Aminul Islam and M. Ziaul Ahsan, *Am. J. Nanosci.*, 2020, **6**, 6.
293 H. Tan, G. Tang, Z. Wang, Q. Li, J. Gao and S. Wu, *Anal. Chim. Acta*, 2016, **940**, 136–142.
294 H. Yoo, J. Shin, J. Sim, H. Cho and S. Hong, *Biosens. Bioelectron.*, 2020, **168**, 112561.
295 S. Zhou, M. Jin, R. Tan, Z. Shen, J. Yin, Z. Qiu, Z. Chen, D. Shi, H. Li, Z. Yang, H. Wang, Z. Gao, J. Li and D. Yang, *Chemosphere*, 2021, 132995.
296 L. Ye, X. Zhang, N. Yang, S. Zhao, H. Wang and Z. Wang, *J. Biomed. Nanotechnol.*, 2021, **17**, 606–614.
297 R. Wu, B. Meng, M. Corredig and M. W. Griffiths, *Food Microbiol.*, 2022, **102**, 103921.
298 B. Yin, W. K. H. Ho, Q. Zhang, C. Li, Y. Huang, J. Yan, H. Yang, J. Hao, S. H. D. Wong and M. Yang, *ACS Appl. Mater. Interfaces*, 2022, **14**, 4714–4724.
299 K. Wu, R. Saha, D. Su, V. D. Krishna, J. Liu, M. C.-J. Cheeran and J.-P. Wang, *ACS Appl. Nano Mater.*, 2020, **3**, 9560–9580.
300 D. Su, K. Wu, V. D. Krishna, T. Klein, J. Liu, Y. Feng, A. M. Perez, M. C.-J. Cheeran and J.-P. Wang, *Front. Microbiol.*, 2019, **10**, 1077.
301 K. Wu, T. Klein, V. D. Krishna, D. Su, A. M. Perez and J.-P. Wang, *ACS Sens.*, 2017, **2**, 1594–1601.
302 J. Zhong, E. L. Rösch, T. Viereck, M. Schilling and F. Ludwig, *ACS Sens.*, 2021, **6**, 976–984.
303 K. Wu, J. Liu, R. Saha, D. Su, V. D. Krishna, M. C.-J. Cheeran and J.-P. Wang, *ACS Appl. Mater. Interfaces*, 2020, **12**, 13686–13697.
304 P. P. Sharma, E. Albisetti, M. Massetti, M. Scolari, C. La Torre, M. Monticelli, M. Leone, F. Damin, G. Gervasoni, G. Ferrari, F. Salice, E. Cerquaglia, G. Falduti, M. Cretich, E. Marchisio, M. Chiari, M. Sampietro, D. Petti and R. Bertacco, *Sens. Actuators, B*, 2017, **242**, 280–287.
305 L. Li, K.-Y. Mak and Y. Zhou, *Chin. Phys. B*, 2020, **29**, 88701.
306 M. Sayhi, O. Ouerghi, K. Belgacem, M. Arbi, Y. Tepeli, A. Ghram, Ü. Anik, L. Österlund, D. Laouini and M. F. Diouani, *Biosens. Bioelectron.*, 2018, **107**, 170–177.
307 T. Wu, X. Li, Y. Fu, X. Ding, Z. Li, G. Zhu and J. Fan, *Talanta*, 2020, **209**, 120550.
308 J. Lee, K. Takemura, C. N. Kato, T. Suzuki and E. Y. Park, *ACS Appl. Mater. Interfaces*, 2017, **9**, 27298–27304.
309 A. B. Ganganboina, A. D. Chowdhury, I. M. Khoris, F. Nasrin, K. Takemura, T. Hara, F. Abe, T. Suzuki and E. Y. Park, *Biosens. Bioelectron.*, 2020, **157**, 112169.
310 K. C. Sanjaya, A. Ranzoni, J. Hung, M. A. T. Blaskovich, D. Watterson, P. R. Young and M. A. Cooper, *Anal. Chim. Acta*, 2020, **1107**, 85–91.
311 L. Luo, J. Yang, K. Liang, C. Chen, X. Chen and C. Cai, *Talanta*, 2019, **202**, 21–26.
312 C. Wang, C. Wang, X. Wang, K. Wang, Y. Zhu, Z. Rong, W. Wang, R. Xiao and S. Wang, *ACS Appl. Mater. Interfaces*, 2019, **11**, 19495–19505.
313 F. Zhang, L. Luo, H. Gong, C. Chen and C. Cai, *RSC Adv.*, 2018, **8**, 32262–32268.
314 A. Barrios-Gumiel, D. Sepúlveda-Crespo, J. L. Jiménez, R. Gómez, M. Á. Muñoz-Fernández and F. J. de la Mata, *Colloids Surf., B*, 2019, **181**, 360–368.
315 X. Peng, G. Luo, Z. Wu, W. Wen, X. Zhang and S. Wang, *ACS Appl. Mater. Interfaces*, 2019, **11**, 41148–41156.
316 Z. Wu, T. Zeng, W.-J. Guo, Y.-Y. Bai, D.-W. Pang and Z.-L. Zhang, *ACS Appl. Mater. Interfaces*, 2019, **11**, 5762–5770.
317 F. Luo, C. Long, Z. Wu, H. Xiong, M. Chen, X. Zhang, W. Wen and S. Wang, *Sens. Actuators, B*, 2020, **310**, 127831.
318 B. Tian, J. Fock, G. A. S. Minero and M. F. Hansen, *Biosens. Bioelectron.*, 2020, **160**, 112219.
319 M. Pirzada and Z. Altintas, *Micromachines*, 2020, **11**, 356.
320 H. Yanagawa, A. Inoue, H. Sugimoto, M. Shioi and M. Fujii, *MRS Commun.*, 2019, **9**, 1079–1086.
321 J. F. F. Ribeiro, M. I. A. Pereira, L. G. Assis, P. E. Cabral Filho, B. S. Santos, G. A. L. Pereira, C. R. Chaves, G. S. Campos, S. I. Sardi, G. Pereira and A. Fontes, *J. Photochem. Photobiol., B*, 2019, **194**, 135–139.
322 A. M. J. Jimenez, A. Moulick, L. Richtera, L. Krejcova, L. Kalina, R. Datta, M. Svobodova, D. Hynek, M. Masarik,

Z. Heger and V. Adam, *Sens. Actuators, B*, 2018, **258**, 295–303.
323 R. Q. Zhang, S. L. Hong, C. Y. Wen, D. W. Pang and Z. L. Zhang, *Biosens. Bioelectron.*, 2018, **100**, 348–354.
324 G. R. Bardajee, M. Zamani, H. Mahmoodian, H. Elmizadeh, H. Yari, L. Jouyandeh, R. Shirkavand and M. Sharifi, *Spectrochim. Acta, Part A*, 2022, **269**, 120702.
325 L. Meng, K. Xiao, X. Zhang, C. Du and J. Chen, *Sens. Actuators, B*, 2020, **305**, 127480.
326 H. Ashiba, Y. Sugiyama, X. Wang, H. Shirato, K. Higo-Moriguchi, K. Taniguchi, Y. Ohki and M. Fujimaki, *Biosens. Bioelectron.*, 2017, **93**, 260–266.
327 N. A. S. Omar, Y. W. Fen, J. Abdullah, M. H. M. Zaid, W. M. E. M. M. Daniyal and M. A. Mahdi, *Opt. Laser Technol.*, 2019, **114**, 204–208.
328 Y. Zhao, J. Chen, Z. Hu, Y. Chen, Y. Tao, L. Wang, L. Li, P. Wang, H.-Y. Li, J. Zhang, J. Tang and H. Liu, *Biosens. Bioelectron.*, 2022, **202**, 113974.
329 F. Sabzehparvar, T. Rahmani Cherati, A. Mohsenifar, T. Roodbar Shojaei and M. Tabatabaei, *Spectrochim. Acta, Part A*, 2019, **212**, 173–179.
330 L. Luo, F. Zhang, C. Chen and C. Cai, *Anal. Chem.*, 2019, **91**, 15748–15756.
331 Y. Ma, G. Mao, W. Huang, G. Wu, W. Yin, X. Ji, Z. Deng, Z. Cai, X.-E. Zhang, Z. He and Z. Cui, *J. Am. Chem. Soc.*, 2019, **141**, 13454–13458.
332 M. Bao, E. Jensen, Y. Chang, G. Korensky and K. Du, *ACS Appl. Mater. Interfaces*, 2020, **12**, 43435–43443.
333 B. Babamiri, R. Hallaj and A. Salimi, *Sens. Actuators, B*, 2018, **254**, 551–560.
334 Z. Ranjbar-Navazi, Y. Omidi, M. Eskandani and S. Davaran, *TrAC, Trends Anal. Chem.*, 2019, **118**, 386–400.
335 F. Zhang, D. Yi, H. Sun and H. Zhang, *J. Nanosci. Nanotechnol.*, 2014, **14**, 1409–1424.
336 D. B. Ngo, T. Chaibun, L. S. Yin, B. Lertanantawong and W. Surareungchai, *Anal. Bioanal. Chem.*, 2021, **413**, 1027–1037.
337 J. Chen, Y. Kong, W. Wang, H. Fang, Y. Wo, D. Zhou, Z. Wu, Y. Li and S. Chen, *Chem. Commun.*, 2016, **52**, 4025–4028.
338 S. R. Ahmed and S. Neethirajan, *Glob. Challenges*, 2018, **2**, 1700071.
339 O. J. Achadu, K. Takemura, I. M. Khoris and E. Y. Park, *Sens. Actuators, B*, 2020, **321**, 128494.
340 H. Malekzad, P. Sahandi Zangabad, H. Mirshekari, M. Karimi and M. R. Hamblin, *Nanotechnol. Rev.*, 2017, **6**, 301–329.
341 Z. Bognár, M. I. De Jonge and R. E. Gyurcsányi, *Nanoscale*, 2022, **14**, 2296–2303.
342 N. Wu, H.-C. Zhang, X.-H. Sun, F.-N. Guo, L.-X. Feng, T. Yang and J.-H. Wang, *Sens. Actuators, B*, 2022, **352**, 131041.
343 L. L. Zheng, X. J. Shuai, Y. Liu, C. M. Li, S. J. Zhen, J. J. Liu, Y. F. Li and C. Z. Huang, *Chem. Eng. J.*, 2022, **434**, 134658.
344 Y. Tao, K. Yi, H. Wang, H.-W. Kim, K. Li, X. Zhu and M. Li, *J. Colloid Interface Sci.*, 2022, **613**, 406–414.
345 Y. Tao, Y.-H. Lao, K. Yi, Y. Xu, H. Wang, D. Shao, J. Wang and M. Li, *Talanta*, 2021, **234**, 122675.
346 N. Gao, F. Gao, S. He, Q. Zhu, J. Huang, H. Tanaka and Q. Wang, *Anal. Chim. Acta*, 2017, **951**, 58–67.
347 F. Jin, H. Li and D. Xu, *Anal. Chim. Acta*, 2019, **1077**, 297–304.
348 A. D. Kurdekar, L. A. A. Chunduri, S. M. Chelli, M. K. Haleyurgirisetty, E. P. Bulagonda, J. Zheng, I. K. Hewlett and V. Kamisetti, *RSC Adv.*, 2017, **7**, 19863–19877.
349 V. I. Kukushkin, N. M. Ivanov, A. A. Novoseltseva, A. S. Gambaryan, I. V. Yaminsky, A. M. Kopylov and E. G. Zavyalova, *PLoS One*, 2019, **14**, e0216247.
350 N. N. Durmanov, R. R. Guliev, A. V. Eremenko, I. A. Boginskaya, I. A. Ryzhikov, E. A. Trifonova, E. V. Putlyaev, A. N. Mukhin, S. L. Kalnov, M. V. Balandina, A. P. Tkachuk, V. A. Gushchin, A. K. Sarychev, A. N. Lagarkov, I. A. Rodionov, A. R. Gabidullin and I. N. Kurochkin, *Sens. Actuators, B*, 2018, **257**, 37–47.
351 E. Khristunova, J. Barek, B. Kratochvil, E. Korotkova, E. Dorozhko and V. Vyskocil, *Bioelectrochemistry*, 2020, **135**, 107576.
352 M. Awan, S. Rauf, A. Abbas, M. H. Nawaz, C. Yang, S. A. Shahid, N. Amin and A. Hayat, *J. Mol. Liq.*, 2020, **317**, 114014.
353 Y. Khristunova, E. Korotkova, B. Kratochvil, J. Barek, E. Dorozhko, V. Vyskocil, E. Plotnikov, O. Voronova and V. Sidelnikov, *Sensors*, 2019, 19.
354 L. Gou, Y. Sheng, Q. Peng, J. Ling, H. Yue, F. Chen and H. Tang, *Sens. Actuators, B*, 2020, **312**, 127987.
355 V. M. Generalov, O. V. Naumova, B. I. Fomin, S. A. P'yankov, I. V. Khlistun, A. S. Safatov, B. N. Zaitsev, E. G. Zaitseva and A. L. Aseev, *Optoelectron. Instrum. Data Process.*, 2019, **55**, 618–622.
356 M. Uhm, J.-M. Lee, J. Lee, J. H. Lee, S. Choi, B.-G. Park, D. M. Kim, S.-J. Choi, H.-S. Mo, Y.-J. Jeong and D. H. Kim, *Sensors*, 2019, 19.
357 S. Choi, H.-S. Mo, J. Kim, S. Kim, S. M. Lee, S.-J. Choi, D. M. Kim, D.-W. Park and D. H. Kim, *Curr. Appl. Phys.*, 2020, **20**, 828–833.
358 K. A. Malsagova, T. O. Pleshakova, R. A. Galiullin, I. D. Shumov, A. F. Kozlov, T. S. Romanova, V. P. Popov, A. V. Glukhov, V. A. Konev, A. I. Archakov and Y. D. Ivanov, *Coatings*, 2020, 10.
359 K. A. Malsagova, T. O. Pleshakova, R. A. Galiullin, A. L. Kaysheva, I. D. Shumov, M. A. Ilnitskii, V. P. Popov, A. V. Glukhov, A. I. Archakov and Y. D. Ivanov, *Anal. Methods*, 2018, **10**, 2740–2749.
360 A. A. Leonardi, M. J. Lo Faro, S. Petralia, B. Fazio, P. Musumeci, S. Conoci, A. Irrera and F. Priolo, *ACS Sens.*, 2018, **3**, 1690–1697.
361 M. M. N. Nuzaihan, U. Hashim, M. K. Md Arshad, S. R. Kasjoo, S. F. A. Rahman, A. R. Ruslinda, M. F. M. Fathil, R. Adzhri and M. M. Shahimin, *Biosens. Bioelectron.*, 2016, **83**, 106–114.
362 K. A. Gonchar, S. N. Agafilushkina, D. V. Moiseev, I. V. Bozhev, A. A. Manykin, E. A. Kropotkina, A. S. Gambaryan and L. A. Osminkina, *Mater. Res. Express*, 2020, **7**, 35002.

363 M. B. Gongalsky, U. A. Tsurikova, J. V. Samsonova, G. Z. Gvindzhiliiia, K. A. Gonchar, N. Y. Saushkin, A. A. Kudryavtsev, E. A. Kropotkina, A. S. Gambaryan and L. A. Osminkina, *Results Mater.*, 2020, **6**, 100084.
364 C. Singhal, A. Ingle, D. Chakraborty, A. K. P. N., C. S. Pundir and J. Narang, *Int. J. Biol. Macromol.*, 2017, **98**, 84–93.
365 N. Wiriyachaiporn, S. Sirikaew, S. Bamrungsap, T. Limcharoen, P. Polkankosit, P. Roeksrungruang and K. Ponlamuangdee, *Anal. Methods*, 2021, **13**, 1687–1694.
366 J. Zhou, M. Ren, W. Wang, L. Huang, Z. Lu, Z. Song, M. F. Foda, L. Zhao and H. Han, *Anal. Chem.*, 2020, **92**, 8802–8809.
367 L. Ding, C. Xiang and G. Zhou, *Talanta*, 2018, **181**, 65–72.
368 S. Chen, L. Luo, L. Wang, C. Chen, H. Gong and C. Cai, *Analyst*, 2021, **146**, 3924–3932.
369 Y. Liu, T. Shen, L. Hu, H. Gong, C. Chen, X. Chen and C. Cai, *Sens. Actuators, B*, 2017, **253**, 1188–1193.
370 B. Yang, H. Gong, C. Chen, X. Chen and C. Cai, *Biosens. Bioelectron.*, 2017, **87**, 679–685.
371 W. S. Lee, J. Ahn, S. Jung, J. Lee, T. Kang and J. Jeong, *BioChip J.*, 2021, **15**, 260–267.
372 M. E. Klaczko, K. Lucas, A. T. Salminen, M. C. McCloskey, B. Ozgurun, B. M. Ward, J. Flax and J. L. McGrath, *Analyst*, 2022, **147**, 213–222.
373 M. S. Draz, M. Venkataramani, H. Lakshminarayanan, E. Saygili, M. Moazeni, A. Vasan, Y. Li, X. Sun, S. Hua, X. G. Yu and H. Shafiee, *Nanoscale*, 2018, **10**, 11841–11849.
374 C. Singhal, C. S. Pundir and J. Narang, *Biosens. Bioelectron.*, 2017, **97**, 75–82.
375 E. P. Simão, D. B. S. Silva, M. T. Cordeiro, L. H. V. Gil, C. A. S. Andrade and M. D. L. Oliveira, *Talanta*, 2020, **208**, 120338.
376 F. Khosravi-Nejad, M. Teimouri, S. Jafari Marandi and M. Shariati, *Appl. Phys. A: Mater. Sci. Process.*, 2019, **125**, 616.
377 M. Shariati, M. Sadeghi and S. H. R. Shojaei, *Anal. Chim. Acta*, 2022, **1195**, 339442.
378 M. H. Nguyen, H. H. Nguyen and A. T. Mai, *Sens. Actuators, A*, 2020, **312**, 112171.
379 M. Shariati and M. Sadeghi, *Anal. Bioanal. Chem.*, 2020, **412**, 5367–5377.
380 F. Zhao, Y. Bai, L. Cao, G. Han, C. Fang, S. Wei and Z. Chen, *J. Electroanal. Chem.*, 2020, **867**, 114184.
381 S. H. Baek, C. Y. Park, T. P. Nguyen, M. W. Kim, J. P. Park, C. Choi, S. Y. Kim, S. K. Kailasa and T. J. Park, *Food Control*, 2020, **114**, 107225.
382 C.-C. Chen, Z.-L. Lai, G.-J. Wang and C.-Y. Wu, *Biosens. Bioelectron.*, 2016, **77**, 603–608.
383 J. Kim, J. H. Kwon, J. Jang, H. Lee, S. Kim, Y. K. Hahn, S. K. Kim, K. H. Lee, S. Lee, H. Pyo, C.-S. Song and J. Lee, *Biosens. Bioelectron.*, 2018, **112**, 209–215.
384 A. Mehranfar, M. Khavani and M. Izadyar, *J. Mol. Liq.*, 2022, **345**, 117852.
385 Y. Xia, Y. Chen, Y. Tang, G. Cheng, X. Yu, H. He, G. Cao, H. Lu, Z. Liu and S.-Y. Zheng, *ACS Sens.*, 2019, **4**, 3298–3307.
386 G. Biasotto, J. P. C. Costa, P. I. Costa and M. A. Zaghete, *Appl. Phys. A: Mater. Sci. Process.*, 2019, **125**, 821.
387 R. van den Hurk, M. Baghelani, J. Chen, M. Daneshmand and S. Evoy, *Sens. Actuators, A*, 2019, **296**, 186–191.
388 J. Liu, M. Xu, B. Tang, L. Hu, F. Deng, H. Wang, D.-W. Pang, Z. Hu, M. Wang and Y. Zhou, *Small*, 2019, **15**, 1803788.
389 W. Hou, Y. Li, W. Kang, X. Wang, X. Wu, S. Wang and F. Liu, *Sci. Rep.*, 2019, **9**, 1307.
390 J. Liu, M. Su, X. Chen, Z. Li, Z. Fang and L. Yi, *J. Biomater. Appl.*, 2022, 08853282211063298.
391 Q. Zhang, J. Li, Y. Li, G. Tan, M. Sun, Y. Shan, Y. Zhang, X. Wang, K. Song, R. Shi, L. Huang, F. Liu, Y. Yi and X. Wu, *Biosens. Bioelectron.*, 2022, 113978.
392 K.-I. Joo, Y. Lei, C.-L. Lee, J. Lo, J. Xie, S. F. Hamm-Alvarez and P. Wang, *ACS Nano*, 2008, **2**, 1553–1562.
393 Z.-Y. Hong, Z.-L. Zhang, B. Tang, J. Ao, C. Wang, C. Yu and D.-W. Pang, *Anal. Chem.*, 2018, **90**, 14020–14028.
394 L.-J. Zhang, S. Wang, L. Xia, C. Lv, H.-W. Tang, Z. Liang, G. Xiao and D.-W. Pang, *mBio*, 2020, **11**, e00135–20.
395 L.-J. Zhang, L. Xia, S.-L. Liu, E.-Z. Sun, Q.-M. Wu, L. Wen, Z.-L. Zhang and D.-W. Pang, *ACS Nano*, 2018, **12**, 474–484.
396 L. L. Zheng, C. M. Li, S. J. Zhen, Y. F. Li and C. Z. Huang, *Nanoscale*, 2017, **9**, 7880–7887.
397 J. A. Coultas, R. Smyth and P. J. Openshaw, *Thorax*, 2019, **74**, 986–993.
398 Y.-B. Yang, Y.-D. Tang, Y. Hu, F. Yu, J.-Y. Xiong, M.-X. Sun, C. Lyu, J.-M. Peng, Z.-J. Tian, X.-H. Cai and T.-Q. An, *Nano Lett.*, 2020, **20**, 1417–1427.
399 E.-Z. Sun, A.-A. Liu, Z.-L. Zhang, S.-L. Liu, Z.-Q. Tian and D.-W. Pang, *ACS Nano*, 2017, **11**, 4395–4406.
400 Q.-M. Wu, S.-L. Liu, G. Chen, W. Zhang, E.-Z. Sun, G.-F. Xiao, Z.-L. Zhang and D.-W. Pang, *Small*, 2018, **14**, 1702841.
401 L. L. Zheng, C. M. Li, S. J. Zhen, Y. F. Li and C. Z. Huang, *Nanoscale*, 2016, **8**, 18635–18639.
402 J. Liu, C. Yu, J.-F. Gui, D.-W. Pang and Q.-Y. Zhang, *Front. Microbiol.*, 2018, **9**, 2797.
403 L. Wen, Y. Lin, Z.-L. Zhang, W. Lu, C. Lv, Z.-L. Chen, H.-Z. Wang and D.-W. Pang, *Biomaterials*, 2016, **99**, 24–33.
404 Y. Ma, M. Wang, W. Li, Z. Zhang, X. Zhang, T. Tan, X.-E. Zhang and Z. Cui, *Nat. Commun.*, 2017, **8**, 15318.
405 A. Pramanik, Y. Gao, S. Patibandla, D. Mitra, M. G. McCandless, L. A. Fassero, K. Gates, R. Tandon and P. C. Ray, *J. Phys. Chem. Lett.*, 2021, **12**, 2166–2171.
406 R. Cheng, F. Zhu, M. Huang, Q. Zhang, H. H. Yan, X. H. Zhao, F. K. Luo, C. M. Li, H. Liu, G. L. Liang, C. Z. Huang and J. Wang, *Biosens. Bioelectron.*, 2022, **202**, 114001.
407 H. Zhao, B. Ni, X. Jin, H. Zhang, J. J. Hou, L. Hou, J. H. Marsh, L. Dong, S. Li, X. W. Gao, D. Shi, X. Liu and J. Xiong, *Appl. Opt.*, 2022, **61**, 546–553.
408 J. C. Abrego-Martinez, M. Jafari, S. Chergui, C. Pavel, D. Che and M. Siaj, *Biosens. Bioelectron.*, 2022, **195**, 113595.
409 G. Pang, Y. Zhang, X. Wang, H. Pan, X. Zhang, Y. Li, S. Zhang, C. Yan, L. Sun, H. Wang and J. Chang, *Nano Today*, 2021, **40**, 101264.

410 T. Wiegand, M. Fratini, F. Frey, K. Yserentant, Y. Liu, E. Weber, K. Galior, J. Ohmes, F. Braun, D.-P. Herten, S. Boulant, U. S. Schwarz, K. Salaita, E. A. Cavalcanti-Adam and J. P. Spatz, *Nat. Commun.*, 2020, **11**, 32.

411 F. Xu, A. Bandara, H. Akiyama, B. Eshaghi, D. Stelter, T. Keyes, J. E. Straub, S. Gummuluru and B. M. Reinhard, *Proc. Natl. Acad. Sci. U. S. A.*, 2018, **115**, E9041 LP–E9050.

412 R. Schubert, S. Trenholm, K. Balint, G. Kosche, C. S. Cowan, M. A. Mohr, M. Munz, D. Martinez-Martin, G. Fläschner, R. Newton, J. Krol, B. G. Scherf, K. Yonehara, A. Wertz, A. Ponti, A. Ghanem, D. Hillier, K.-K. Conzelmann, D. J. Müller and B. Roska, *Nat. Biotechnol.*, 2018, **36**, 81–88.

413 V. Marjomäki, T. Lahtinen, M. Martikainen, J. Koivisto, S. Malola, K. Salorinne, M. Pettersson and H. Häkkinen, *Proc. Natl. Acad. Sci. U. S. A.*, 2014, **111**, 1277 LP–1281.

414 L. Luo, F. Zhang, C. Chen and C. Cai, *Microchim. Acta*, 2020, **187**, 140.

415 M. Shamsipur, L. Samandari, L. Farzin and A. Besharati-Seidani, *Microchem. J.*, 2021, **160**, 105714.

416 J. Xu, F. Merlier, B. Avalle, V. Vieillard, P. Debré, K. Haupt and B. Tse Sum Bui, *ACS Appl. Mater. Interfaces*, 2019, **11**, 9824–9831.

417 S. Wankar, N. W. Turner and R. J. Krupadam, *Biosens. Bioelectron.*, 2016, **82**, 20–25.

418 M. Pirzada and Z. Altintas, in *Molecular Imprinting for Nanosensors and Other Sensing Applications*, ed. A. Denizli, Elsevier, Amsterdam, 1st edn, 2021, pp. 367–406.

419 A. J. Ruiz-Sanchez, C. Parolo, B. S. Miller, E. R. Gray, K. Schlegel and R. A. McKendry, *J. Mater. Chem. B*, 2017, **5**, 7262–7266.

420 N. A. S. Omar, Y. W. Fen, S. Saleviter, Y. M. Kamil, W. M. E. M. M. Daniyal, J. Abdullah and M. A. Mahdi, *Sens. Actuators, A*, 2020, **303**, 111830.

421 C. Liu, J. Dong, S. Ning, J. Hou, G. I. N. Waterhouse, Z. Cheng and S. Ai, *Microchim. Acta*, 2018, **185**, 423.

422 J. Yang, W. Feng, K. Liang, C. Chen and C. Cai, *Talanta*, 2020, **212**, 120744.

423 M. Antipchik, D. Polyakov, E. Sinitsyna, A. Dzhuzha, M. Shavlovsky, E. Korzhikova-Vlakh and T. Tennikova, *Sensors*, 2020, 20.

424 C.-Z. Wang, H.-H. Han, X.-Y. Tang, D.-M. Zhou, C. Wu, G.-R. Chen, X.-P. He and H. Tian, *ACS Appl. Mater. Interfaces*, 2017, **9**, 25164–25170.

425 W. Diao, M. Tang, S. Ding, X. Li, W. Cheng, F. Mo, X. Yan, H. Ma and Y. Yan, *Biosens. Bioelectron.*, 2018, **100**, 228–234.

426 J. Ma, W. Wang, Y. Li, Z. Lu, X. Tan and H. Han, *Anal. Chem.*, 2021, **93**, 2090–2096.

427 Z. Su, D. Tang, X. Yang, Y. Peng, B. Wang, X. Li, J. Chen, Y. Hu and X. Qin, *Microchem. J.*, 2022, **174**, 107038.

428 H.-Q. Zhao, G.-H. Qiu, Z. Liang, M.-M. Li, B. Sun, L. Qin, S.-P. Yang, W.-H. Chen and J.-X. Chen, *Anal. Chim. Acta*, 2016, **922**, 55–63.

429 B. Sun, H.-Q. Zhao, B.-P. Xie, L.-P. Bai, Z.-H. Jiang and J.-X. Chen, *J. Inorg. Biochem.*, 2017, **176**, 17–23.

430 H.-Q. Zhao, S.-P. Yang, N.-N. Ding, L. Qin, G.-H. Qiu, J.-X. Chen, W.-H. Zhang, W.-H. Chen and T. S. A. Hor, *Dalton Trans.*, 2016, **45**, 5092–5100.

431 L. Xue, Y. Yang, S. Wu, Y. Huang, J. Li, Y. Xiang and G. Li, *Anal. Chem.*, 2020, **92**, 2972–2978.

432 B.-P. Xie, G.-H. Qiu, P.-P. Hu, Z. Liang, Y.-M. Liang, B. Sun, L.-P. Bai, Z.-H. Jiang and J.-X. Chen, *Sens. Actuators, B*, 2018, **254**, 1133–1140.

433 Y. Pan, S. Zhan and F. Xia, *Anal. Biochem.*, 2018, **546**, 5–9.

434 G.-H. Qiu, Z.-H. Weng, P.-P. Hu, W.-J. Duan, B.-P. Xie, B. Sun, X.-Y. Tang and J.-X. Chen, *Talanta*, 2018, **180**, 396–402.

435 B.-P. Xie, G.-H. Qiu, B. Sun, Z.-F. Yang, W.-H. Zhang, J.-X. Chen and Z.-H. Jiang, *Inorg. Chem. Front.*, 2019, **6**, 148–152.

436 S.-P. Yang, W. Zhao, P.-P. Hu, K.-Y. Wu, Z.-H. Jiang, L.-P. Bai, M.-M. Li and J.-X. Chen, *Inorg. Chem.*, 2017, **56**, 14880–14887.

437 T. Matsubara, M. Ujie, T. Yamamoto, Y. Einaga, T. Daidoji, T. Nakaya and T. Sato, *ACS Sens.*, 2020, **5**, 431–439.

438 H. Que, D. Zhang, B. Guo, T. Wang, H. Wu, D. Han and Y. Yan, *Biosens. Bioelectron.*, 2019, **143**, 111610.

439 A.-L. Sun, *Analyst*, 2018, **143**, 487–492.

440 Y. Mustapha Kamil, S. H. Al-Rekabi, M. H. Yaacob, A. Syahir, H. Y. Chee, M. A. Mahdi and M. H. Abu Bakar, *Sci. Rep.*, 2019, **9**, 13483.

441 B. Babamiri, R. Hallaj and A. Salimi, *Methods Appl. Fluoresc.*, 2018, **6**, 35013.

442 H. C. Nguyen, H. Park, H.-J. Shin, N. M. Nguyen, A. T. V. Nguyen, T.-T. T. Trinh, T. H. Y. Duong, H. T. Tuong, V. T. Hoang, G.-E. Seo, H.-J. Sohn and S.-J. Yeo, *Intervirology*, 2019, **62**, 145–155.

443 M. Gast, S. Kühner, H. Sobek, P. Walther and B. Mizaikoff, *Anal. Chem.*, 2018, **90**, 5576–5585.

444 Z. Altintas, in *Advanced Molecularly Imprinting Materials*, ed. A. Tiwari and L. Uzun, 2016, pp. 389–411.

445 W. Feng, C. Liang, H. Gong and C. Cai, *New J. Chem.*, 2018, **42**, 3503–3508.

446 M. Du, N. Li, G. Mao, Y. Liu, X. Wang, S. Tian, Q. Hu, X. Ji, Y. Liu and Z. He, *Anal. Chim. Acta*, 2019, **1084**, 116–122.

447 Q. Yan, Y. Yang, Z. Tan, Q. Liu, H. Liu, P. Wang, L. Chen, D. Zhang, Y. Li and Y. Dong, *Biosens. Bioelectron.*, 2018, **103**, 151–157.

448 X. Zhu, X. Wang, L. Han, T. Chen, L. Wang, H. Li, S. Li, L. He, X. Fu, S. Chen, M. Xing, H. Chen and Y. Wang, *Biosens. Bioelectron.*, 2020, **166**, 112437.

449 P. Piedimonte, L. Sola, M. Cretich, A. Gori, M. Chiari, E. Marchisio, P. Borga, R. Bertacco, A. Melloni, G. Ferrari and M. Sampietro, *Biosens. Bioelectron.*, 2022, 113996.

450 K. H. Cho, D. H. Shin, J. Oh, J. H. An, J. S. Lee and J. Jang, *ACS Appl. Mater. Interfaces*, 2018, **10**, 28412–28419.

451 C. L. Pirich, R. A. de Freitas, R. M. Torresi, G. F. Picheth and M. R. Sierakowski, *Biosens. Bioelectron.*, 2017, **92**, 47–53.

452 N. Dey, D. Bhagat and S. Bhattacharya, *ACS Sustainable Chem. Eng.*, 2019, **7**, 7667–7675.

453 C. Song, Y. Sun, J. Zhang, T. Wang, Y. Wang, Y. Liu and L. Wang, *Analyst*, 2020, **145**, 5475–5481.
454 H. Zhang, X. Xu and W. Jiang, *Chem. Sci.*, 2020, **11**, 7415–7423.
455 G.-X. Liang, S.-Y. Ye, H.-M. Yu, K.-R. Zhao, P.-F. Liu, Z.-J. Liu and L. Wang, *Sens. Actuators, B*, 2022, **354**, 131199.
456 Y. Liu, H. Xu, C. Liu, L. Peng, H. Khan, L. Cui, R. Huang, C. Wu, S. Shen, S. Wang, W. Liang, Z. Li, B. Xu and N. He, *J. Biomed. Nanotechnol.*, 2019, **15**, 790–798.
457 T. Zhao, K. Asawa, T. Masuda, A. Honda, K. Kushiro, H. Cabral and M. Takai, *J. Colloid Interface Sci.*, 2021, **601**, 825–832.
458 M. Fratini, T. Wiegand, C. Funaya, Z. Jiang, P. N. M. Shah, J. P. Spatz, E. A. Cavalcanti-Adam and S. Boulant, *ACS Infect. Dis.*, 2018, **4**, 1585–1600.
459 M. Gast, F. Wondany, B. Raabe, J. Michaelis, H. Sobek and B. Mizaikoff, *Anal. Chem.*, 2020, **92**, 3050–3057.
460 Y. Wu, L. Li, L. Frank, J. Wagner, P. Andreozzi, B. Hammer, M. D'Alicarnasso, M. Pelliccia, W. Liu, S. Chakrabortty, S. Krol, J. Simon, K. Landfester, S. L. Kuan, F. Stellacci, K. Müllen, F. Kreppel and T. Weil, *ACS Nano*, 2019, **13**, 8749–8759.
461 H.-O. Kim, W. Na, M. Yeom, J.-W. Lim, E.-H. Bae, G. Park, C. Park, H. Lee, H. K. Kim, D. G. Jeong, K.-S. Lyoo, V. P. Le, S. Haam and D. Song, *ACS Appl. Mater. Interfaces*, 2020, **12**, 6876–6884.
462 Y. Zhang, C. Yurdakul, A. J. Devaux, L. Wang, X. G. Xu, J. H. Connor, M. S. Ünlü and J.-X. Cheng, *Anal. Chem.*, 2021, **93**, 4100–4107.